

**MECHANICAL AND DYNAMICAL PROCESS MODEL FOR GENERAL
MILLING TOOLS IN MULTI-AXIS MACHINING**

by

Ömer Mehmet ÖZKIRIMLI

Submitted to the Graduate School of Engineering and Natural Sciences

in partial fulfillment of

the requirements for the degree of

Master of Science

Sabancı University

February, 2011

© Ömer Mehmet Özkırmı, 2011

All Rights Reserved

to my family...

MECHANICAL AND DYNAMICAL PROCESS MODELLING FOR GENERAL MILLING TOOLS IN MULTI-AXIS MACHINING

Ömer Mehmet Özkırmılı

Industrial Engineering, MSc Thesis, 2011

Thesis Supervisor: Assoc. Prof. Dr. Erhan Budak

Keywords: Cutting mechanics, cutting dynamics, multi-axis milling, general cutting tools, serrated tools, variable tools, process model

Abstract

Multi-axis milling operations are widely used in many industries such as aerospace, automotive and die-mold for machining intricate sculptured surfaces. The most important aspects in machining operations are the dimensional integrity, surface quality and productivity. Process models are employed in order to predict feasible and proper process conditions without relying on empirical methods based on trial and error cutting and adaptation of previous experiences. However, previously developed process models are often case specific where the model can only be employed for some particular milling tools or they are not applicable for multi-axis operations. In many cases, custom tools with intricate profile geometries are compatible with the surface profile to be machined. On the other hand, for more robust and stable cutting operations, tools with wavy cutting edge profiles and varying geometric edge distributions are utilized.

In this thesis, a complete numerical mechanic and dynamic process model is proposed where the tool is modeled as a point cloud in the cylindrical coordinates along the tool axis. The tool geometry is extracted from CAD data enabling to form a model for any custom tool. In addition, the variation in the cutting edge geometry, where serrated and variable helix/pitch cutting edges can be adapted for any milling tool is taken into account. The cutting engagement boundaries are identified numerically using a Boolean

intersection scheme. Moreover, a Z-mapping algorithm is integrated in the proposed multi-axis mechanistic force model to predict cutting forces for a continuous process. As for the multi-axis milling dynamics, previous single-frequency stability models are extended to encompass all possible tool geometries taking the time delay variation introduced by irregular cutting edge geometries. The proposed model is experimentally verified with different tool geometries investigating cutting forces and also predicting the stable cutting conditions.

ÇOK EKSENLİ FREZELEME OPERASYONUNDA GENEL TAKIM GEOMETRİLERİ İÇİN MEKANİK VE DİNAMİK SÜREÇ MODELLEMESİ

Ömer Mehmet Özkırmı

Endüstri Mühendisliği, Yüksek Lisans Tezi, 2011

Tez Danışmanı: Doç. Dr. Erhan Budak

Anahtar Kelimeler: Kesme mekaniği, kesme dinamiği, çok-eksen frezeleme, genel kesici takımlar, kaba işlem takımları, değişken takımlar, süreç modeli

Özet

Çok eksenli frezeleme operasyonları havacılık, otomotiv ve kalıpcılık gibi birçok sektörde karmaşık yüzeyleri işlemek için kullanılmaktadır. Boyutsal bütünlük, yüzey kalitesi ve verimlilik talaşlı imalattaki en önemli kıstaslardır. Uygun ve verimli kesme parameterelerinin doğru olarak belirlenmesinde süreç modelleri deneysel ve deneyime dayalı yöntemlere nazaran büyük avantaj sağlamaktadır. Literatürde bulunan çoğu süreç modeli belirli kesici takımlara ya da süreçlere özel olarak geliştirilmiş olup farklı durumlara uyarlanamamaktadır. Çoğu üretim sürecinde, özel üretim takım profil geometrileri oluşturulacak olan yüzey geometrisyle eş olacak şekilde tasarlanmaktadır. Öte yandan, daha dinamik açıdan daha kararlı kesme operasyonları için, değişken ağız aralıklı ve değişken sarmal açılı veya dalgalı kesici kenar geometrilerine sahip kesici takımlar kullanılmaktadır.

Bu çalışmada, kesici takımın üç boyutlu nokta bulutu olarak tanımlandığı, tam bir sayısal mekanik ve dinamik süreç modeli geliştirilmiştir. Herhangi bir karmaşık form takımını kolaylıkla modellemek için takımların geometric bilgileri CAD verilerinden elde edilmektedir. Aynı zamanda, değişken ve dalgalı kesici kenar formları düşünülerek, kesici kenarların geometrik değişkenlikleri de modele uyarlanabilmektedir. Takım-iş parçası çakışım alanları geliştirilen Boolean kesişim modeliyle bulunmaktadır. Ek

olarak, geliştirilen mekanik model Z-haritalama yöntemiyle birleştirilerek uzun değişken operasyonlar esnasında kesme kuvvetleri hesaplanmış ve testlerle doğrulanmıştır. Süreç dinamiği yönündense, önceden geliştirilmiş tek frekansa dayalı kararlılık modeli olası bütün takım geometrilerini kapsayacak şekilde geliştirilmiştir. Ortaya konulan süreç modeli yapılan mekanik kesme ve kararlılık analiz testleriyle doğrulanmış ve işlevselliği kanıtlanmıştır.

Acknowledgement

I owe my deepest gratitude to my advisor, Prof. Dr. Erhan Budak, for his intellectual input, guidance, encouragement and inspiration throughout my graduate studies that enabled me to excel both academically and technically. It has been and always will be a great pleasure to work with him at all times.

I would like to thank my family for their love and support that was immeasurable and constant. I dedicate this thesis to them for being my driving force not only for my academic journey but for all my life and for always trying to show me what is best and virtuous.

I would like to thank my love, Gizem Ekiz, for always being on my side patiently throughout my university adventure and bringing joy to every second of my life.

It is a pleasure to thank every single member of Manufacturing Research Group (MRL) and Maxima Manufacturing R&D. I am very grateful for the technical and academic support and guidance of my colleagues, Dr. Emre Özlü, Dr. L. Taner Tunç, Dr. Erdem Öztürk, Volkan Aran, Esma Baytok, İpek Güven and Burak Aksu. I also would like to thank Mehmet Güler and Süleyman Tutkun for their contributions and help in the manufacturing laboratory.

I would like to thank Anıl Can, Halil Şen, Çetin Suyabatmaz, Nihan Özşamlı, Mahir Umman Yıldırım and all of my friends in the Manufacturing System Laboratory for their support at the most desperate times and for the happy times that we shared.

I would like to thank Mr. Aykut Aşık from Makina Takım Endüstri (MTE) and engineers in Artı Takım for their interest in the subject and especially for providing custom cutting tools for the verification tests.

Table of Contents

Abstract.....	ii
Özet.....	iv
CHAPTER 1 INTRODUCTION.....	1
1.1 Organization of the thesis.....	2
1.2 Literature survey.....	3
CHAPTER 2 MILLING TOOL GEOMETRY.....	8
2.1 Tool shape geometry.....	11
2.1.1 Parametric standard helical tools.....	13
2.1.2 Multi-segmented helical tools.....	17
2.1.3 Inserted face milling tools.....	20
2.2 Variable cutting edge geometry.....	27
2.3 Summary.....	33
CHAPTER 3 MULTI-AXIS CUTTING PROCESS GEOMETRY.....	34
3.1 Multi-axis milling geometry.....	34
3.1.1 Coordinate transformations.....	36
3.1.2 Relation between cutter contact and cutter tip points.....	37
3.2 Process geometry and cutter engagement zones.....	39
3.2.1 Arbitrary cutting scenario.....	39
3.2.2 Following cut scenario.....	42

3.3	Summary	45
CHAPTER 4 FORCE MODEL		47
4.1	Mechanistic cutting force model.....	47
4.2	Uncut chip thickness formulation for serrated general variable helix/pitch tools 50	
4.3	Identification of milling cutting force coefficients	56
4.4	Model verification and experimental results.....	58
4.4.1	Multi-axis cutting force verification for a ball end mill tool	58
4.4.2	Multi-axis cutting force verification for a standard milling tool	60
4.4.3	Cutting force verification for a custom profiling tool with multiple profile segments.....	62
4.4.4	Cutting force verification for inserted face milling tool	64
4.4.5	Cutting force verification tests for a serrated end mill	66
4.4.6	Cutting force verification for variable helix/pitch cutters	68
4.4.7	Cutting force verification for a process simulation case employing Z- mapping70	
4.5	Summary	75
CHAPTER 5 DYNAMIC STABILITY MODEL		76
5.1	Chatter stability model for constant time delayed systems.....	77
5.2	Chatter stability model for varying time delayed systems	83
5.3	Model verification and simulation results.....	86
5.3.1	Stability analysis of an inverted cone bull end mill during 5-axis operation 88	

5.3.2	Radial stability analysis of multi-segmented profiling tool.....	90
5.3.3	Stability limit verification of inserted milling tool	93
5.3.4	Stability limit of serrated milling tool	94
CHAPTER 6 CONCLUSION		96
6.1	Summary and contributions	96
6.2	Future works	98
Bibliography		100

List of Figures

Figure 1.1: Mechanic and Dynamic process model schematic.....	3
Figure 2.1: Different tool geometries (a) standard helical tools, (b) custom profiling tools, (c) face milling inserted tools.....	9
Figure 2.2: Different cutting edge profile geometries [22].....	10
Figure 2.3: Milling tool and corresponding geometrical parameters.....	10
Figure 2.4: Lag angle and immersion angle definition for a cutting flute	11
Figure 2.5: IGES file example and its sections.....	12
Figure 2.6: Geometry of standard milling cutters with APT parameters.....	14
Figure 2.7: Standard milling cutter shapes and corresponding parameters	14
Figure 2.8: Taper ball end mills with constant lead and constant helix [17]	16
Figure 2.9: Example standard milling cutter representations with helical flutes.....	17
Figure 2.10: Fir tree tool and machining of the turbine blade slots.....	17
Figure 2.11: Multi-segmented tool geometry with corresponding segment parameters	18
Figure 2.12: <i>Example multi-segmented cutter representation with cutting flutes</i>	19
Figure 2.13: Schematic representation of inserted face milling tools with curved 4-sided inserts (a), curved 3-sided inserts and (c) circular inserts.....	20
Figure 2.14: Insert representation with tool and insert coordinate systems.....	20
Figure 2.15: Insert coordinate systems and geometrical parameters of (a) curved 4-sided, (b) curved 3-sided and (c) circular insert bodies	21
Figure 2.16: Insert orientation; (a) Insert coordinate systems with no orientation, (b) Axial rake angle, β (c) Lead angle, δ (d) Index angle, α	22

Figure 2.17: Two example inserted face milling tools with circular [Tool 1 - (a)] and curved squared [Tool 2 - (b)] insert geometries	26
Figure 2.18: Cutting flute geometry and corresponding parameters;	28
Figure 2.19: Maximum safe rotary speed values corresponding to maximum permissible residual unbalance value for different balanca quality grades, G 0.....	30
Figure 2.20: Custom variable tool AOT.318.001, (a) unfolded tool geometry, (b) separation angle variation	31
Figure 2.21: Custom variable tool AOT.318.002, (a) unfolded tool geometry, (b) separation angle variation	32
Figure 2.22: Custom variable tool AOT.318.003, (a) unfolded tool geometry, (b) separation angle variation	32
Figure 3.1: Machining coordinate systems	35
Figure 3.2: Lead and tilt angle representations	36
Figure 3.3: CL and CC point representations in process coordinates.....	37
Figure 3.4: Arbitrary cutting case and corresponding engagement surface	39
Figure 3.5: Engagement boundary conditions and total engagement.....	40
Figure 3.6: Engagement of a standard milling tool with an arbitrary workpiece; (a-b) Engagement zone shown on tool, (c) Cutter engagement boundary map, $CEB(\phi,z)$	42
Figure 3.8: Engagement of a tapered bull end mill performing following cutting; (a) Engagement zone shown on tool, (b) Cutter engagement boundary map, $CEB(\phi,z)$, (c) Previous tool boundaries (blue and red points) and current tool (black points).....	45
Figure 4.1: Multi-axis differential cutting force and differential chip representation	48
Figure 4.2: Chip load of an exemplary conventional milling tool.....	52
Figure 4.3: Chip load of an exemplary variable helix/pitch milling tool	52

Figure 4.4: Chip load of a serrated cutter having equally separated circular wave formed edges	53
Figure 4.5: Detailed Uncut chip thickness definition for a serration profile	55
Figure 4.6: Orthogonal and oblique cutting geometries 0	56
Figure 4.7: Results of the 1 st force verification test (a) cutter engagement boundary, (b) cutter engagement zone on tool, (c) simulated versus measured forces (simulated in thin line, measured in dashed).....	59
Figure 4.8: Inverted cone bull end mill tool (ISCAR MMHT) geometrical parameters	60
Figure 4.9: Results of the 2 nd force verification test (a) cutter engagement boundary, (b) cutter engagement zone on tool, (c) simulated versus measured forces (simulated in thin line, measured in dashed).....	61
Figure 4.10: Custom profiling tool (a) CMM output of the profile for the custom multi-segmented tool, (b) actual tool photograph	62
Figure 4.11: Results of the 3 rd force verification test (a) cutter engagement boundary, (b) cutter engagement zone on tool, (c) simulated versus measured forces (simulated in thin line, measured in dashed).....	64
Figure 4.12: Inserted face milling tool (Fette FCT 11355) and respective geometry.....	64
Figure 4.13: Force verification results of the inserted face milling tool.....	65
Figure 4.14: Force verification results for serrated end mills the 1 st test condition	67
Figure 4.15: Force verification results for serrated end mills the 2 nd for test condition.	67
Figure 4.16: Force verification results for AOT.318.002 variable helix tool.....	69
Figure 4.17: Force verification results for AOT.318.003 variable helix/pitch tool.....	69
Figure 4.18: Applicatinn of the Z-map method [52]	71
Figure 4.19: Virtual CAM operation and resulting surfaces	72

Figure 4.20: Simulated machined surface profiles from Z-mapping algorithm	73
Figure 4.21: Simulated and measured process forces.....	74
Figure 5.1: Block diagram for the closed loop chatter generation system.....	76
Figure 5.2: The chatter vibration on the tool and corresponding dynamic chip thickness definition.....	78
Figure 5.3: Dynamic cutting forces and discrete height definitions.....	78
Figure 5.4: Pseudocode for generating stability diagrams for non-time varying machine tool systems.....	83
Figure 5.5: Pseudocode for generating stability diagrams for varying time delay machine tool systems.....	86
Figure 5.6: Frequency response function (FRF) measurement setups (a) impact hammer with accelerometer, (b) impact hammer with vibrometer.....	87
Figure 5.7: Frequency response function plots for inverted cone bull end cutter in X (a) and Y (b) directions	89
Figure 5.8: Stability lobe diagram for inverted bull end mill with corresponding stability test points (green dot representing stable operations, red dot representing chatter vibrations).....	89
Figure 5.9: Magnitude of FRF for custom profiling tool with tool overhang length 190mm	91
Figure 5.10: 3D plot of axial stability lobe diagrams with corresponding radial depth of cuts for custom profiling tool	92
Figure 5.11: Radial stability limit diagram for custom profiling tool	92
Figure 5.12: Magnitude of FRF for inserted tool (Table 2.2 - Tool 2) with overhang length 170mm	93
Figure 5.13: Stability lobe diagram for inserted tool (Table 2.2 - Tool 2).....	93

Figure 5.14: Stability lobe diagram serrated milling tool (see Table 4.8) 94

List of Tables

Table 2.1: Geometric definitions in the Parameter Data section of an IGES file.....	13
Table 2.2: Properties of the example face milling tools	27
Table 2.3: Calculated rotation angles for example face milling tools	27
Table 2.4: Cutting flute parameters for custom made variable tools.....	31
Table 4.1: Tool and process properties for 1 st force model verification test case	58
Table 4.2: Material database parameters for Ti ₆ Al ₄ V.....	59
Table 4.3: Tool and process properties for 2 nd force model verification test case	60
Table 4.4: Material database parameters for Al7075-T6.....	61
Table 4.5: Tool and process properties for 2 nd force model verification test case	63
Table 4.6: Orthogonal database for GH210 steel	65
Table 4.7: Process parameters for inserted face milling tool force verification test	65
Table 4.8: Tool properties for serrated flat end mill verification tests	66
Table 4.9: Process conditions for serrated end mill force verification tests.....	66
Table 4.10: Cutting edge geometric parameters for variable helix/pitch tools used for force verification tests.....	68
Table 4.11: Process parameters for milling tools with variable cutting edge geometry.	68
Table 4.12: Cutting conditions for process simulation verification tests	72
Table 4.13: Simulation times for the process model	73
Table 5.1: Modal parameters for the inverted cone bull end mill cutter with 94mm overhang length.....	88

Table 5.2: Modal parameters for custom profiling tool with tool overhang length 190mm	91
Table 5.3: Modal parameters for serrated milling tool (see Table 4.8)	94

CHAPTER 1

INTRODUCTION

In manufacturing industry, among many different types of shape forming operations, machining or metal cutting is the most dominant one. Machining is a fast, versatile and accurate solution and different types of machining operations exist for different purposes; turning, broaching, drilling, milling, etc. For all of the machining operations, the aim is to be as productive as possible by satisfying desired tolerances and improved surface finish. In general, the process parameters controlling the rate of production are chosen using trial and error based methods which mainly depend on the experience of the operator. However, poor choices of machining parameters may result in stall of the machine tools, excessive part and tool deflection or tool breakages due to high cutting forces. To determine optimal cutting parameters, process models and simulations can be employed to predict key aspects of machining operations such as cutting forces, machine tool vibration.

Due to its flexibility, milling is the most widely used machining technique producing wide ranges of shapes in many industries such as aerospace, automotive and die-mold, etc. Multi-axis milling operations are often classified the number of degrees of freedom in movement and orientation, such as 2½ axis, 3 axis, 5 axis, etc. where the integer number designates the number of simultaneously altering translational or rotational axes during operations. Mechanical parts having freeform and complex surfaces are often manufactured using multi-axis milling operations. In milling operations, there are infinitely many methods to machine a part considering the choice of milling tool, process parameters and machining strategies. Finding an optimal solution might not be possible; however, through process modeling encompassing different type of milling tools and multi-axis operations, feasible sets of solutions can be simulated and chosen.

In this study, the objective is to constitute a complete process model for multi-axis machining to predict first the cutting forces secondly the stable cutting conditions through construction of the stability lobe curves for any type of milling tool performing multi-axis operations. Furthermore, the model is applied to tools with unconventional cutting edge geometries such as serrated and variable helix cutters.

1.1 Organization of the thesis

The thesis is organized as follows;

- Chapter 2 presents the geometric modeling of different types of tools and identification of cutting edge point parameters in cylindrical coordinates by discretizing the milling tool axially constructing radial cross sections.
- Chapter 3 discusses the geometry of multi-axis machining by introducing formulations of translational and rotational transformations of the milling tool with respect to machined part and finally introducing a numerical methodology to identify cutter engagement boundaries required in the following process models.
- In Chapter 4, force modeling of generalized milling tools for multi-axis operations is presented as an extension of the model proposed by Ozturk and Budak [44]. Linear edge force model approach is utilized and discrete uncut chip thickness formulations are given for the most general case such as serrated, unevenly spaced and non-uniform helical general end mills. Experimental verifications of the proposed models are given at the end of the chapter
- In chapter 5, the chatter stability model utilizing zero-order frequency domain solution is introduced first for milling tools with uniform straight helical edges as an extension to the model proposed for 5 axis ball end mills by Ozturk and Budak [43]. Secondly, chatter stability model is constructed for milling tools with varying cutting edge profiles introducing variable time delay as an extension to the model proposed by Campomanes [43] for serrated flat-end

mills. Experimental verifications of the proposed models are given at the end of the chapter.

- In Chapter 6, process simulation model for force prediction through a whole operation cycle is introduced for which the surface update model and cutter engagement zone information is proposed by Tunc [52] utilizing the Z-mapping technique.

The adapted methodology of the thesis to calculate mechanic and dynamic aspects of the multi-axis milling operation is summarized in Figure 1.1.

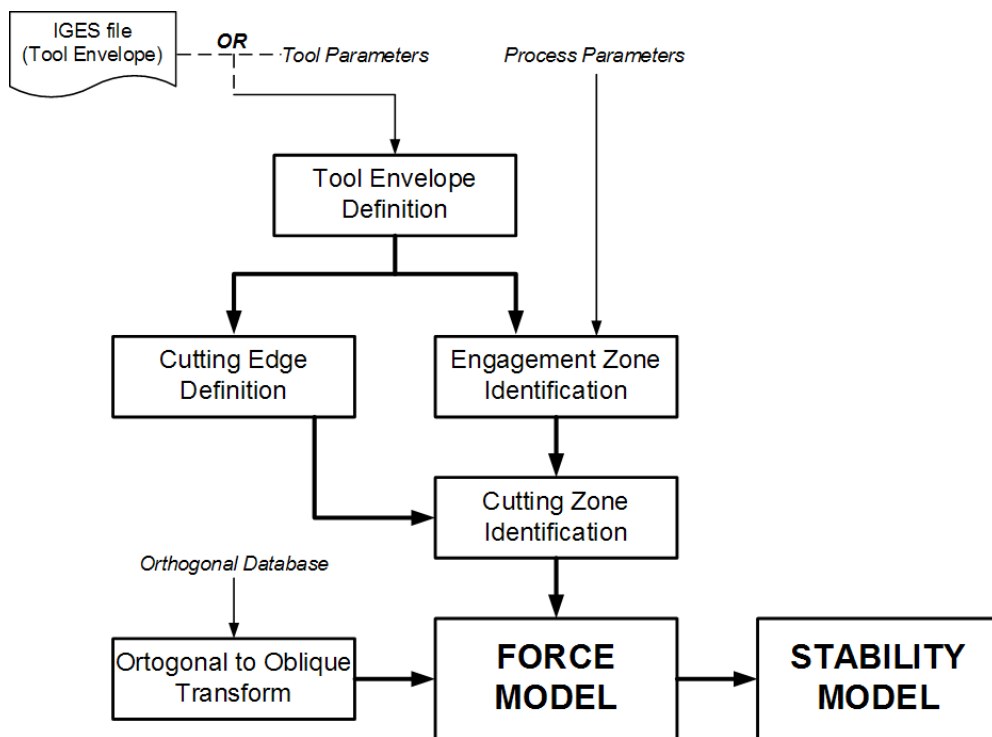


Figure 1.1: Mechanic and Dynamic process model schematic

1.2 Literature survey

In the literature, there is extensive amount of publication on the mechanics and dynamic of cutting for different tool types considering both the envelope of the cutter and the effect of cutting edge geometry on the process using different approaches. In this section, some of the important work are presented to shed light on the subject matter of this thesis.

The mechanics of simple milling operations for flat end mills was examined by Martelotti [37] which is followed by Kline et. al. [30] who calculated average cutting forces for varying feed rates and process parameters by modeling chip load and cutting geometry for milling. Later, Altintas and Spence [4] developed a semi-analytical force model which can be integrated into CAD systems. Budak et. al. [11] proposed an accurate cutting coefficient transformation model where cutting coefficient obtained orthogonal database are transformed into helical milling conditions considering the oblique cutting mechanism. Employing this model, Lee and Altintas modeled the mechanics and dynamics of helical flat end cutters [32] and later improved their model to calculate cutting forces for ball end mill tools [33]. For standad milling tools, the first complete geometrical model was developed by Engin and Altintas [17] covering all standard end mill geometries. They modeled helical cutting edge geometries wrapped around these tools and analyzed the mechanics and dynamics of cutting by verifying their model with exemplary tests. Considering the former model and employing the same methodology proposed by Budak et. al. [11], Gradisek et. al. [21] developed an analytical average force coefficient calculation model for general milling geometries.

For multi-axis machining, due to the variation in tool position and orientation, mechanic and dynamic modeling approaches have to consider the workpiece conditions. The most challenging part of these models is to predict the cutter engagement boundaries defining the surface area of the cutting tool engaging with the workpiece surface during cutting in terms of tool orientation angles. For 3 axis operations, the first mechanic models are developed by Lazoglu and Liang [31] for sculptured surfaces and analytical approach is presented to predict the engagement boundaries. This model is verified by airfoil machining experiments. Both analytical and numerical methods are present in the literature, however analytical models are very limited due to complexity of the multi-axis machining operations. Therefore, numerical methods where the milling tool and workpiece surface are modeled using different types of discrete elements are developed and utilized for their robustness. Z-mapping and Octree methods are among the most popular and robust models proposed in the literature. In Z-mapping method [26]-[36], the workpiece is represented with arbitrary vectors in the Z direction and the height of these vectors is updated by the intersection of the swept volume of the cutter body during cutting. In Octree method, the workpiece material is divided into cubic elements and as in the Z-mapping methodology arbitrary cubes engaging with the swept volume

of the cutter are further decreased in size to finally find an accurate solution. On the other hand, there are also few analytical models developed for mostly case specific or tool specific conditions. For 5-axis milling operations, an analytical engagement model considering the orientation of the cutting tool with respect cutting surface is developed by Ozturk and Budak [44]. They also predicted the cutting forces during multi-axis operations which further improves the model proposed by Lee and Altintas [33]. A case specific semi-analytical model for taper ball end mills used mainly in the manufacturing of bladed disks for aerospace industry is developed by Ferry and Altintas [19]. All of these models for multi-axis machining are limited due to their case specific structures which can only handle a set of cutting tools for designated milling conditions. In this thesis, a very general numerical multi-axis process model is proposed which can handle any tool shape.

As for the inserted cutter and especially face milling cutter used in die-mold industry the research mainly focuses on predicting feasible productive process parameters. Li et al. [34] developed a force model for calculation of forces in face milling with inserted cutters. They included dynamics of the structure and run out in force calculations. For inserted cutting tools, the orientations of cutting inserts with respect to the tool body complicate the definition of cutting edge geometry. Until the work of Engin and Altintas [4], these orientation angles had not been taken into account. Engin and Altintas [18] proposed a model for the mechanics and dynamics of the inserted cutters and verified them experimentally. They presented experimental results only for rectangular inserts. Kim et al. [28] modelled cutting forces for cutting tools with rectangular and circular inserts. They verified their model experimentally for both rectangular and circular inserts. They also employed feed rate scheduling to keep cutting forces around a predefined value during the process. Lopez de Lacalle et al. [35] developed force and deflection models and used them in die machining. Considering hardness variations in workpiece and calculated tool deflections, they modified the process parameters, and demonstrated the benefits of the model for die industry. Afterward, Campa et al. [13] modelled the dynamics of bull-nose end mills and verified the predicted stability diagrams experimentally.

Machine tool vibrations resulting from the self-excitation mechanism in the generation of varying chip thickness modulations are considered as chatter vibrations. Both the machine tool and the workpiece are flexible bodies and once they are excited by varying

cutting forces around one of the structural modes, they start to oscillate. The oscillations may cease in time or build up and induce instability of the machine tool-workpiece system. During milling, consecutive cutting edges machine surfaces cut by previous edges. Hence, if there exists a wave profile (outer modulation) left from the dynamic oscillations during the previous tooth period, the uncut chip thickness during the present tooth period varies in accordance with the cutting forces resulting in a new wave profile on the surface in phase or out of phase with respect to the previous modulation. Out of phase modulations results in chatter vibrations and causes an exponential rise in machine tool vibrations in addition to cutting forces.

Research on the stability of the multi-axis machining operation for general milling tools on the other hand is missing in the literature. Accurate solutions with different methods are obtained for 3 axis operations. For milling applications, Minis et. al. [40] modeled milling stability using an iterative method. Budak et al., [12] proposed single and multi-frequency methods and were the first researchers to identify stability regions in milling analytically. Later Bavyl et al. [8] applied the time temporal finite element (TFEA) analysis and Insperger et al. [24] proposed the semi-discretization method to predict stable cutting regions. Altintas et al. [5] applied the single-frequency method to 3 axis ball-end milling. Ozturk et al. [43] proposed an iterative multi-frequency method for 5-axis ball-end machining considering tool axis orientation extended from Altintas et al.'s [5] work. Ferry [20] investigated the dynamics of serrated taper ball-end mills with variable tooth separations through Nyquist criterion.

Serrated milling tools used extensively for roughing operations due to their high material removal rate performance. The advantage of serrated cutters is that their wavy cutting edge profile and axial phase shift of the wave between consecutive teeth induces irregular chip removal rate. This irregularity both decreases the chip load and also increases the stability of the cutting system drastically. Tlustý et al. [50] were the first researchers investigating the chatter stability of the serrated milling cutters where they examined non-helical (straight) fluted cutter geometries. Campomanes [14] established a mechanic and dynamic model for helical serrated cutters with sinusoidal wave form. He formulated the uncut chip thickness for serrated cutters and proposed a dynamical model based on [1] where the effect of serration form was taken as an average regeneration quantity. Merdol and Altintas [39] developed a model for serrated flat, ball and taper end mills utilizing B-spline representation for the serration waves. Zhang et. al.

[57] developed a sectional numerical model to identify cutting forces and effective cutting force coefficients. Dombovari et. al. [16] employing the semi-discretization model developed by Insperger and Stephan [23]-[24] established a new chatter stability model for helical serrated flat end mill cutters. In this thesis, the single-frequency formulation proposed by Campomanes [14] is improved to handle multi-axis milling operations.

Currently, especially in finishing operations for low radial cutting cases, in order to increase stability of the milling system for passive vibration cutting tools with irregular helix and variable pitched milling tools are utilized. These geometrical parameters of these types of tools are often chosen through trial and error methods by the tool manufacturers and their aim is to suppress first the forced vibrations during cutting. However, the literature on these types of tools is very limited. Budak et al. [9]-[2] investigated the dynamics and stability of variable pitch cutters with uneven tooth separation by improving their previous model [1] and proposed an optimization methodology for choosing right tooth pitch angles for desired cutting speeds. For similar tools, Olgac and Sipahi [42] developed an optimization model by analyzing the dynamic characteristic equation of the system using cluster treatment method. Later, Ferry [20] developed a mechanical and dynamical model to predict stable cutting regions for serrated variable pitch cutting tools using Nyquist criteria. For variable helix tools on the other hand, the literature is very limited. By applying the method [9] developed for variable pitch cutters to variable helix cutters, Turner et. al. [53] obtained coherent results for low radial cutting cases. Zatarin et al. investigated the effect of helix angle on the chatter stability for low radial cutting conditions and concluded that flip bifurcation or period doubling effects should be also considered for low radial cutting conditions where cutting is very interrupted. Finally, Sims et. al. [48]-[55] by comparing and investigating three different dynamic modeling approaches (semi-discretization [23]-[24], time averaged semi-discretization with similar assumptions of Budak et. al.'s work [9], and temporal-finite element method (TFEA) [55]) investigated the chatter dynamic of variable helix variable pitch cutters analytically and proposed an optimization methodology.

CHAPTER 2

MILLING TOOL GEOMETRY

The key element of a productive milling operation is the choice of milling tool in order to obtain the desired surface profile in the most effective way. In industry, multi-purpose standard tools or process specific custom tools are utilized. Example of standard tools are flat end mills, ball end mills, taper end mills, bull nose mills, etc. (Figure 2.1a). Due to their simple geometries, these type of tools are flexible for machining any type of surfaces with a multi-axis machine tool. However, to increase productivity and achieve superior surface quality, custom tools based on the surface profile to be formed are utilized in case of specific operations (Figure 2.1b). Inserted tools facilitate the maintenance of the milling tool through easily interchangeable cutting inserts and give more flexibility in terms of cutting edge profile regarding the distribution of the inserts (Figure 2.1c).

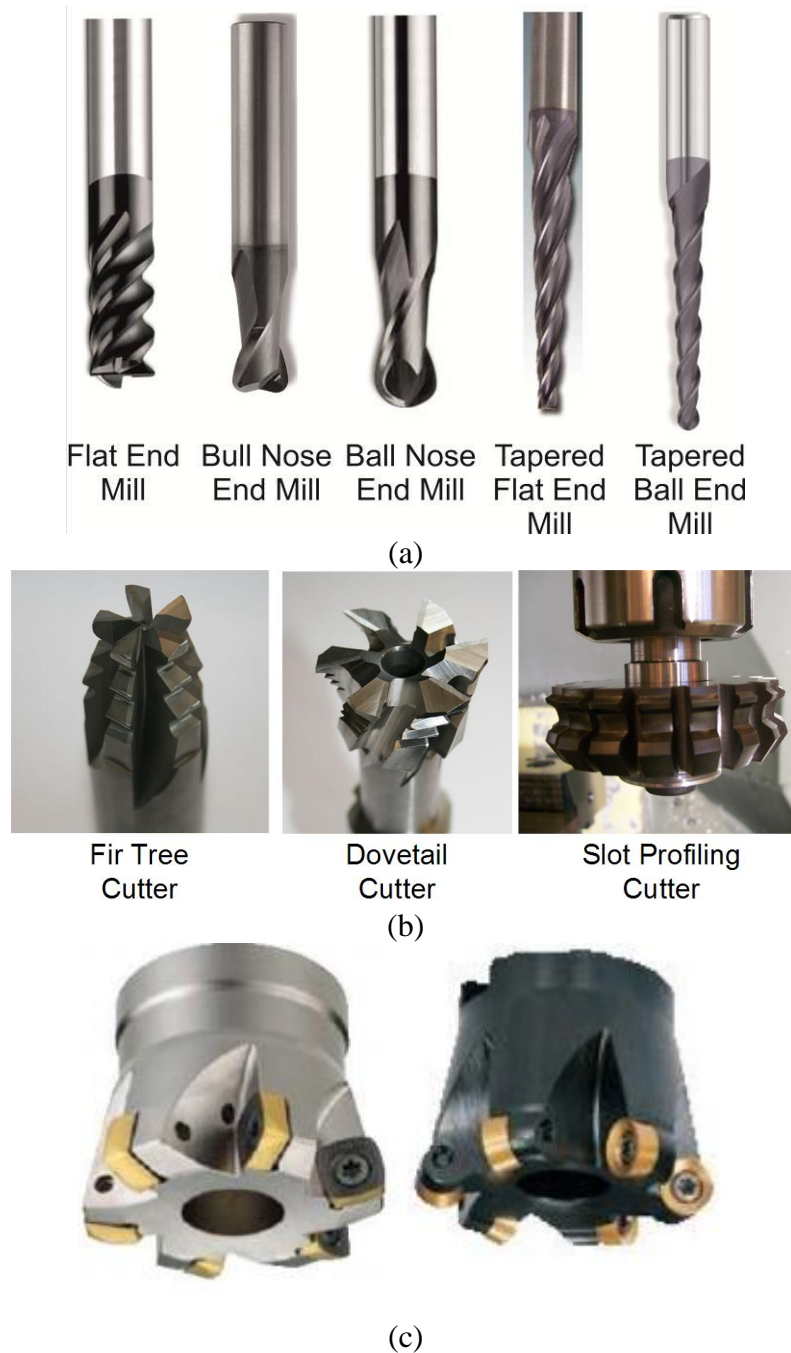


Figure 2.1: Different tool geometries (a) standard helical tools, (b) custom profiling tools, (c) face milling inserted tools

Other than the profile geometry, in order to increase productivity through reduced cutting forces and chatter vibration effects, cutting edges of the milling tools may have different geometries. Specifically, for roughing operations where the surface finish is not an important criterion and high material removal rates are sought, milling tools with serrated edges profiles are utilized. Moreover, milling tools in order to suppress undesirable chatter vibrations may possess variable cutting edge inclination and angular distribution.

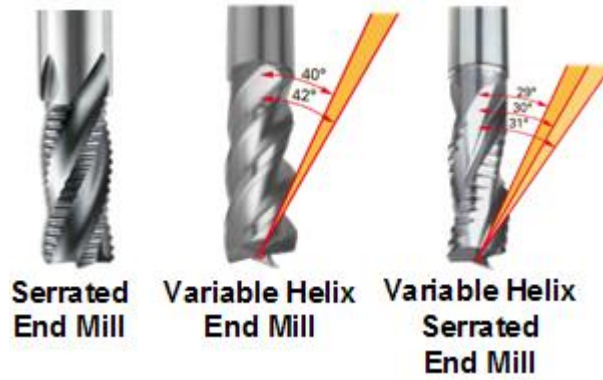


Figure 2.2: Different cutting edge profile geometries [22]

In this study, a milling tool is geometrically defined as a point cloud representing the outer envelope of the tool and the cutting edges. The cutting tool is presented in tool coordinate system, xyz where x , y and z defines the feed, cross-feed and tool axis directions, respectively. The cutter is divided into axial elements along the tool axis direction and the points on the axial sections are represented in polar coordinates. A point P on a helical cutting flute is defined in cylindrical coordinates by characterizing radial distance $r(z)$, the axial immersion angle $\kappa(z)$ which is the angle between the tool axis and the normal vector of the cutting edge and the radial lag angle $\psi(z)$. (Figure 2.3).

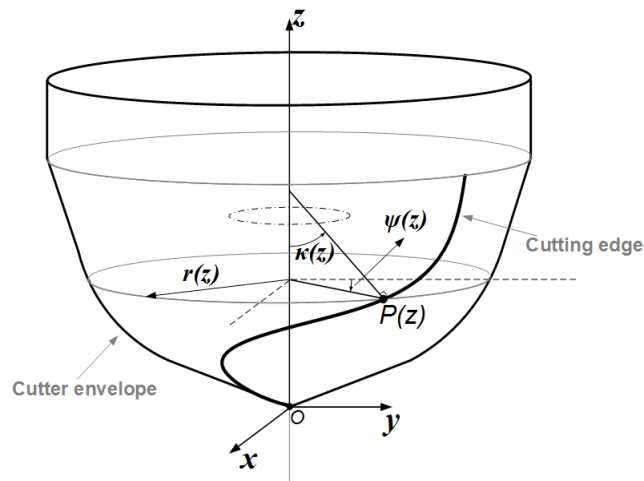


Figure 2.3: Milling tool and corresponding geometrical parameters

Due to helical cutting flutes, cutting points at different elevations are shifted rotationally along the periphery of the cutter body with respect to each other. This rotational shift at elevation z is defined as the lag angle, $\psi(z)$. The relation between the lag angle and rotation angle ϕ of the tool during cutting defines the exact definition of the immersion angle of the corresponding cutting tooth.

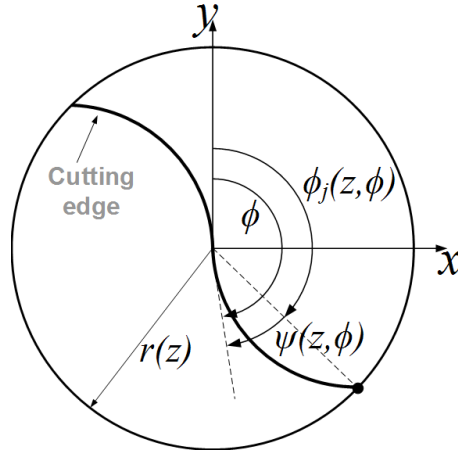


Figure 2.4: Lag angle and immersion angle definition for a cutting flute

For general cutting tools with variable helix and variable tooth pitch separation, generalized local immersion angle $\phi_j(z)$ definition of the j^{th} cutting edge is then given as;

$$\phi_j(z) = \phi + \phi_{p,j} - \psi_j(z) \quad (2.1)$$

where $\phi_{p,j}$ and ψ_j represents the angular position of j^{th} cutting edge with respect to previous $j-1^{\text{th}}$ edge (pitch angle) and axial lag angle shift of the j^{th} cutting edge having a specific helix angle.

2.1 Tool shape geometry

A milling tool can be considered as a union of basic geometric 3D units which are tori and cones. Each basic unit defines a segment of the milling tool. These basic geometric units can be constructed as a revolve surface where the required contour defines the outer body of the milling tool. Most standard milling tools can be expressed as a union of three or less segments and can therefore be represented parametrically. However, parametric representation of custom tools with intricate multi segmented (union of more than three basic geometric unit) geometries is not an efficient way to define the tool geometry because of the large amount of parameters to be defined to identify each segment. It is convenient to obtain the geometric properties of the cutter envelope by decoding the CAD data.

The tool envelope should be first constructed as a sketch on XZ plane in the CAD environment using lines to describe cones and arcs to describe tori. The CAD data is

then converted to IGES. In this study, IGES formatting is chosen because its widely used, standardized and most of the commercial CAD software can both encode or decode this format.

SolidWorks IGES file using analytic representation for surfaces							S	1	Start section
1H,,1H;,25HIscar_MMHT120N06R3.SLDPRT,49HC:\Users\ozkirimli\Desktop\IscarG							1		
_MMHT120N06R3.IGS,15HSolidWorks 2009,15HSolidWorks 2009,32,308,15,308,						G	2		Global section
15,25HIscar_MMHT120N06R3.SLDPRT,1.,2,2HMM,50,0.125,13H100715.140813,						G	3		
1E-008,499990.,9Hozkirimli,,11,0,13H100715.140813;						G	4		
124	1	0	0	0		00000000D	1		
124	0	0	1	0		0D	2		
110	2	0	0	0	1	00020000D	3		
110	0	0	1	0		0D	4		
110	3	0	0	0	1	00020000D	5		
110	0	0	1	0		0D	6		
110	4	0	0	0	1	00020000D	7		
110	0	0	1	0		0D	8		
110	5	0	0	0	1	00020000D	9		Directory Entry section
110	0	0	1	0		0D	10		
100	6	0	0	0	1	00020000D	11		
100	0	0	1	0		0D	12		
100	7	0	0	0	1	00020000D	13		
100	0	0	1	0		0D	14		
402	8	0	0	0		00000000D	15		
402	0	0	1	16	2DSKETCH	1D	16		
314	9	0	0	0		00000200D	17		
314	0	8	1	0		0D	18		
124,1.,0.,0.,0.,0.,0.,1.,0.,0.,0.,0.,1.,0.;							1P	1	
110,0.,0.345824206,0.,2.63439197,0.022361545,0.;							3P	2	
110,5.977638455,3.36560803,0.,5.16303755,20.,0.;							5P	3	
110,0.,0.345824206,0.,-2.63439197,0.022361545,0.;							7P	4	Parameter Data Section
110,-5.977638455,3.36560803,0.,-5.16303755,20.,0.;							9P	5	
100,0.,3.,3.,2.63439197,0.022361545,5.977638455,3.36560803;							11P	6	
100,0.,-3.,3.,-5.977638455,3.36560803,-2.63439197,0.022361545;							13P	7	
402,1,6,1,3,5,7,9,11,13;							15P	8	
314,75.2941176470588,75.2941176470588,75.2941176470588,;							17P	9	
S	1G	4D	18P	9			T	1	Terminate section

Figure 2.5: IGES file example and its sections

The IGES file constitutes five main sections shown in Figure 2.5. Parameter data section holds the geometric information of each entity with its corresponding type in a matrix form. Each row in this section starts with the declaration of the entity type (ie. for lines “110”, for arcs “100”) which is followed by the geometric values corresponding to the coordinates of the entity boundaries and arc centers. With respect to the entity type, the corresponding definition of the geometric values in each entity column differs which are shown in Table 2.1.

Table 2.1: Geometric definitions in the Parameter Data section of an IGES file

Line (110)

1	2	3	4	5	6	7
Type (110)	X_{st}	0	Z_{st}	X_{fi}	0	Z_{fi}

Arc (100)

1	2	3	4	5	6	7	8
Type (100)	0	X_{ce}	Z_{ce}	X_{st}	Z_{st}	X_{fi}	Z_{fi}

where $X_{st} - Z_{st}$, $X_{fi} - Z_{fi}$ and $X_{ce} - Z_{ce}$ represent entity start, finish and arc center points, respectively. Thus, for every segment, the coordinates of the bounding points are known, and this information will be utilized in the following sections.

Once the segment envelope information is known, the points on the cutter envelope can be calculated parametrically along the tools axis at each dz elevation step and revolving the calculating point around the tool axis with $d\phi$ angular increment gives the 3D point cloud of the cutter.

2.1.1 Parametric standard helical tools

Tool envelope of standard milling cutters can be identified using APT (Automatic Programmed Tools) representation consisting of seven geometric parameters which are D , R , R_r , R_s , α , β , H as shown Figure 2.6. A standard end mill can be divided into three main segments which are the tip part shown by line [OM] with inclination angle α , the torus part shown by arc [MN] with center point C and radius R and the taper part shown by line [NS] with taper angle β . According to assigned tool parameters some of these segments may vanish. Engin and Altintas [17] investigated standard milling tool geometries and proposed a complete model to analytically present tool envelope and helical flutes in tool coordinate system.

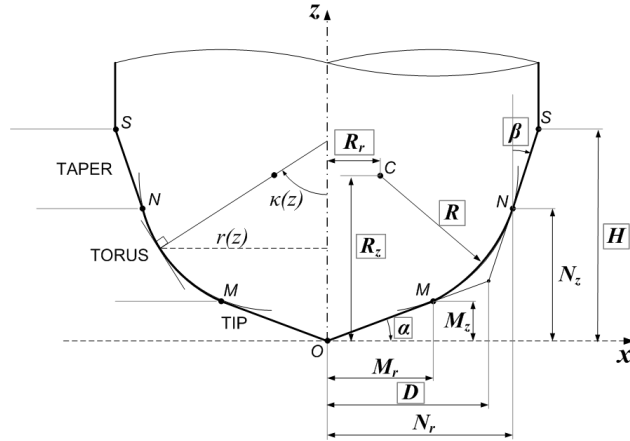


Figure 2.6: Geometry of standard milling cutters with APT parameters

In general there are six types of milling tools used in industry which are namely flat end mill, ball end mill, bull nose mill, taper end mill, taper ball end mill, conic end mill ().

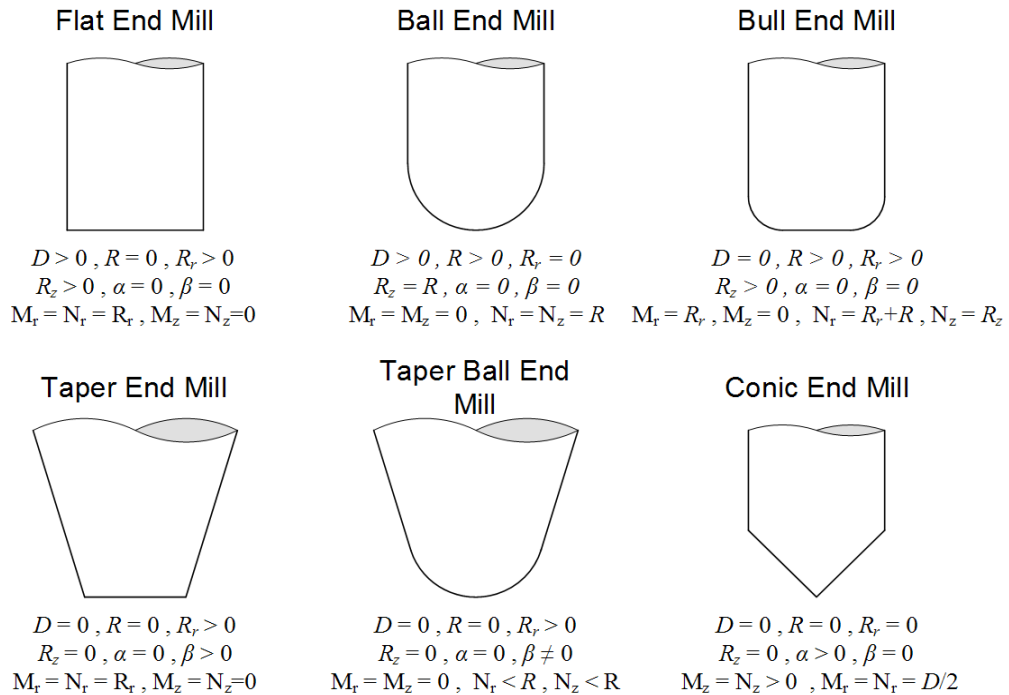


Figure 2.7: Standard milling cutter shapes and corresponding parameters

The segment boundary points lying on the cutter envelope which are in this case O, M, N and S are geometrically defined in the IGES file as explained in the previous section. For each segment of the cutter envelope at each elevation level, radial distance and immersion angle are defined as follows;

$$\left. \begin{aligned} r(z) &= \frac{z - M_z}{\tan \alpha} \\ \kappa(z) &= \alpha \end{aligned} \right\} \text{ for TIP part (OM)} \quad (2.2)$$

$$\left. \begin{aligned} r(z) &= \sqrt{R^2 - (R_z - z)^2} + R_r \\ \kappa(z) &= \sin^{-1} \left(\frac{r(z) - R_r}{R} \right) \end{aligned} \right\} \text{ for TORUS part (MN)} \quad (2.3)$$

$$\left. \begin{aligned} r(z) &= N_r + (z - N_z) \tan \beta \\ \kappa(z) &= \frac{\pi}{2} - \beta \end{aligned} \right\} \text{ for TAPER part (NS)} \quad (2.4)$$

For standard milling tools with more than one segment, the lag angle varies from segment to segment due to the change in the geometry of the profile. The lag angle at the tip conical part, designated by line [OM], for a given helix angle i_0 is defined as follows;

$$\psi(z) = \psi_{TIP}(z) = \frac{\ln(z \cot \alpha) \tan i_0}{\cos \alpha} \quad (2.5)$$

For the torus section, the lag angle deviation and the lag angle for a point at the torus segment are defined as follows:

$$\left. \begin{aligned} \psi_{TORUS}(z) &= \frac{(R + z - R_z) \tan i_0}{R} \\ \psi(z) &= \psi_{TORUS}(z) - \psi_{TORUS}(M_z) + \psi_{TIP}(M_z) \end{aligned} \right\} \quad (2.6)$$

The taper part of standard milling tools can be ground either with constant helix or constant lead scheme (Figure 2.8). For constant helix tools, the helix angle i_0 used in the previous segments is maintained. However for constant lead tools at the taper part, the flutes are ground with constant pitch length p_l .

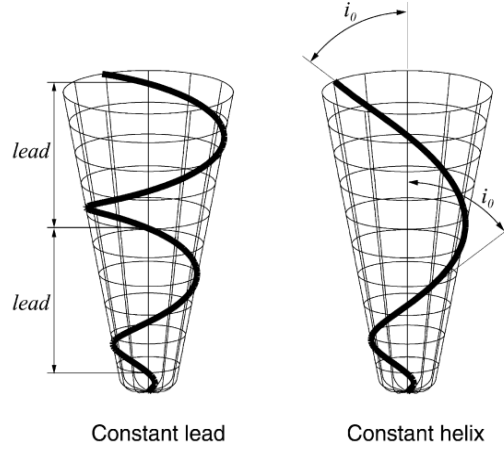


Figure 2.8: Taper ball end mills with constant lead and constant helix [17]

For constant helix case, the lag angle definition in the taper segment is as follows;

$$\left. \begin{aligned} \psi_{TAPER_{helix}}(z) &= \frac{\ln(N_r - (N_z - z) \tan \beta) \tan i_0}{\sin \beta} \\ \psi(z) &= \psi_{TAPER_{helix}}(z) - \psi_{TAPER_{helix}}(N_z) + \psi_{TORUS}(N_z) \end{aligned} \right\} \quad (2.7)$$

In the constant lead case, the variable helix angle i_s due to constant pitch length p_l is calculated as follows;

$$i_s = \tan^{-1} \left(\frac{2\pi N_r}{p_l \cos \beta} \right) \quad (2.8)$$

Accordingly, the lag angle of a point in the taper zone with constant lead is defined as;

$$\psi(z) = \underbrace{\frac{(z - N_z) \tan i_s}{N_r}}_{\psi_{TAPER_{lead}}(z)} + \psi_{TORUS}(N_z) \quad (2.9)$$

In Figure 2.9, some sample tool envelopes extracted from IGES data and constructed in 3D with helical flutes are demonstrated.

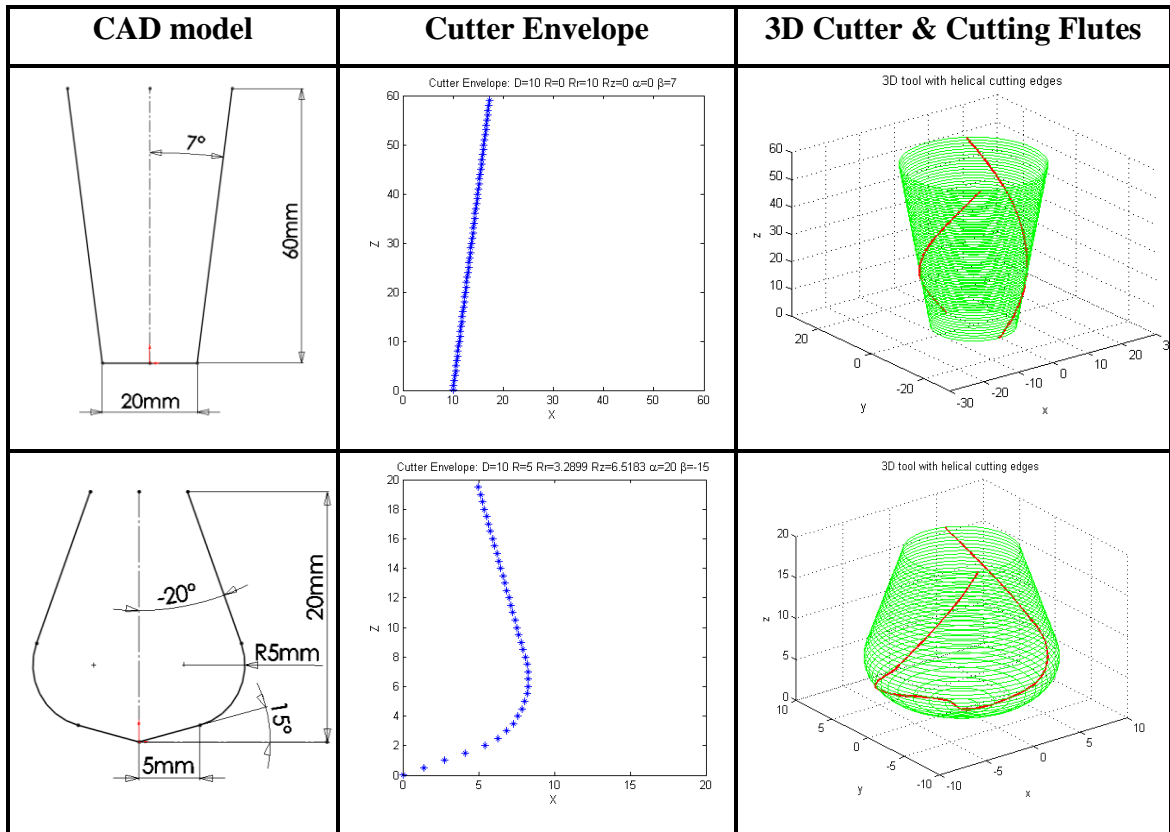


Figure 2.9: Example standard milling cutter representations with helical flutes

2.1.2 Multi-segmented helical tools

Different phases of the process may require various types of cutters and custom tooling play a major role to obtain desired features accurately and with increased productivity. Custom tools such as fir tree tools used for machining turbine blade root slots of monolithic rotors. They are manufactured according to the surface to be machined and often have non-uniform cutter envelope profiles (Figure 2.10). Standard tool definition mentioned in the above section is not sufficient to express tools with multiple segments which are often used as custom profiling tools. A more general mathematical definition must be given to calculate required geometrical parameters.



Figure 2.10: Fir tree tool and machining of the turbine blade slots

The cutter envelope is modeled in a CAD environment as a combination of lines and arcs corresponding to each segment. IGES data format is adequate for obtaining the boundary information of the individual segments. In Figure 2.11, an exemplary multi-segmented tool geometry involving 4 arcs and 5 lines with corresponding geometrical parameters is given. Lines are represented with S_i and E_i points being start and end points, respectively. In addition to S_i and E_i , arcs are represented with an additional of center point C_i where index i denotes the segment number starting from the tool tip.

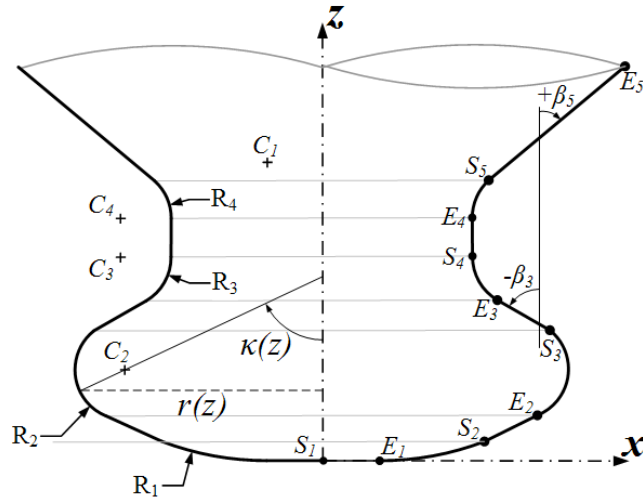


Figure 2.11: Multi-segmented tool geometry with corresponding segment parameters

Considering a linear segment profile, the radial distance $r(z)$, the axial immersion angle $\kappa(z)$ are given as;

$$\left. \begin{aligned} r(z) &= \frac{z - S_{i,z}}{\tan \beta_i} + S_{i,x} \\ \kappa(z) &= \beta_i \end{aligned} \right\} \quad (2.10)$$

where β_i is the inclination angle of the line segment. Ramaraj [46] gives the differential equation for a helical flute wrapping a cone as the derivative of a developed continuous line as follows

$$\frac{dr}{d\psi} - \frac{\sin \beta_i}{\tan i_0} r = 0 \quad (2.11)$$

for which the solution for r is given as;

$$r = e^{(\sin \beta_i / \tan i_0) \psi} \quad (2.12)$$

For a tapered conic part represented with a line segment, the lag angle definition is given as;

$$\psi_L = \frac{\ln(r(z)) \tan i_0}{\sin \beta_i} \quad (2.13)$$

A circle segment represents a torus unit element in the cutter body. For a torus, the radial distance $r(z)$, the axial immersion angle $\kappa(z)$ are given as follows;

$$\left. \begin{aligned} r(z) &= \sqrt{R^2 - (R_{z,s} - z)^2} \\ \kappa(z) &= \sin^{-1} \left(\frac{r(z) - R_{r,s}}{R} \right) \end{aligned} \right\} \quad (2.14)$$

and the lag angle expression for the arc segment is;

$$\psi_A = \frac{(R_i - C_{i,z} + z) \tan i_0}{R_i} \quad (2.15)$$

Final lag angle at elevation z is calculated with respect to current and previous segment definitions to ensure continuity;

$$\psi(z) = \psi_{L/A} + \psi_{pre} - \psi_{cur} \quad (2.16)$$

where ψ_{pre} is the final lag angle of the previous segment at the starting point of the current one and ψ_{cur} is the lag angle of the current segment at its starting point.

In Figure 2.12 some sample tool envelopes extracted from IGES data and constructed 3D cutter body with helical cutting flutes are shown.

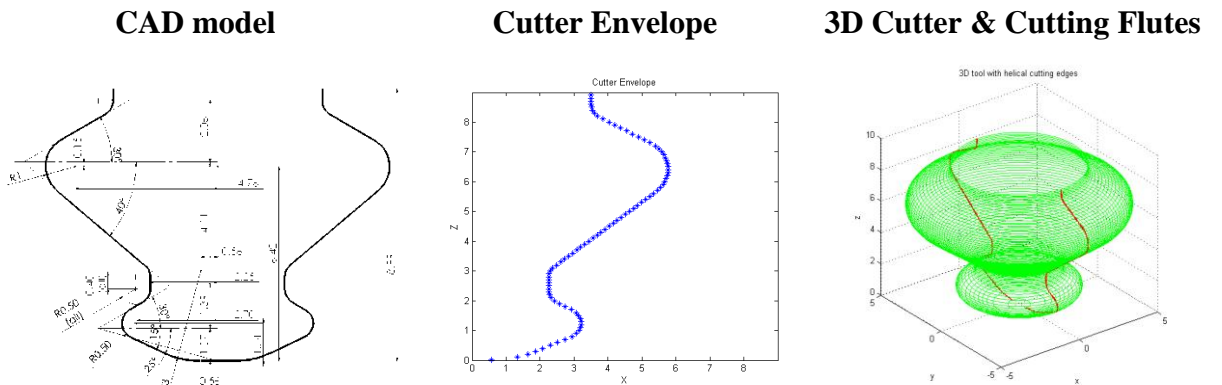


Figure 2.12: Example multi-segmented cutter representation with cutting flutes

2.1.3 Inserted face milling tools

In this section, the geometrical identification and parameter definitions for an inserted face milling tool is given. Inserted tools may have different insert geometries, and the ones that are considered in this work are shown in Figure 2.13.

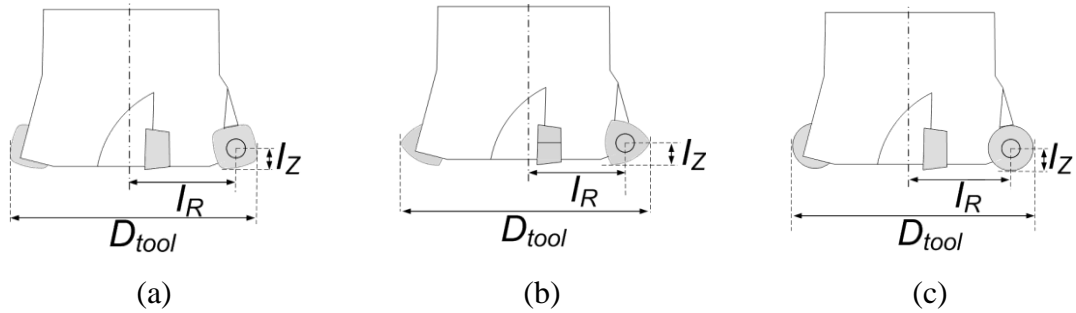


Figure 2.13: Schematic representation of inserted face milling tools with curved 4-sided inserts (a), curved 3-sided inserts and (c) circular inserts

In the modeling, positions of points on the cutting edge have to be formulated for which two coordinate systems are used, namely tool and insert coordinate systems. The tool coordinate system consists of x , y and z directions as it was for the previous type of tools mentioned in the above sections (Figure 2.14).

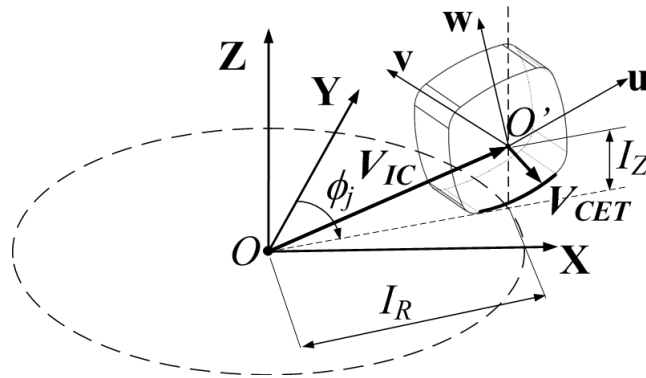


Figure 2.14: Insert representation with tool and insert coordinate systems

The insert coordinate system consists of u , v and w directions with its origin at the center of the insert face containing the cutting edge. The tool and the insert coordinate systems are aligned with each another when immersion angle of the insert is 90° before orientations on the insert are applied (Figure 2.14). The position of the insert center with respect to the tool coordinate system is defined by V_{IC} vector as follows:

$$\mathbf{V}_{IC} = \sin(\phi)I_R\mathbf{i} + \cos(\phi)I_R\mathbf{j} + I_Z\mathbf{k} \quad (2.17)$$

where I_R is the radial offset in the XY plane and I_Z is the axial offset in Z direction. These offset values are not generally given in the tool catalogues; hence, these values need to be calculated which is explained in the next section. $\mathbf{i}, \mathbf{j}, \mathbf{k}$ are unit vectors in x, y and z directions, respectively.

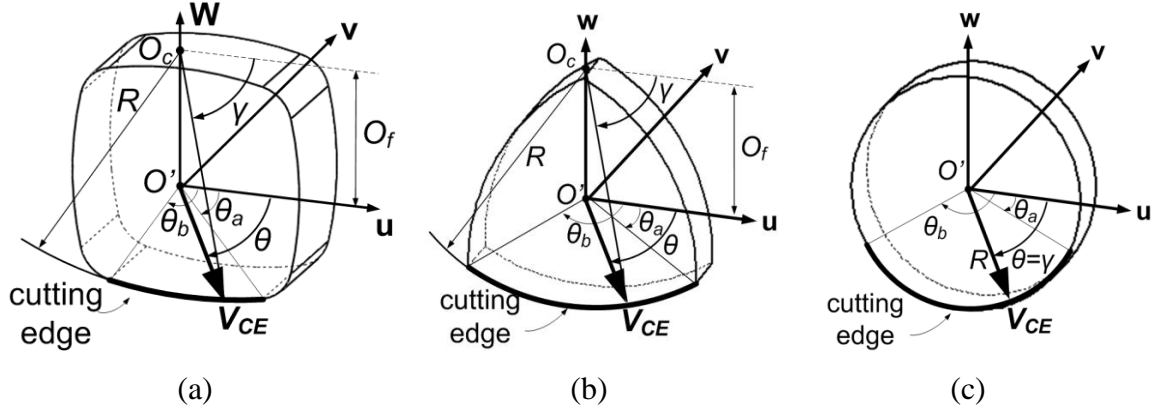


Figure 2.15: Insert coordinate systems and geometrical parameters of (a) curved 4-sided, (b) curved 3-sided and (c) circular insert bodies

Inserts considered in this work have curved edges with or without a center offset with respect to the insert center. Center offset, O_f , defines the distance between the insert center (O') and center of the curvature of the cutting edge, O_c , as shown in Figure 2.15a and Figure 2.15b for some example inserts. An insert without a center offset is also presented in Figure 2.15c. The position of a point on the cutting edge with respect to the insert center is shown with the \mathbf{V}_{CE} vector in insert coordinate system:

$$\mathbf{V}_{CE} = a\mathbf{u} + b\mathbf{v} + c\mathbf{w} \quad (2.18)$$

where a, b and c are measure numbers of \mathbf{V}_{CE} vector in \mathbf{u}, \mathbf{v} and \mathbf{w} directions, respectively. These are calculated using the equations given as (Figure 2.15);

$$\left. \begin{array}{l} a = R \cos \gamma \\ b = 0 \\ c = -R \sin \gamma \end{array} \right\} \text{where } \gamma = \theta + \sin^{-1}\left(\frac{O_f}{R} \cos \theta\right) \quad (2.19)$$

R is defined as the radius of curvature of the cutting edge and γ angle shown in Figure 2.15 is defined between θ_a and θ_b which are the limits of cutting edge. θ represents the angle between the \mathbf{V}_{CE} vector and u direction. Inserts are designed with different orientation angles on cutting tools depending on the application. Their orientation are

determined by three orientation angles, namely, axial rake angle, β , lead angle, δ and index angle, α which are presented in Figure 2.16.

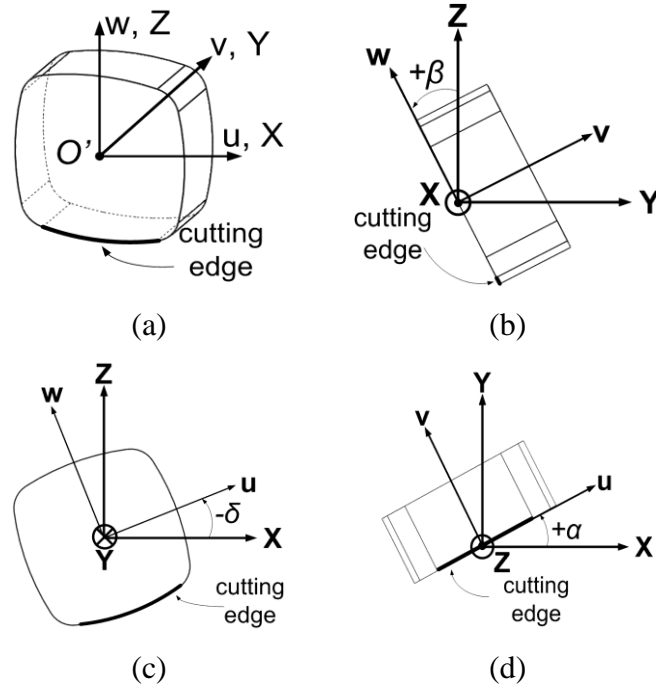


Figure 2.16: Insert orientation; (a) Insert coordinate systems with no orientation, (b) Axial rake angle, β (c) Lead angle, δ (d) Index angle, α

These orientation angles are defined for the instant where the immersion angle of the corresponding insert is 90° . At that instant, insert coordinates uvw and tool coordinates xyz coincide before orientations are applied (Figure 2.16a). Axial rake angle, β is the angle on xy plane between the w direction and z -axis. Lead angle, δ represents the angle between the u direction and x -axis on xz plane. Lastly, index angle α is the angle between the u direction and x -axis on xy plane. These orientations are represented in terms of three rotation angles: β^{rot} , δ^{rot} and α^{rot} which are rotations about x , y and z directions, respectively. After including the effects of the orientation angles by rotation angles and considering the rotation effect of the immersion angle ϕ on the inserts, \mathbf{V}_{CE} vector can be transformed to the tool coordinate system as follows:

$$\mathbf{V}_{CET} = T_M \mathbf{V}_{CE} \quad (2.20)$$

where T_M is a transformation matrix consisting of four rotations $R_x(\beta^{rot})$, $R_y(\delta^{rot})$, $R_z(\alpha^{rot})$ and $R_z(\phi^{rot})$ which are defined in the following equations :

$$T_M = R_Z(\phi^{rot})R_Z(\alpha^{rot})R_Y(\delta^{rot})R_X(\beta^{rot}) \quad (2.21)$$

$$R_X(\beta^{rot}) = \begin{bmatrix} 1 & 0 & 0 \\ 0 & \cos \beta^{rot} & -\sin \beta^{rot} \\ 0 & \sin \beta^{rot} & \cos \beta^{rot} \end{bmatrix}, R_Y(\delta^{rot}) = \begin{bmatrix} \cos \delta^{rot} & 0 & \sin \delta^{rot} \\ 0 & 1 & 0 \\ -\sin \delta^{rot} & 0 & \cos \delta^{rot} \end{bmatrix}, \quad (2.22)$$

$$R_Z(\alpha^{rot}) = \begin{bmatrix} \cos \alpha^{rot} & -\sin \alpha^{rot} & 0 \\ \sin \alpha^{rot} & \cos \alpha^{rot} & 0 \\ 0 & 0 & 1 \end{bmatrix}, R_Z(\phi^{rot}) = \begin{bmatrix} \cos \phi^{rot} & -\sin \phi^{rot} & 0 \\ \sin \phi^{rot} & \cos \phi^{rot} & 0 \\ 0 & 0 & 1 \end{bmatrix}$$

where ϕ^{rot} is defined as the complementary angle of ϕ .

Orientation angles, (axial rake, lead and index angles) are often given by the tool manufacturer as the values of all transformations combined and measured directly on the insert itself. However, rotation angles mentioned above may differ from the given angles due to individual transformations. Calculation of rotation angles from given orientation angles is similar to an inverse kinematics problem. Required rotation angles about x , y and z directions which results in the specified orientations of inserts are determined in this section. The rotations and orientations are defined for the instant where local immersion angle on an insert is 90° . For that reason, ϕ^{rot} angle does not affect the transformation matrix T_M defined in (2.21).

Firstly, u and w vectors are represented in tool coordinate system as u_T and w_T , respectively as the orientation angles (β, δ, α) depend on u and w directions in the tool coordinate system.

$$u_T = T_M [1 \ 0 \ 0]^T, w_T = T_M [0 \ 0 \ 1]^T \quad (2.23)$$

where superscript T represents the transpose operation. Using the definitions of axial rake angle (β), lead angle (δ) and index angle (α), the following equations can be written to relate orientation angles (β, δ, α), and rotation angles ($\beta^{rot}, \delta^{rot}, \alpha^{rot}$):

$$\begin{aligned}
\beta &= -\tan^{-1}\left(\frac{w_T(2)}{w_T(3)}\right) \\
\delta &= -\tan^{-1}\left(\frac{u_T(3)}{u_T(1)}\right) \\
\alpha &= \tan^{-1}\left(\frac{u_T(2)}{u_T(1)}\right)
\end{aligned} \tag{2.24}$$

The indexes 1, 2, 3 represent the elements of the vectors u_T and w_T in X, Y and Z directions, respectively. Solving (2.24) simultaneously, the rotation angles can be determined explicitly as follows:

$$\begin{aligned}
\alpha^{rot} &= \alpha \\
\delta^{rot} &= \tan^{-1}(\tan \delta \cos \alpha^{rot}) \\
\beta^{rot} &= \tan^{-1}\left(\frac{\tan \beta \cos \delta^{rot} + \sin \alpha^{rot} \sin \delta^{rot}}{\cos \alpha^{rot}}\right)
\end{aligned} \tag{2.25}$$

From (2.25), it is seen that the rotational angle α^{rot} is equal to the orientation angle α . This is because α^{rot} is the last rotation according to the transformation matrix defined in Eq. (2.21).

The final position vector of the points on the cutting edge (\mathbf{V}_P) with respect to the tool coordinate system can be written as (Figure 2.14):

$$\mathbf{V}_P = \mathbf{V}_{IC} + \mathbf{V}_{CET} \tag{2.26}$$

As a result, using the presented procedure, x , y and z coordinates of points on cutting edges can be calculated in the tool coordinate system. Moreover, local immersion angle, $\phi(z)$, of points on the j^{th} insert's cutting edge can be determined using X and Y coordinates of the corresponding points as follows:

$$\phi_j(Z) = \text{atan2}(X, Y) \tag{2.27}$$

The radial offset in the xy plane (I_R) and the axial offset in z direction (I_Z) need to be determined in order to fully describe the cutting edges of the inserts (Figure 2.14). These parameters are not typically given in the tool catalogs, hence they must be calculated. Once these are known, x , y and z coordinates of every point on the cutting edges of the inserts can be calculated. Although several approaches are present in the literature for modeling of inserted face mills [25]-[28], an explicit formulation for radial and axial offsets has not been presented. In this work, these parameters are calculated

using vectorial representation presented previously. As the immersion angle of the tool has no effect on the offset values, the offset calculations are performed for $\phi = 90^\circ$. For any point on the cutting edge curve, the distance from that point to the insert center in z direction can be calculated using equation (2.26) by equating the z component of \mathbf{V}_P vector to zero. A closed form formula for this distance (Z_d) as a function of θ can be then obtained as follows:

$$Z_d(\theta) = R \sin \delta^{rot} \cos \left(\theta + \sin^{-1} \left(\frac{O_f}{R} \sin \theta \right) \right) - \cos \delta^{rot} \cos \beta^{rot} \left(-R \sin \left(\theta + \sin^{-1} \left(\frac{O_f}{R} \sin \theta \right) \right) + O_f \right) \quad (2.28)$$

The maximum value of $Z_d(\theta)$ among all the cutting edge points gives the axial offset, I_z , of the insert at its oriented position. The point that maximizes $Z_d(\theta)$ is the actual contact point of the insert on the cutting surface (Figure 2.14).

A similar approach is utilized to calculate the offset in the radial direction, I_R . The radius of the tool (R_{tool}) is known and this time X component of \mathbf{V}_{IP} vector in equation (2.26) is equated to R_{tool} . A closed form formula for the distance between the insert center and tool center in the radial direction, $R_d(\theta)$, can be obtained as;

$$R_d(\theta) = R_{tool} - R \cos \alpha^{rot} \cos \delta^{rot} \cos \left(\theta + \sin^{-1} \left(\frac{O_f}{R} \sin \theta \right) \right) - \left(\sin \alpha^{rot} \sin \beta^{rot} + \cos \alpha^{rot} \sin \delta^{rot} \cos \beta^{rot} \right) \cdot \left(R \sin \left(\theta + \sin^{-1} \left(\frac{O_f}{R} \sin \theta \right) \right) + O_f \right) \quad (2.29)$$

Finding the radial offset values of the points lying only on the cutting edge will not suffice to determine I_R because the farthest point from the tool center in the radial direction can be on any of the insert edges. For that reason, all of the edges of the insert must be investigated and the actual radial offset value I_R is found at the point where $R_d(\theta)$ is minimized.

Finally, to complete the geometrical definition of the inserted face milling tools, the axial immersion angle $\kappa(z)$ is given as follows;

$$\kappa(z) = \cos^{-1}(-\mathbf{k} \cdot \mathbf{u}) \quad (2.30)$$

where \mathbf{k} is the unit vector along z direction and \mathbf{u} is the unit outward vector in tool coordinate system (xyz). Unit outward normal vector in insert coordinate system (\mathbf{u}_i) is defined as follows;

$$\mathbf{u}_i = \begin{bmatrix} \cos \gamma \\ 0 \\ -\sin \gamma \end{bmatrix} \quad (2.31)$$

Considering the insert orientations, the unit outward vector in tool coordinate system is calculated by transforming \mathbf{u}_i using transformation matrix \mathbf{T}_M defined in (2.21);

$$\mathbf{u} = \mathbf{T}_M \mathbf{u}_i \quad (2.32)$$

For two example cutting tools, the calculated xyz coordinates of cutting edges for the immersion angle of $\phi_j=0$ deg. are presented in Figure 2.17. The properties of the example tools are tabulated in Table 2.2. Some of these geometrical properties for the first tool are obtained from [47].

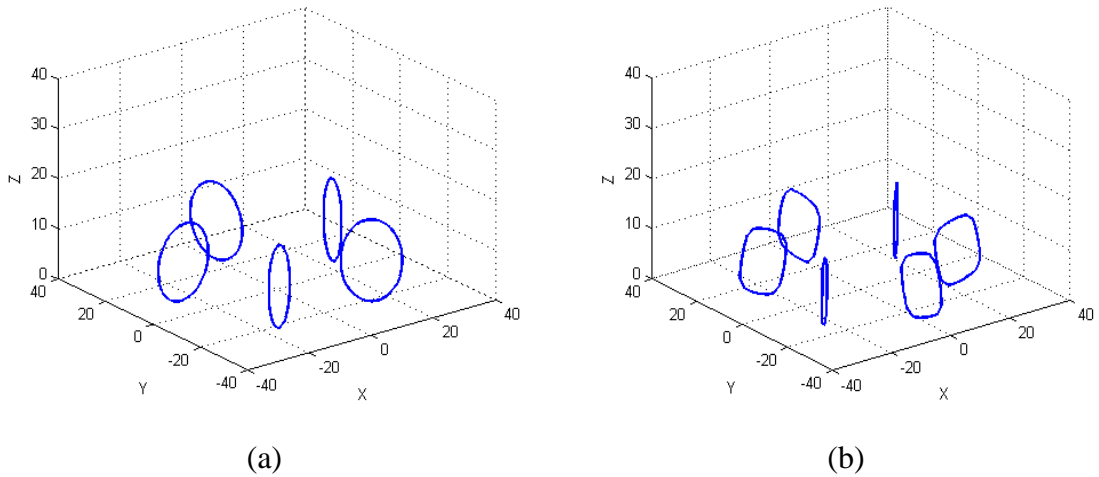


Figure 2.17: Two example inserted face milling tools with circular [Tool 1 - (a)] and curved squared [Tool 2 - (b)] insert geometries

Table 2.2: Properties of the example face milling tools

Tool properties	Tool 1	Tool 2
Tool diameter (mm)	66	66
Number of teeth	5	6
Radius of curvature of cutting edge (mm)	8	19.75
Rake angle of the insert, α_{ins}	6°	6°
Axial rake angle (β)	7°	0°
Lead angle (δ)	0°	-14.5°
Index angle (α)	18°	17°
O_f (mm)	0	13.4
I_z (mm)	7.9342	6.7215
I_R (mm)	25.3849	26.4464
θ_a	0°	53.79°
θ_b	180°	126.21°

For the two example tools properties of which are tabulated in Table 2.2, the calculated rotation angle values are presented in Table 2.3. It is seen that depending on the magnitudes of orientation angles, the difference between orientation angles and rotation angles can be significant. Hence, the calculated rotation angles should be used in the mathematical model, instead of directly using orientation angles as rotation angles as done in [18].

Table 2.3: Calculated rotation angles for example face milling tools

Rotation angles	Tool 1	Tool 2
β^{rot} (deg)	7.3564	-
δ^{rot} (deg)	-	-13.89
α^{rot} (deg)	18	17

2.2 Variable cutting edge geometry

In the previous section, the profile properties of cutting tools are given and the uniform helix geometries are explained. Although, the profile geometry constitutes the major part of the operation, hence the process simulation, the helical flute geometry and its variations play a bigger role in the mechanics and dynamics of the process. The time

delay differences between adjacent cutting flutes removing material affects the cutting forces but more importantly disturbs the regenerative chatter mechanisms. In this section, the geometrical variation and non-uniform distribution of helical flute geometries will be given and a general formulation encompassing all possible variations will be introduced.

Variation of helix angle from flute to flute and the pitch angle between adjacent teeth changes the immersion angle definition (2.1) which directly effects the time delay at each elevation level and as a consequence the chip thickness variation. Equation (2.1) can be examined in two parts in this scope. First, the variation of the pitch angle is denoted by $\phi_{p,j}$ representing the angular position of j^{th} cutting edge with respect to previous $j-1^{th}$ edge and secondly, the lag angle for level z of the j^{th} cutting edge is represented by $\psi_j(z)$ depending on helix angle of the j^{th} cutting edge, $i_{o,j}$. In Figure 2.18, a 4 fluted flat end mill with variable helix and variable pitch angles is shown to identify previously mentioned parameters.

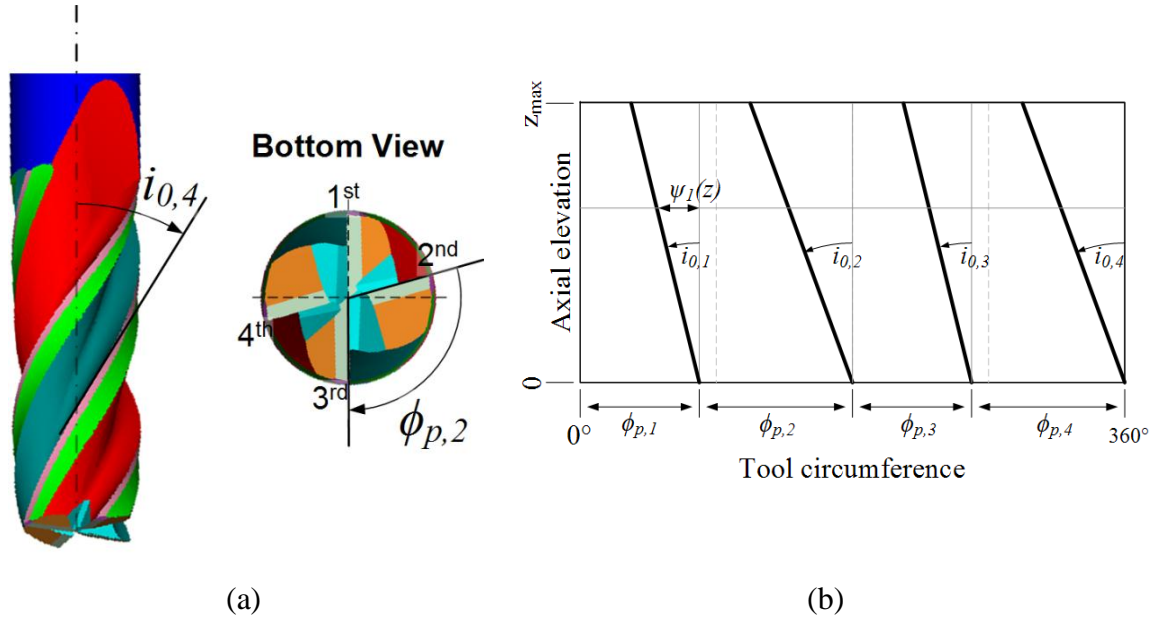


Figure 2.18: Cutting flute geometry and corresponding parameters;

(a) 3D representation, (b) Unfolded representation

In order to find the delay between each flute at elevation z , the separation angle, $\delta\phi_j(z)$ is calculated for each axial level, z . The separation angle defines the flute geometry of the cutting tool as an angle in terms of radian from tool axis to the cutting edge for flute j . It is calculated as the difference of immersion angle (refer to Eq.(2.1)) values $\phi_j(z)$ of j^{th} and $j+1^{th}$ cutting flutes;

$$\delta\phi_j(z) = \phi_{j+1}(z) - \phi_j(z) \quad (2.33)$$

In practice there are infinitely many combinations to construct a variable milling tool; each flute may have different helix angles and the pitch angle between each tooth at each z level may be different from each other. However, there are some constraints to consider in constructing such tools. First, the flutes may coincide in the upper region of the tool due to non-uniform distribution of helix angles. Even though, manufacturers produce crossing fluted tools for some specific operations [51], this must be avoided for the purpose of improved chatter stability and a better surface finish. To find whether any of two or more tool flutes cross each other, the sign of separation angle must be controlled. A negative separation angle value indicates flute crossing.

Non-uniform helix and pitch angles result in unbalance on the tool. In high rotational speeds, the unbalance induces forced vibrations resulting in extra radial load and poor surface quality. A balance test should be conducted to predict critical maximum spindle speed values above which the eccentricity disturbs the system. In the International Standard ISO 1940/1, the maximum secure rotary speed values are charted with respect to the balance quality value G of the rotor and its corresponding permissible residual unbalance e_{per} . Permissible residual unbalance can be considered as the displacement of the center of mass in μm [7]. In Figure 2.19 the maximum critical speed values are shown on a log chart for increasing center of mass deviations with respect to different balance quality values. Below relation extracted from ISO 1940/1 can also be utilized to calculate maximum critical spindle speed value, n_{crit} ;

$$n_{crit} = 9549 \cdot \frac{G}{e_{per}} \quad (2.34)$$

where G is selected according to type of rotors and it is convenient to choose $G=2.5$ for medium sized cutting tools.

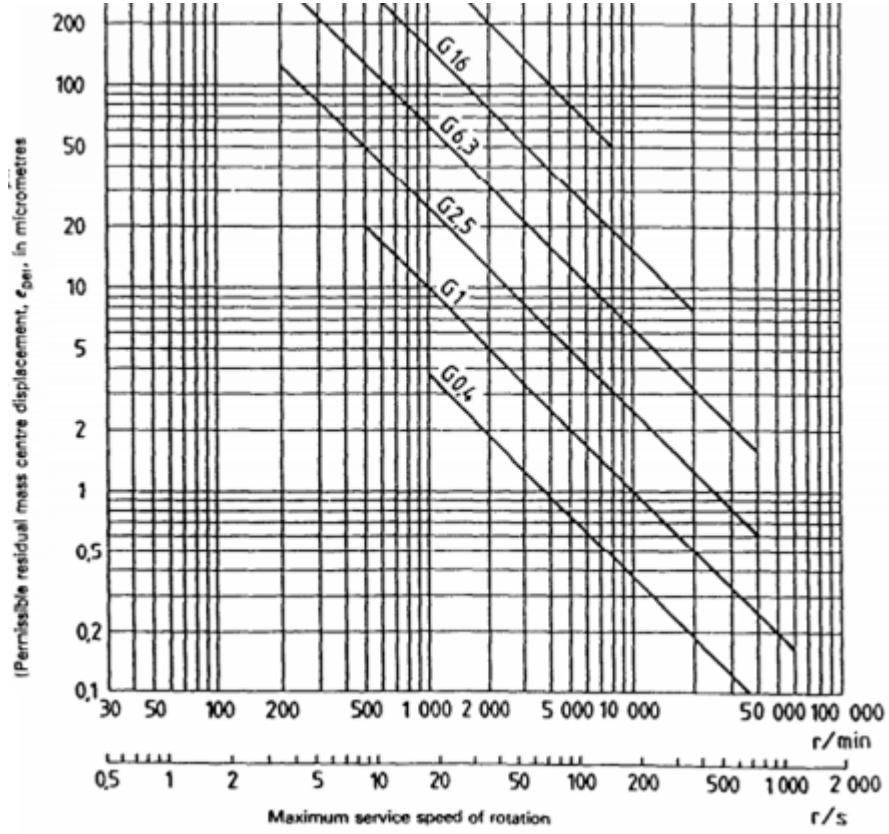


Figure 2.19: Maximum safe rotary speed values corresponding to maximum permissible residual unbalance value for different balanca quality grades, G [7]

In this work, for pitch angle distribution, two common variation patterns are examined which are linear pitch distribution and alternating pitch distribution. For both cases, a pitch angle variation measure ΔP is introduced. For each type, the pitch angles for an N_t fluted tool are given as;

$$\left. \begin{aligned} &P_0, P_0 + \Delta P, P_0 + 2\Delta P, \dots, P_0 + (N_t - 1)\Delta P \\ &P_0 = \frac{2\pi}{N_t} - \frac{(N_t - 1)\Delta P}{2} \end{aligned} \right\} \text{Linear} \quad (2.35)$$

$$\left. \begin{aligned} &P_0, P_0 + \Delta P, P_0, \dots, P_0 + \begin{cases} \Delta P & N_t \text{ even} \\ 0 & N_t \text{ odd} \end{cases} \\ &P_0 = \frac{2\pi}{N_t} - \frac{(N_t - 1)\Delta P}{2} \end{aligned} \right\} \text{Alternating} \quad (2.36)$$

where P_0 is the initial pitch angle.

Three custom tools with different combinations are designed to see the effects of variable helix geometry. All of the tools have 4 cutting flutes, diameter of 12mm and flute length of 26mm. These tools in the further chapters are compared in the scope of

mechanics and dynamics of machining. The cutting flute geometry parameters of these tools are given in Table 2.4.

Table 2.4: Cutting flute parameters for custom made variable tools

Tool code	Helix angle (deg), $i_{0,1...4}$	Pitch angle variation measure (deg), ΔP	Pitch distribution type	Pitch angles (deg) $\phi_{p,1...4}(\theta)$
AOT.318.001	30 – 33 – 30 – 33	0	-	90 – 90 – 90 – 90
AOT.318.002	30 – 32 – 34 – 36	0	-	90 – 90 – 90 – 90
AOT.318.003	30 – 33 – 30 – 33	2	Alternating	87 – 93 – 87 – 93

Unfolded tool geometry in terms of rotation angle and the separation angle $\delta\phi_j(z)$ for each tool corresponding to varying elevation levels are plotted in Figure 2.20 - Figure 2.22. For each figure the graph on the left shows the angular position of each cutting edge on the unfolded tool geometry for $\phi=0$ (tool at initial position). Each point on a specific elevation level z corresponds to the immersion angle value $\phi_j(z)$. On the right hand side, the separation angles for each cutting flute at each elevation level z is plotted according to equation (2.33).

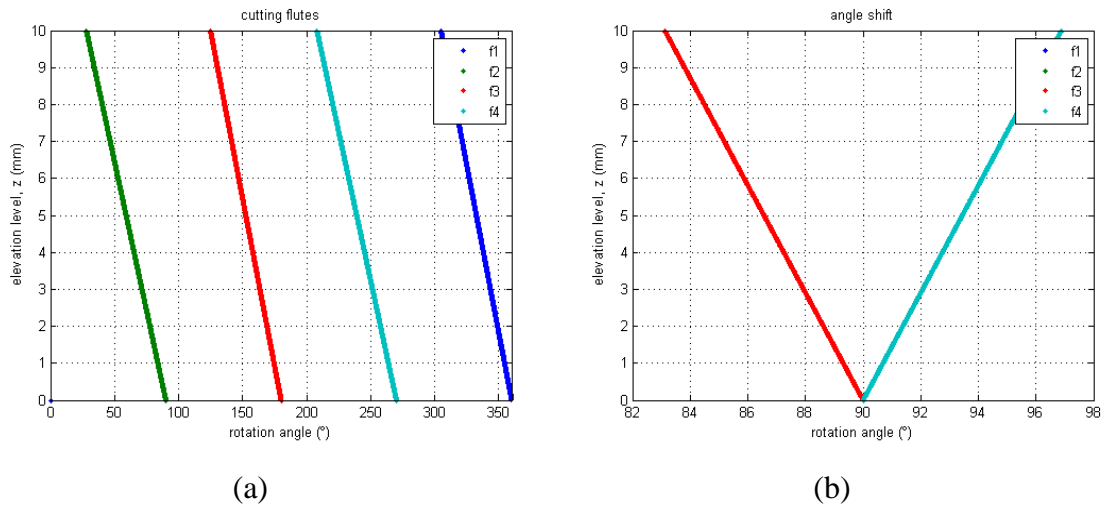


Figure 2.20: Custom variable tool AOT.318.001, (a) unfolded tool geometry, (b) separation angle variation

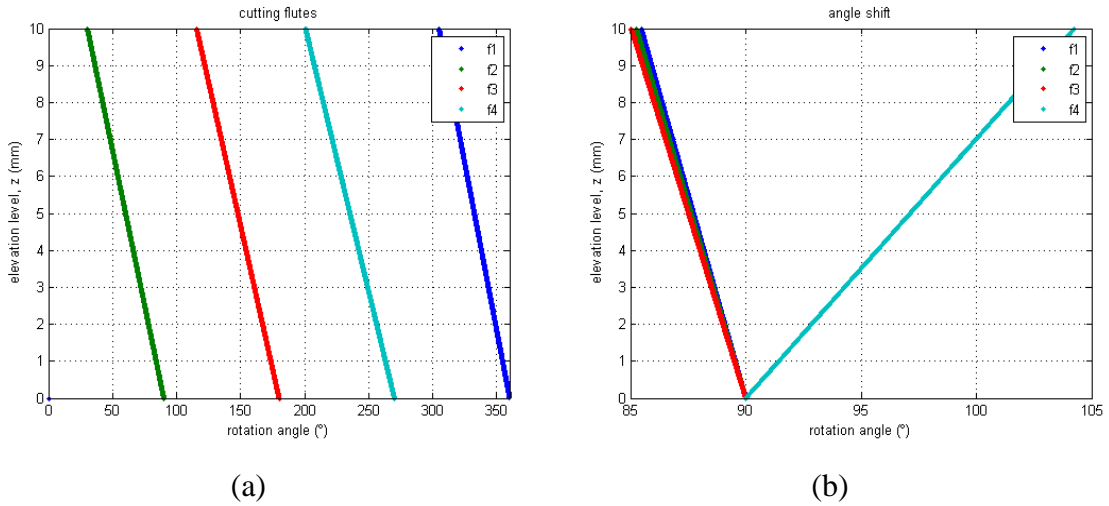


Figure 2.21: Custom variable tool AOT.318.002, (a) unfolded tool geometry, (b) separation angle variation

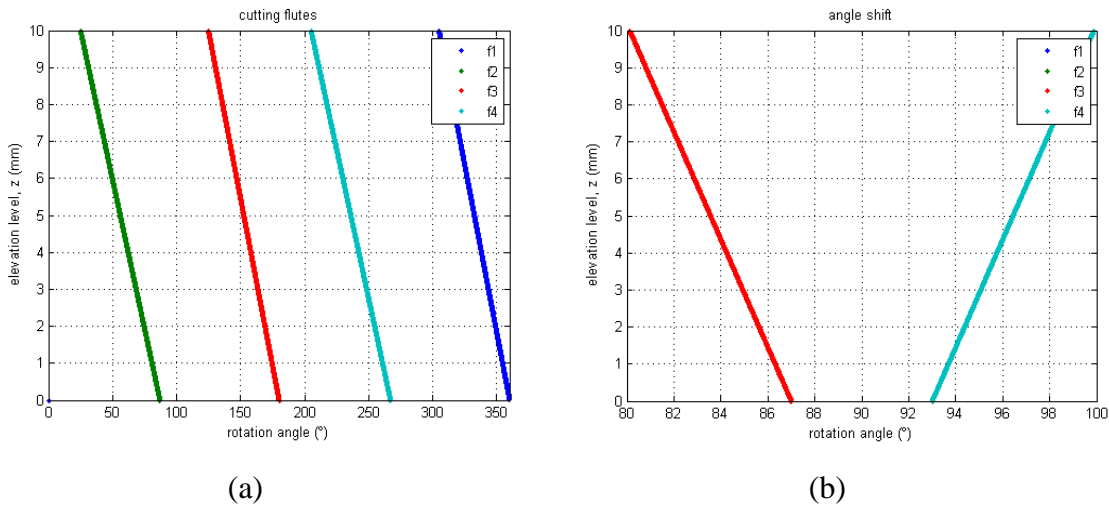


Figure 2.22: Custom variable tool AOT.318.003, (a) unfolded tool geometry, (b) separation angle variation

For each case, in the unfolded tool geometry graphs, the difference between the rotation angles of consecutive teeth at the lowermost point ($z = 0$) designates the tooth pitch angles which also corresponds to the $z=0$ value at for the separation angle variation graph. For the first two cases, as the initial pitch angles is constant and equal to 90° ($\phi_{p,j}=2\pi/N_i$), in the separation angle variation graphs on the right, the initial separation is also constant. On the other hand, due to varying helix angles of the consecutive teeth, for the first case due to alternating distribution of the helix angles, the separation angle between consecutive teeth varies alternatingly (ie. for the separation at $z=3$ for 1st, 2nd and 3rd and 4th teeth is equal to 88° but for 2nd, 3rd and 4th and 1st teeth is equal to

94°). However, for the last cutter, due to the variation of both pitch and helix angles, the separation between adjacent is always different from each other starting from $z=0$. This causes a varying time delay for every axial level and the time delay between consecutive teeth tend to increase axially.

2.3 Summary

In this chapter, the identification of the cutting tool geometries are given. For the process model, cutting tools are defined as as 3D point clouds where the points on all of the cutting edges are defined with respect to their radial immersion angle $\phi_j(z)$, axial immersion angle $\kappa(z)$ and local radius $r_j(z)$. In industry, as many custom tools are utilized and their profile geometries are intricate, in this chapter a new methodology to extract the cutter geometry information from CAD data is explained. Tool envelope geometry is divided into segments (either arc or line) and thus for tool with varying tool geometries along the cutter axis are classified as “multi-segmented tools”. To establish a complete model for different tool geometries, inserted cutters are also defined according to the above convension where the insert body is first identified and the relative position of each insert is defined in tool coordinate system regarding the insert orientations and radial and axial center offsets (I_R and I_Z).

Finally, varying cutting edge geometries are explained. The varying tool cutting edge point definition in terms of radial immersion angles is explained and for different cases the separation angle ($\delta\phi_j(z)$) definition is introduced. The variation of the separation angles introduces time delay between consecutive teeth which induces uncut chip thickness variation for different edges along the cutter axis and also interrupted chatter vibration cycles. For tools with varying cutting edges, because of the asymmetry of the tool, balance problem is also considered. It is shown that as the center of mass of the tool deviates from the tool axis radially, the spindle speeds values for which a safe non-vibrating operation can be conducted decreases.

CHAPTER 3

MULTI-AXIS CUTTING PROCESS GEOMETRY

To model the milling processes, the workpiece and the respective position and orientation of the tool with respect to it should also be considered. The aim is to identify the engagement region of the tool with the workpiece. During cutting at any point there exist a contact area between the tool and the workpiece altering with respect to process parameters such as depth of cuts and tool orientations. In this chapter the effect of these two aspects will be discussed and a formulation to find the cutter engagement boundaries (CEB) will be proposed.

In this chapter, the geometry of multi-axis machining operations will be given in the light of the mentioned coordinate systems and process conditions. First, the coordinate transformations and tool axis orientations will be defined. Secondly, cutter contact point identification will be given. In the last part of the section, the numerical engagement boundary identification method will be introduced.

3.1 Multi-axis milling geometry

Multi-axis milling operations are classified according to the movement of the cutting tool with respect to workpiece surface and denoted by the number of axial and rotational degree of freedom utilized during the operation such as; 2½ axis, 3 axis, 5 axis, etc. machining operations. Before introducing different types of machining operations, it will be useful to introduce the coordinate systems used in order to describe cutting tool, machined surface and machine with respect to each other.

For multi-axis machining, three coordinate systems are defined (Figure 3.1). Machine coordinates are denoted with *XYZ* and is positioned such that it is fixed to the $-X$, $-Y$

and $-Z$ is fixed axis of the machine tool. The second coordinate system is used to identify the process itself. Process coordinate system (FCN), consists of the feed, F , the cross-feed, C and the surface normal N . The orientation and the position of process coordinate system change according to the position of the tool and also according to the surface characteristic of the machined surface. Tool coordinate system xyz is defined on the cutter contact point (CC) of the tool while z is aligned with the tool axis (TA), x with the feed direction and y with the cross-feed direction. Both process coordinate system and tool coordinate system shares the same origin at cutter contact point.

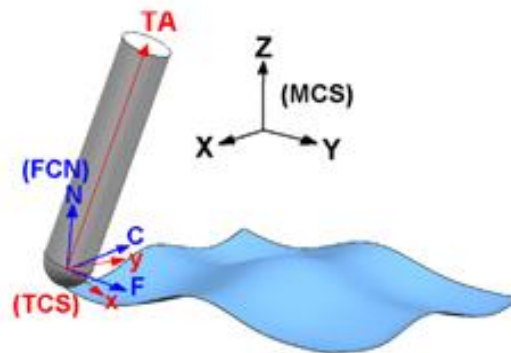


Figure 3.1: Machining coordinate systems

2½ axis machining is used to create flat surfaces while the tool is moving on the XY plane while the Z level is fixed. Mostly face milling tools, flat end mills and majority of the multi-segmented profiling tools are utilized for this type of machining while the cutter periphery is directly imprinted to the surface. In 3 axis machining, the tool is free to move in X, Y and Z directions simultaneously while tool axis z is fixed at Z direction. Tools with spherical tips such as ball end mills, taper ball end mills, bull-nose end mills etc. are preferred for this type of machining while the aim is to machine a contoured surface. Finally, in 5 axis machining, the tool is free to move both in X, Y, Z directions as it was for 3 axis machining and also the tool axis is free to rotate around feed (F) and cross-feed (C) directions giving the ability to follow a surface maintaining a constant approach angle providing an even depth of cut for most of the cases. Flank milling operations used to machine turbine blade sides is one of the best examples for this type of operations. The purpose of flank milling is to remove as much material as the operation allows with few deep cutting passes while the entire flank surface of the tool is in contact with the machined surface.

3.1.1 Coordinate transformations

In multi-axis machining, the tool axis and the machine table normal are not parallel to each other in the presence of rotation angles. Tool rotation angles are defined with respect to the rotations around these coordinates. Lead angle is defined as the rotation about cross-feed direction C whereas tilt angle is the rotation about the feed direction as shown in Figure 3.2. T_{FCN} defines the Euler transformation for lead and tilt rotations represented as l and t :

$$T_{FCN} = \begin{bmatrix} 1 & 0 & 0 \\ 0 & \cos t & -\sin t \\ 0 & \sin t & \cos t \end{bmatrix} \begin{bmatrix} \cos l & 0 & \sin l \\ 0 & 1 & 0 \\ -\sin l & 0 & \cos l \end{bmatrix} \quad (3.1)$$

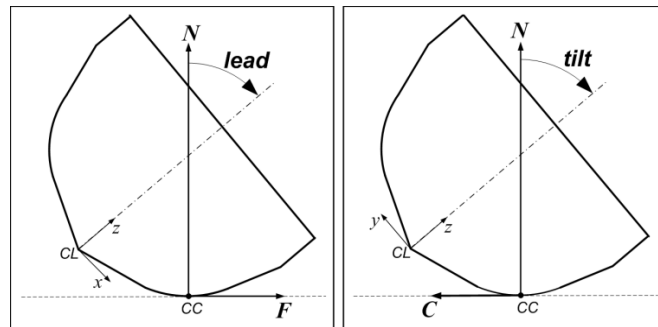


Figure 3.2: Lead and tilt angle representations

Lead and tilt angles are arbitrarily defined parameters. In practice, these angles are not given as process inputs instead a range for them is calculated during toolpath calculations. It is necessary to calculate the exact angles for each process step considering both the surface characteristic defined geometrically by feed and surface normal directions in machine coordinate system MCS , and tool axis vector (\mathbf{TA}) in MCS . Let \mathbf{f} and \mathbf{n} denote the feed and surface normal direction in MCS coordinates, the cross feed direction \mathbf{c} is found as;

$$\mathbf{c} = \mathbf{f} \times \mathbf{n} \quad (3.2)$$

As the lead angle is defined as the rotary angle about cross feed direction, it can be calculated as the angle between feed vector and tool axis vector projected on the plane defined by \mathbf{f} and \mathbf{n} vectors with a surface normal \mathbf{c} . The projection of the tool axis on this plane is defined as;

$$\mathbf{TA}_{\text{pro,fn}} = \mathbf{TA} - (\mathbf{TA} \cdot \mathbf{c})\mathbf{c} \quad (3.3)$$

and the tilt angle t is calculated as;

$$t = \cos^{-1}(\mathbf{c} \cdot \mathbf{TA}_{\text{pro,fn}}) \quad (3.4)$$

The same procedure is utilized for calculating the lead angle. This time, the projection of the tool axis \mathbf{TA} on the plane defined with its normal \mathbf{f} is considered and lead angle is calculated as the angle between cross feed direction \mathbf{c} and projected tool axis;

$$\mathbf{TA}_{\text{pro,cn}} = \mathbf{TA} - (\mathbf{TA} \cdot \mathbf{f})\mathbf{f} \quad (3.5)$$

$$l = \cos^{-1}(\mathbf{f} \cdot \mathbf{TA}_{\text{pro,cn}}) \quad (3.6)$$

3.1.2 Relation between cutter contact and cutter tip points

Cutter tip point, CL defining the cutter location must be translated due to cutter rotations in order to position the tool tangent to the machined surface. FN plane in process coordinates is considered as the surface to be machined, and FCN coordinate is fixed at the cutter contact location, CC , which is the lowermost point of the cutter envelope on FN plane. CL point location in FCN coordinates (Figure 3.3) can be expressed as the sum of the vectors \mathbf{t}_1 , \mathbf{t}_2 and \mathbf{t}_3 as follows [15];

$$CL_{FCN} = \mathbf{t}_1 + \mathbf{t}_2 + \mathbf{t}_3 \quad (3.7)$$

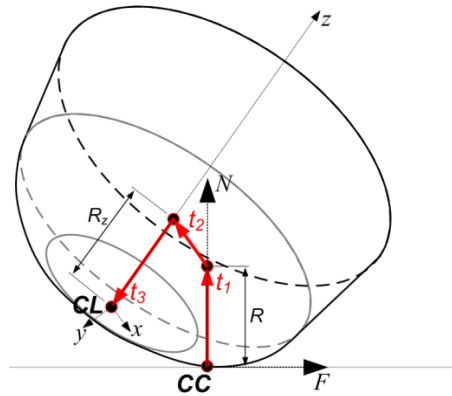


Figure 3.3: CL and CC point representations in process coordinates

The translation vectors are defined as follows:

$$\left. \begin{aligned} \mathbf{t}_1 &= R \cdot \hat{\mathbf{N}} \\ \mathbf{t}_2 &= R_r \cdot \frac{(\hat{\mathbf{N}} \times \hat{\mathbf{z}}) \times \hat{\mathbf{z}}}{\|(\hat{\mathbf{N}} \times \hat{\mathbf{z}}) \times \hat{\mathbf{z}}\|} \\ \mathbf{t}_3 &= -R_z \cdot \hat{\mathbf{z}} \end{aligned} \right\} \quad (3.8)$$

where $\hat{\mathbf{N}}$ is the unit vector of the surface normal direction and $\hat{\mathbf{z}}$ is the unit vector of the oriented tool axis direction.

Thus a point on the tool represented in the tool coordinate system is transformed into process coordinates as follows;

$$\begin{bmatrix} F \\ C \\ N \end{bmatrix} = T_{FCN} \cdot \begin{bmatrix} x \\ y \\ z \end{bmatrix} + \begin{bmatrix} CL_F \\ CL_C \\ CL_N \end{bmatrix} \quad (3.9)$$

A point on the cutter body defined in cylindrical coordinates with respect to tool axis can be represented in process coordinates as follows:

$$\begin{bmatrix} P_F \\ P_C \\ P_N \end{bmatrix} = T_{FCN} \cdot \begin{bmatrix} r(z) \cos(\pi - \phi_j(z)) \\ r(z) \sin(\pi - \phi_j(z)) \\ z \end{bmatrix} + \begin{bmatrix} CL_F \\ CL_C \\ CL_N \end{bmatrix} \quad (3.10)$$

In this chapter, the engagement boundary identification techniques are given. During cutting only a portion of the tool engages the workpiece material, this region is called Cutter Engagement Boundary (CEB). This region depends on the workpiece geometry to be machined, cutting tool geometry and tool orientation. For process simulation, it is necessary to extract the boundary points for each cross-section of the tool which determines the start and exit angles (ϕ_{st} and ϕ_{ex}) in cylindrical coordinate system of the cutter for each cross-section. A point on a cutting flute of the tool can be classified as as in cut if and only if its current immersion angle definitions lies between bounding angles;

$$\phi_{st} \leq \phi_j(\phi, z) \leq \phi_{ex} \pmod{2\pi} \rightarrow \text{point in cut} \quad (3.11)$$

The region of engagement differs according to the process parameters and tool geometry. For simple cases such as flat end milling [10] and 5-axis ball end milling [44] analytical methods are available in the literature, a generalized model which can describe multi-axis machining with intricate tool geometries has not been presented. In this chapter, a new model based on Boolean boundary criteria is given for single process step simulation.

3.2 Process geometry and cutter engagement zones

In this section, first, the cutter engagement boundary identification for an arbitrary cutting scenario will be introduced where a non-machined cubic solid workpiece is cut. Secondly, the following cutting scenario and corresponding cutter engagement boundary formulation will be introduced where a previously machined surface is cut.

3.2.1 Arbitrary cutting scenario

An arbitrary case for multi-axis machining is presented in Figure 3.4 where a block of material having dimensions b and a corresponding to radial and axial depth of cuts respectively is machined.

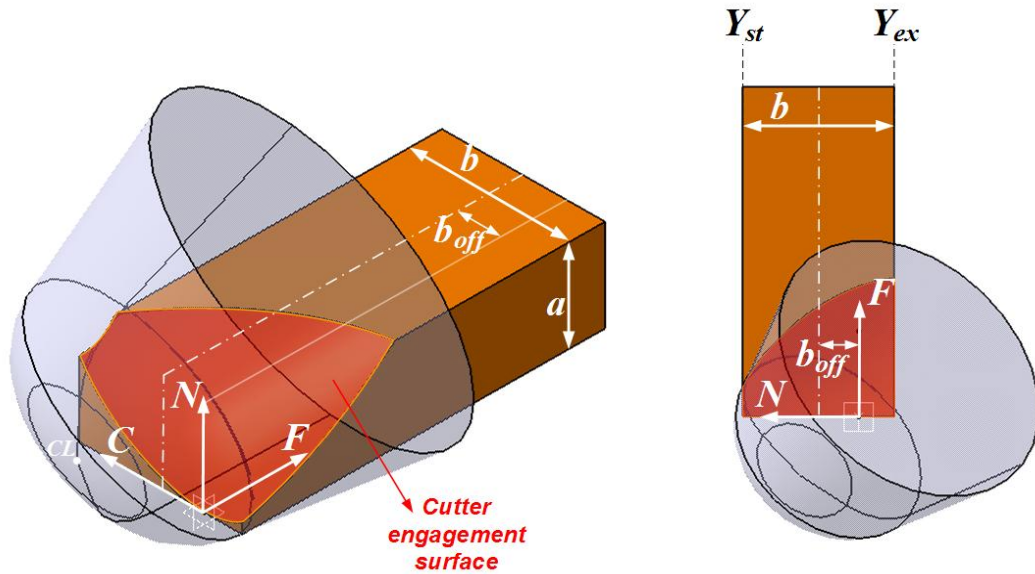


Figure 3.4: Arbitrary cutting case and corresponding engagement surface

The radial offset represented as b_{off} in Figure 3.4 is defined as the positive or negative distance between the midplane of the cutting block and the feed axis F with considering the position of the block. The radial boundaries of the block are calculated as;

$$\begin{aligned} Y_{ex} &= b_{off} - \frac{b}{2} \\ Y_{st} &= b_{off} + \frac{b}{2} \end{aligned} \quad (3.12)$$

Three separate conditions must be evaluated at each level to determine the total engagement boundary. These conditions are uncut chip load condition, radial workpiece boundary and axial workpiece boundary. For each condition, the possible cutting points with respect to this specified limitation is kept as an array of Boolean input (0 or 1) designating whether a point is in cut or not. Finally employing a union operation considering all of the generated Boolean arrays through separate cutting conditions, for each axial cross-section considering all three arrays the points in cut are found.

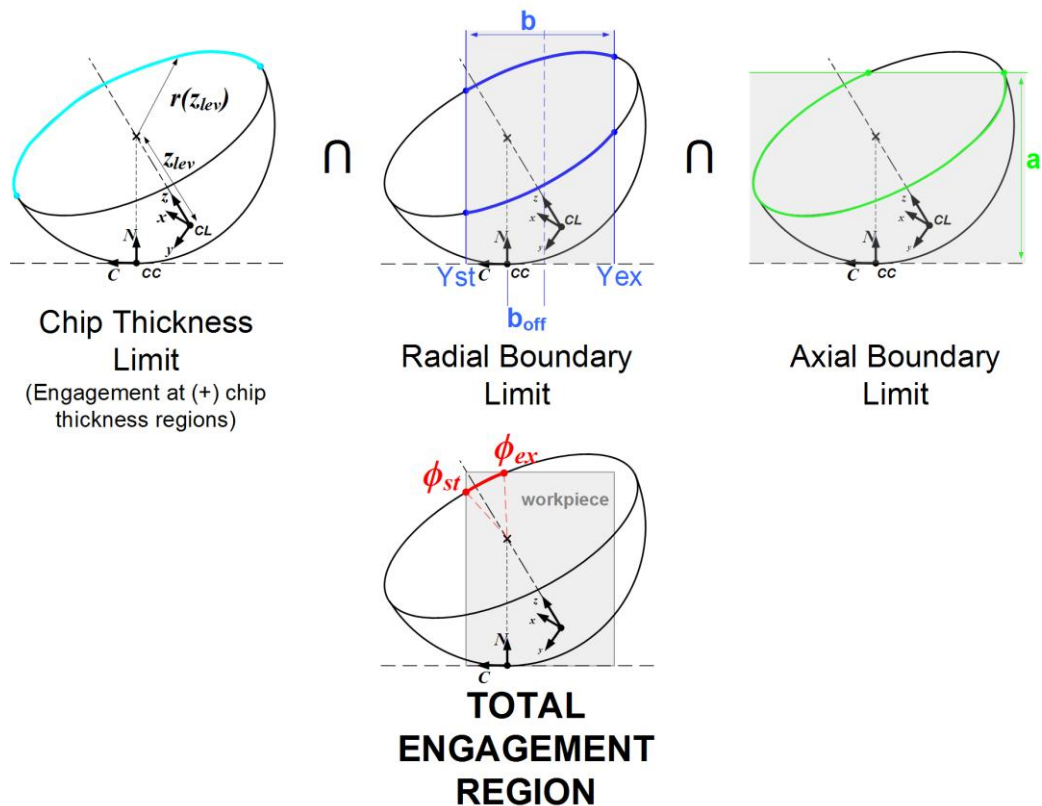


Figure 3.5: Engagement boundary conditions and total engagement

A point on the tool periphery may only cut if there exists un-removed material in the feed direction, F . For each cutting point the sign of the chip thickness must be checked. Only for the positive values of the chip thickness the portion of the tool cross section

can be considered cutting. Negative chip thickness values are neglected and are not included in the CEB. For each axial level along the tool axis, the portion of the tool cross-section in contact with the material can then be found by determining points which have positive-signed chip thickness, $h(\phi, z)$. Formulation for chip thickness calculation will be given in Section 4.2.

In Section 2.1 and Section 3.1.2, the formulation to identify the coordinates of the periphery points of a tool at a given orientation were shown. To determine the engagement region, it is necessary to determine the points lying within the boundaries of the workpiece. As shown in Figure 3.5, the radial and axial boundaries are defined by the width and the height of the workpiece. Possible cutting points within the workpiece region are evaluated as follows;

$$(Y_{st} \geq P_C \geq Y_{ex}) \cap (a \geq P_N) \quad (3.13)$$

where PC and PN are the coordinates of a point on the cutter body defined in process coordinates given in Eq. (3.10). Finally, the intersection of the conditions given above gives the final engagement region for a cross-section in focus. Evaluating all the points on the tool periphery and mapping, the evaluated Boolean value for each point with respect to axial elevation z and radial immersion angle ϕ gives the Cutter Engagement Boundary. An exemplary $CEB(\phi, z)$ map of a standard end mill with positive lead and tilt angles cutting an arbitrary workpiece block is given in Figure 3.6.

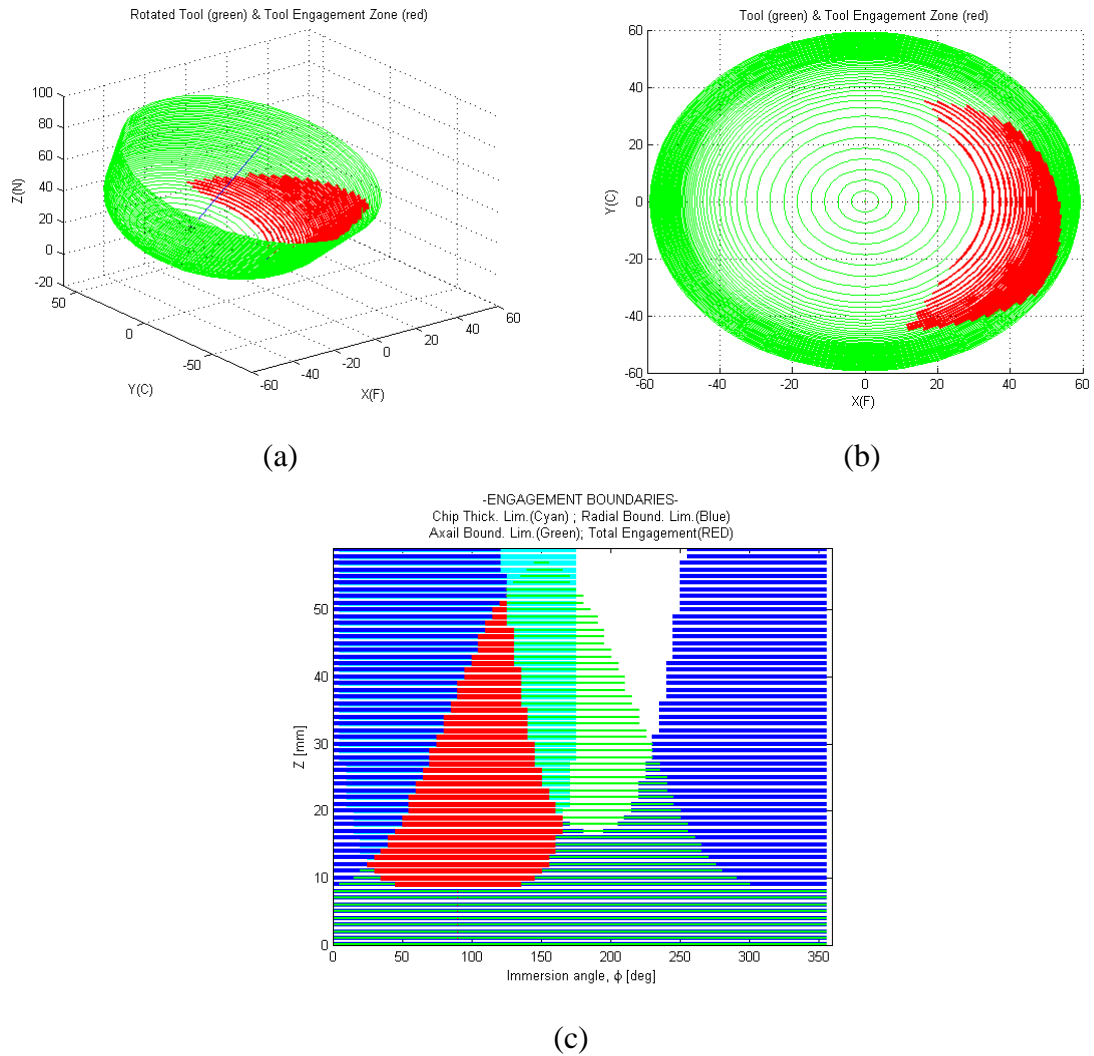


Figure 3.6: Engagement of a standard milling tool with an arbitrary workpiece; (a-b) Engagement zone shown on tool, (c) Cutter engagement boundary map, $CEB(\phi, z)$

3.2.2 Following cut scenario

During machining, as the tool moves in the cross-feed direction from step to step, the surface to be machined is modified. Previously machined surface radial boundary is affected from the previous tool orientation and the step over value, s . The representative schematic for following cut is given in Figure 3.7.

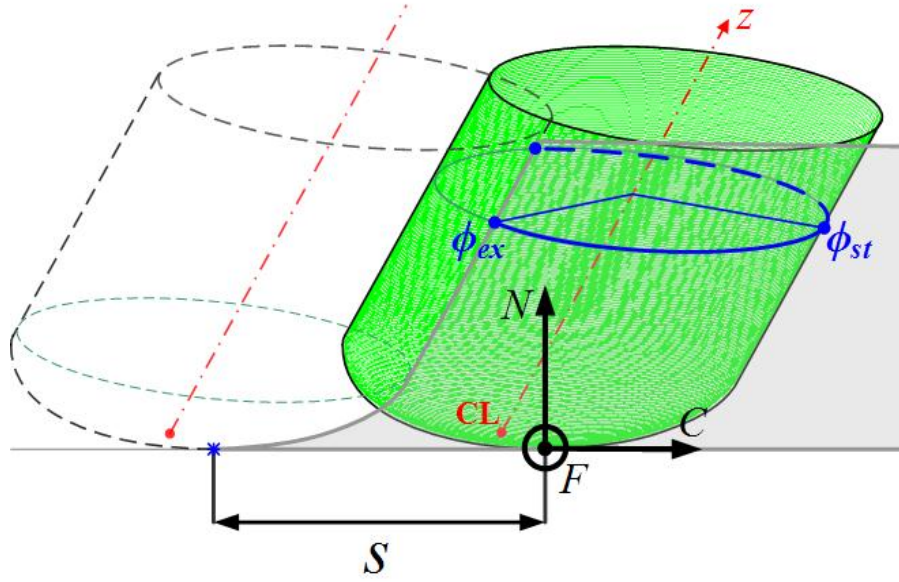


Figure 3.7: Following cutting scenario (for up milling)

The radial boundary in this case is not constant along the surface normal direction N as it was in the previous chapter. The varying geometry is evaluated as the oriented cutter profile of the previous step. The boundary points for simple tool geometries such as flat end and ball end mills can be calculated analytically because of the known profile function and simple transformation. However, for general multi-segmented tool geometries the boundary should be calculated numerically.

The profile boundary points of an oriented tool are found by searching cutter circumference points within a tool cross-section along the surface normal direction N with elevation dN . Among all cutter points lying on a cross-section, the ones having the maximum and minimum values for their C component are noted as the boundary points. These points are denoted as $P_{pre,min}(N)$ and $P_{pre,max}(N)$. The radial boundary for the following pass is then created by shifting the boundary points with respect to step over value and type of milling operation whether it is up of down milling. A following cut boundary according to the type of operation can be either starting ($Y_{st}(N)$) and exit ($Y_{ex}(N)$) radial boundary and in the table their definition are given as;

$$\begin{aligned}
&\text{if Down Milling} \quad \begin{cases} Y_{st}(N) = -\infty \\ Y_{st}(N) = P_{pre,\min}(N) + s \end{cases} \\
&\text{if Up Milling} \quad \begin{cases} Y_{st}(N) = P_{pre,\max}(N) - s \\ Y_{st}(N) = \infty \end{cases}
\end{aligned} \tag{3.14}$$

For the current cutter, these boundaries constitute the varying radial limits. As it was described in Section 3.2.1, to create the cutter engagement boundary map $CEB(\phi, z)$, the cutter periphery points should be compared with the radial, axial boundaries and the chip thickness value of a point must be positive. It should be noted that as the radial boundary for the following cut scenario is discretized along surface normal direction, to form $CEB(\phi, z)$ along z axis, the current cutter points satisfying eq. (3.13) must be found using linear interpolation by taking two adjacent boundary points $Y_{st/ex}(N)$ and calculating the corresponding radial distance $Y_{st/ex}(z)$.

For an arbitrary tapered bull end mill tool the resulting $CEB(\phi, z)$ and corresponding engagement zones on the tool are shown in the below figure. The multi-axis milling operations for 15° lead and 25° tilt angles involves a tapered bull-end mill having 18mm diameter with 6mm corner radius and 6° taper angle performing an up milling following cut with 8 mm step over.

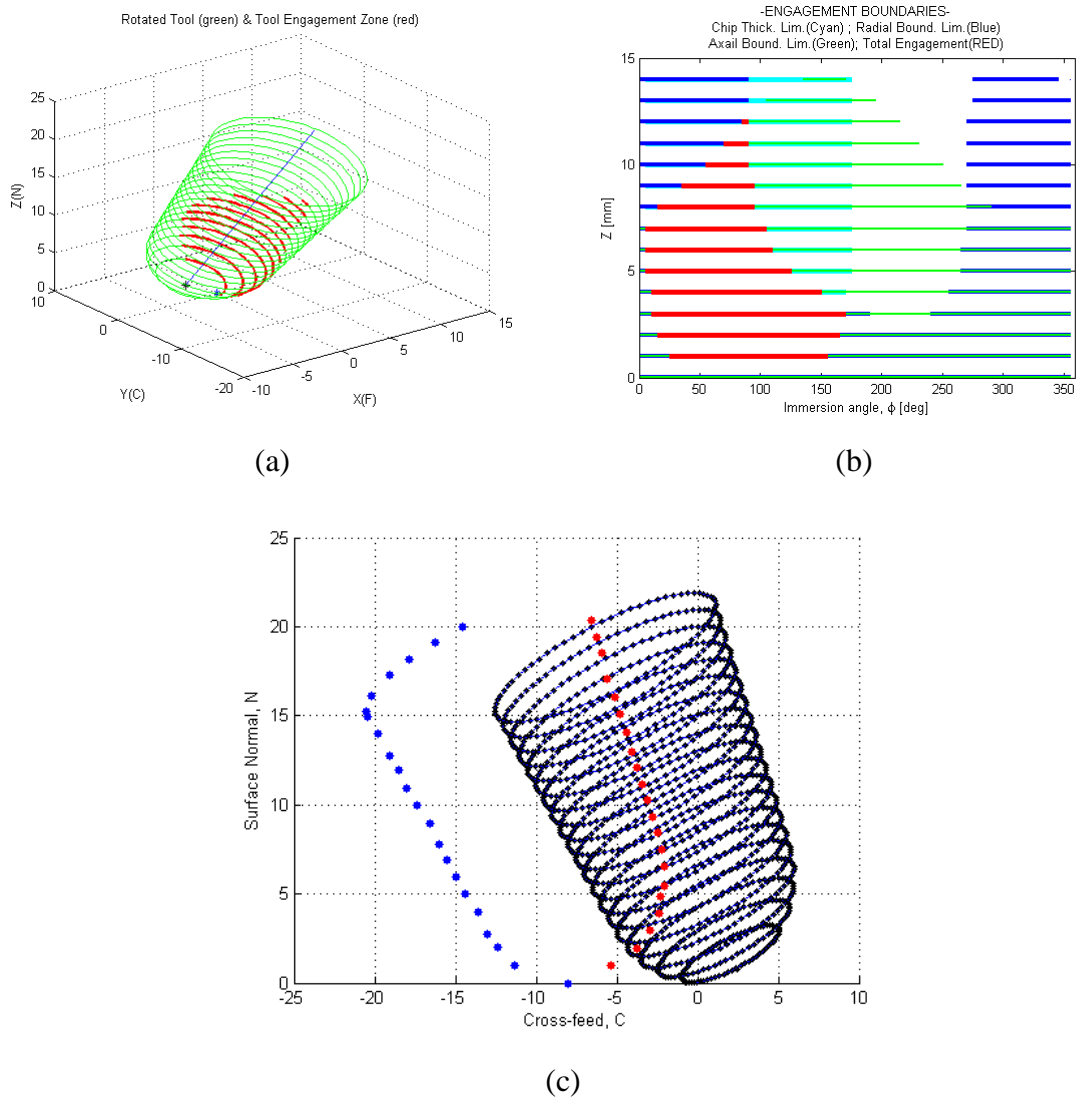


Figure 3.8: Engagement of a tapered bull end mill performing following cutting; (a) Engagement zone shown on tool, (b) Cutter engagement boundary map, $CEB(\phi, z)$, (c) Previous tool boundaries (blue and red points) and current tool (black points)

3.3 Summary

In this chapter, the geometry of multi-axis machining is introduced. In 5-axis milling operations, two additional rotation axis complicate the definition of the process. Three different coordinate system is utilized which correspond to the milling tool, the current process and the machine respectively. In order to find the implication dimensional process parameters (namely depth of cuts) on the milling tool, the tool is defined in the process coordinates using two rotational angles (lead and tilt angles) and the cutter contact (CC) point. In the last section, a numerical method to determine the cutter

engagement boundary identification method is proposed for an arbitrary workpiece cutting scenario and for following cut scenario.

CHAPTER 4

FORCE MODEL

In this chapter, the mechanistic force model formulation for generalized milling cutters is given. Linear edge force modeling technique utilizing uncut chip area and cutting edge contact information with corresponding force coefficients is adapted. The differential cutting forces acting on each tool cross-section point is calculated along a full revolution of the tool considering the contribution of every cutting tooth. Finally these forces are transformed into cutting forces in machine tool coordinates. In this chapter, the generalized uncut chip thickness function is also given for serrated variable helix/pitch general milling tool geometries evaluating multi-axis machining transformations. Finally, verification tests with several different tool geometries are presented in the last section.

4.1 Mechanistic cutting force model

In order to calculate the cutting forces acting on the flutes, differential cutting elements are analyzed using oblique cutting mechanics. In Figure 4.1, the cutting forces acting on a point on the j^{th} cutting edge are shown. A point on a cutting flute, P , is designated in cylindrical coordinates by its elevation from the tool tip along tool axis, z , and the radial immersion $\phi_j(\phi, z)$ (Eq. (2.1)).

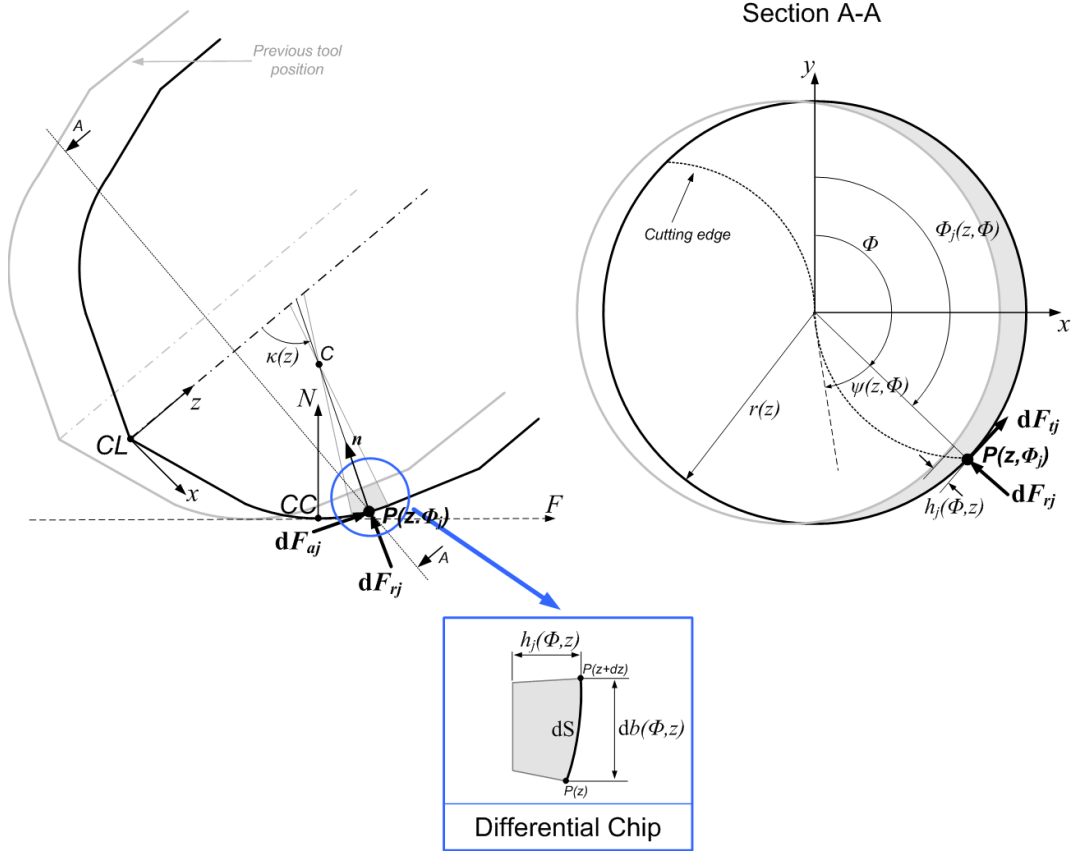


Figure 4.1: Multi-axis differential cutting force and differential chip representation

Differential cutting forces in the radial, axial and tangential directions on a cutting edge point of the j^{th} tooth at elevation z and radial rotation ϕ_j are calculated according to the mechanistic model proposed by Lee and Altintas [32]. Differential forces is the summation of cutting forces originating from the shearing mechanism and edge forces originating from plowing of the clearance face on the machined surface.

$$\begin{bmatrix} dF_{r_j}(z) \\ dF_{t_j}(z) \\ dF_{a_j}(z) \end{bmatrix} = \begin{bmatrix} K_{rc} h_j(\phi_j, z) db + K_{re} dS_j \\ K_{tc} h_j(\phi_j, z) db + K_{te} dS_j \\ K_{ac} h_j(\phi_j, z) db + K_{ae} dS_j \end{bmatrix} \cdot \delta(z) \quad (4.1)$$

where K_{rc}, K_{tc}, K_{ac} and K_{re}, K_{te}, K_{ae} are the cutting and edge force coefficients respectively. These coefficients should be calibrated using orthogonal databases and transformed to oblique counterparts for milling analysis. Chip thickness $h_j(\phi_j, z)$ and chip width db_j define the chip area in contact with the cutting flute whereas differential cutting edge length dS_j information is required for edge forces. Finally, $\delta(z)$ is the Boolean function designating whether the point of interest is in cut or not;

$$\delta(z) = \begin{cases} 1 & \text{if } P(z, \phi_j) \in CEB(\phi, z) \\ 0 & \text{if } P(z, \phi_j) \notin CEB(\phi, z) \end{cases} \quad (4.2)$$

Chip width, db , is defined as the length of the tangent line of the cutting envelope for a differential axial length:

$$db = \frac{dz}{\sin \kappa(z)} \quad (4.3)$$

Cutting edge length at elevation z with differential axial element length dz is expressed as follows:

$$dS = \left\| \begin{array}{l} P_x(z) - P_x(z - dz) \\ P_y(z) - P_y(z - dz) \\ P_z(z) - P_z(z - dz) \end{array} \right\| \quad (4.4)$$

The tangential, radial and axial forces are resolved in tool coordinates considering a transformation in terms of axial and radial immersion angles, κ and ϕ :

$$\begin{bmatrix} F_x \\ F_y \\ F_z \end{bmatrix} = T \cdot \begin{bmatrix} F_r \\ F_t \\ F_a \end{bmatrix} \quad \text{where } T = \begin{bmatrix} -\sin \phi_j \sin \kappa & -\cos \kappa & -\sin \phi_j \cos \kappa \\ -\cos \phi_j \sin \kappa & \sin \kappa & -\cos \phi_j \cos \kappa \\ -\cos \kappa & 0 & -\sin \kappa \end{bmatrix} \quad (4.5)$$

The total milling forces in tool coordinates at a radial immersion ϕ is the summation of the contributions from all teeth in cut:

$$F_k(\phi) = \sum_{j=1}^{N_f} \sum_{i=0}^{L/dz} (dF_{kj}(\phi(i \cdot dz))) \quad k = x, y, z \quad (4.6)$$

Finally, total forces are expressed in process coordinates as follows:

$$\begin{bmatrix} F_F \\ F_C \\ F_N \end{bmatrix} = T_{FCN} \cdot \begin{bmatrix} F_x \\ F_y \\ F_z \end{bmatrix} \quad (4.7)$$

where T_{FCN} is the transformation matrix defined in eq. (3.1) relating tool coordinates to process coordinates.

4.2 Uncut chip thickness formulation for serrated general variable helix/pitch tools

Chip thickness in milling operations is defined as the length of the material removed during trochoidal rotary movement by a cutting flute from the previously machined surface in tool surface normal direction. The trochoidal motion can simply be assumed as a positional shift along the feed vector having a magnitude of effective feed per tooth length $f_{t,j}$. This approximation is valid for large tool diameter over feed per tooth ratios which is generally the case for non-micro tools. Mathematically for general milling tools performing multi-axis milling operations the chip thickness value $h_j(\phi_j, z)$ is defined as:

$$h_j(\phi_j, z) = (\hat{n} \cdot \hat{f}) f_{t,j} \quad (4.8)$$

where \hat{f} is the feed unit vector in tool coordinates xyz . As a convention the feed vector is always considered in plane with tool x direction. Thus the feed unit vector in tool coordinates can be represented as a vector form as a combination of planar feed \hat{f}_x and axial feed \hat{f}_z ;

$$\hat{f} = \begin{bmatrix} \hat{f}_x \\ 0 \\ \hat{f}_z \end{bmatrix} \quad (4.9)$$

The cutting edge point unit outward vector \hat{n} is defined as;

$$\hat{n} = \begin{bmatrix} \sin \kappa \sin \phi_j \\ \sin \kappa \cos \phi_j \\ -\cos \kappa \end{bmatrix} \quad (4.10)$$

where κ or in long form $\kappa_j(z)$ and ϕ_j or in long form $\phi_j(\phi, z)$ are the axial and radial immersion angles for which the definition are given in Section 2.1 for different tool geometries.

Evaluating the general chip thickness equation (4.8), two separate parts are generated: chip thickness in planar direction and in axial direction;

$$h_j(\phi_j, z) = (\hat{f}_x \sin \phi_j \sin \kappa - \hat{f}_z \cos \kappa) f_{t,j}(z) \quad (4.11)$$

For milling tools having N_t number of cutting edges with constant distribution (non-variable helix and pitch angles), the feed per tooth value is simply expressed as;

$$f_{t,j}(z) = \frac{feed}{n.N_t} \quad (4.12)$$

where *feed* is the feed rate in mm/min and n is the spindle speed value in rpm. This results in even distribution of material to be removed in one revolution by all cutting edges.

Variable helix and pitch angles as it is explained in Section 2.2 introduces varying delay between successive cutting edges represented by $\delta\phi_j(z)$ (Eq . (2.33)). This results in varying chip thickness definition. The originating feed per tooth value can thus be expressed;

$$f_{t,j}(z) = \frac{feed}{n} \frac{\delta\phi(z)}{2\pi} \quad (4.13)$$

In the Figure 4.2 and Figure 4.3, the comparison between chip load of a non-variable tool and variable helix and pitch angle tool is given. For both cases milling tools with 4 cutting edges are modeled and the process is a half immersion down milling operation with feed over spindle ratio 0.4mm. For the non-variable tool with constant 30° helix angle for all of the cutting edges, the maximum chip load is equal to 0.05mm/tooth (Figure 4.2). The simulated variable tool in Figure 4.3 has a helix distribution as 30°-36°-30°-36° and the pitch angle variation measure ΔP for alternating pitch angle variation is set to 10°. Due to the variation of the cutting edge properties the instantaneous chip thickness value differs both from one cutting edge to another as well as along the cutting edge itself.

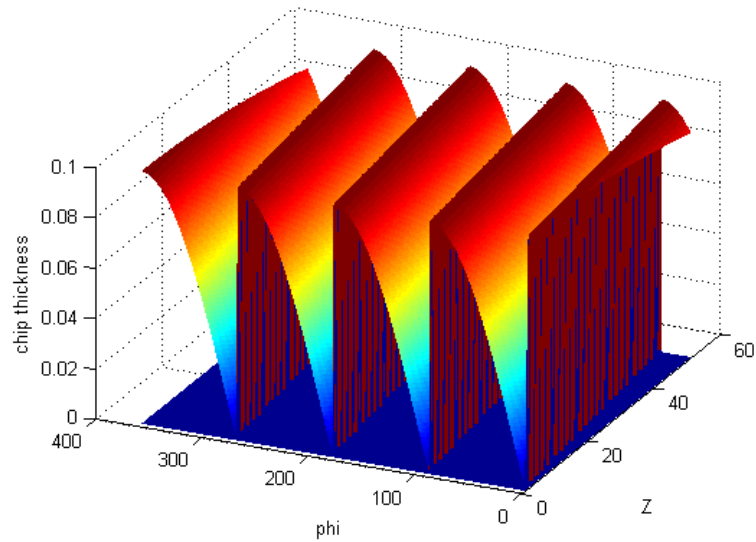


Figure 4.2: Chip load of an exemplary conventional milling tool

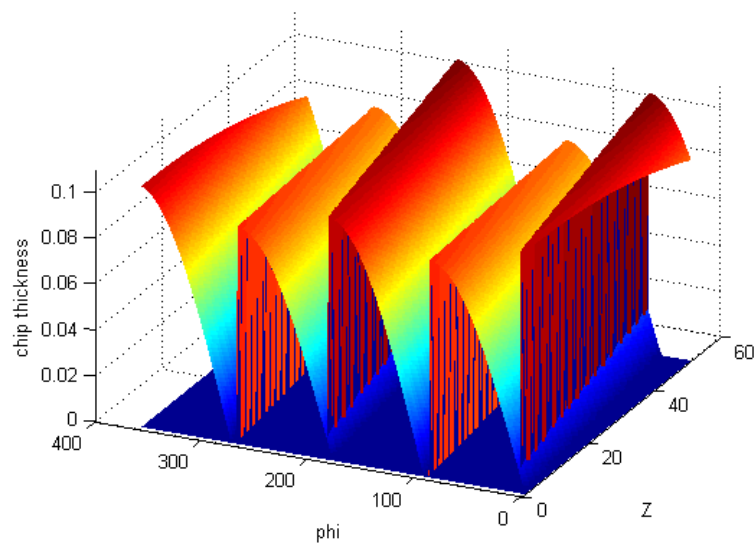


Figure 4.3: Chip load of an exemplary variable helix/pitch milling tool

For serrated cutters, unlike for straight edged milling tools, the local radius at each cross-section of the tool for each cutting edge is different from each other due to wave form in the radial direction. Moreover, serrated milling cutters are ground radially with a wave form. Similar to a tapping tool, the radial profile is ground in a helical form causing phase difference in the wave profile with the adjacent cutting flutes. In Figure 4.4 the phase difference between adjacent teeth are demonstrated. For equally separated milling cutters the phase shift can be denoted as;

$$\theta_{s,j} = 2\pi \frac{j-1}{N_t} \quad (4.14)$$

where j is the tooth number starting from 1.

For serrated milling tools, both the variation of local radius along the cutting edge and the phase difference of the serration wave form for each cutting edge vary along the tool axis. During cutting, because of the noted edge geometry variation, some cutting edges are skipped chip load reduces; some portions of the cutting edges do not engage with the surface machined by the previous edge (Figure 4.4).

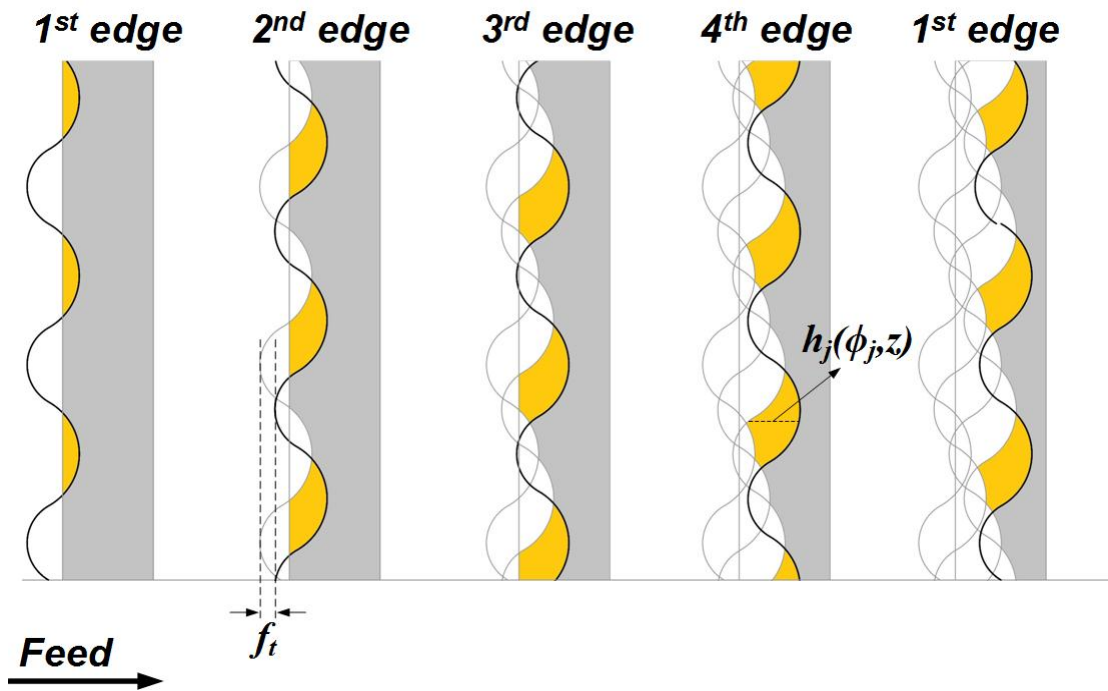


Figure 4.4: Chip load of a serrated cutter having equally separated circular wave formed edges

The chip thickness variation of a serrated cutter can be investigated as if the cutter has a known run-out function along the tool axis. For 2D milling operations, the chip load of cutter having run-out is investigated by Kline and Devor [29] and Wang and Liang [54]. Hence, the definition of the uncut chip thickness for a serrated cutter performing 2½ axis operation is given as follows;

$$h_j(\phi_j, z) = \min_{m=1 \dots N_t} \left[\left(\sum_{p=1}^m f_{t,j}(z) \right) \sin(\phi_j) + r_j(z) - r_{j-m}(z) \right] \sin \kappa_j(z) \quad (4.15)$$

From this expression it can be deduced that the amount of material removed is directly proportional to the feed per tooth value; for large values the chip area increases the separation between consecutive cutting edges widens for a specific immersion angle ϕ . For instance, if the feed per tooth value is larger than the difference of the local radii of the cutting edges (in other words; the wave amplitude of the serration profile) the serration profile is not effective anymore because the $r_j(z) - r_{j-m}(z)$ term in the chip thickness definition along the whole axial level becomes less than the effective uncut chip thickness for immersion angle ϕ .

$$\left(\sum_{p=1}^m f_{t,j}(z) \right) \sin(\phi_j) < r_j(z) - r_{j-m}(z) \quad (4.16)$$

if the expression presented is not satisfied the whole cutting edges engage with the workpiece. Hence, using serrated cutters the feed per tooth value must be chosen according to the wave amplitude of the serration profile.

Eq. (4.15) is only valid for tools performing a $2\frac{1}{2}$ axis operation where a point on the cutting edge at elevation z is always cutting the previously machined surface generated by a previous edge point at the same elevation level z . When the tool performs a multi-axis operation, the exact same cross-section points do not coincide in terms of surface generation. This issue can be neglected for straight fluted cutters because regarding the angular and axial discretization steps of the simulation, the discrete zone can be assumed as two parallel lines depicting previous and cutter edges even though the tool might be a multi-segmented one. However, for serrated cutters with small wave length, the discretization may not be fine enough to deal with the explained issue. The problem is depicted in Figure 4.5, where the feed vector direction is shown by f , the numbers indicate the numeration of cutting edges and corresponding edge points to consider in order to calculate uncut chip thickness.

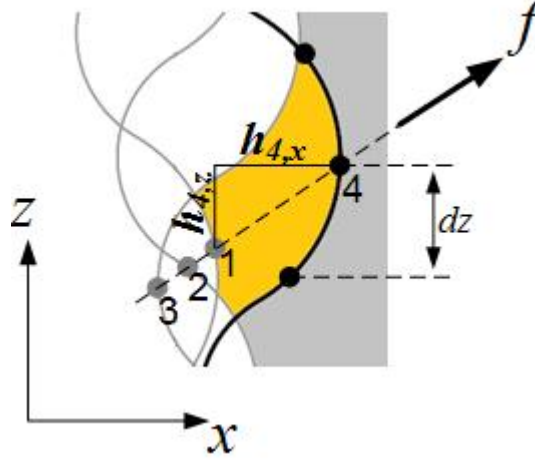


Figure 4.5: Detailed Uncut chip thickness definition for a serration profile

Therefore, the definition for the uncut chip thickness in x direction for a serrated general milling cutter should be updated as follows;

$$h_{j,x}(\phi_j, z) = \min_{m=1 \dots N_t} \left[\left(\sum_{p=1}^m f_{t,j}(z) \right) \hat{f}_x \sin \phi_j + \Delta r_{eff} \right] \sin \kappa_j(z) \quad (4.17)$$

where the effective radius difference, Δr_{eff} is defined as;

$$\Delta r_{eff} = r_j(z) - r_{j-m} \left(z - \left(\sum_{p=1}^m f_{t,j}(z) \right) \hat{f}_z \right) \quad (4.18)$$

On the other hand, the uncut chip thickness in z direction is not affected by this mechanism and can simply be recited as it was in equation (4.11);

$$h_{j,z}(\phi_j, z) = \left(\hat{f}_z \cdot f_{t,j}(z) \right) \cos \kappa(z) \quad (4.19)$$

Finally, the definition of uncut chip thickness for a general serrated variable helix and pitch cutter is given as;

$$h_j(\phi_j, z) = h_{j,x}(\phi_j, z) - h_{j,z}(\phi_j, z)$$

$$h_j(\phi_j, z) = \min_{m=1 \dots N_t} \left[\left(\sum_{p=1}^m f_{t,j}(z) \right) \hat{f}_x \sin \phi_j + \Delta r_{eff} \right] \sin \kappa_j(z) \quad (4.20)$$

$$- \left(\hat{f}_z \cdot f_{t,j}(z) \right) \cos \kappa(z)$$

4.3 Identification of milling cutting force coefficients

Force coefficients relate geometric characteristic, i.e. chip area and edge contact length, of cutting mechanism to forces acting on the cutting edge. Orthogonal cutting coefficients can be determined using a test method where a tube of material is cut orthogonally with a turning machine to obtain an orthogonal database. According to the linear edge model where both shearing mechanism and plowing are taken into account, an orthogonal database can be obtained by considering several different process parameters by varying cutting speeds (V_c), uncut chip thickness (h), rake angles (α_r), etc. Thus force coefficients can be calculated using the identified shear angle, ϕ_c , friction angle, β_f and shear stress, τ_s , parameters varying with respect to process variables.

$$\phi_c, \tau_s, \beta_f = f(V_c, h, \alpha_r) \quad (4.21)$$

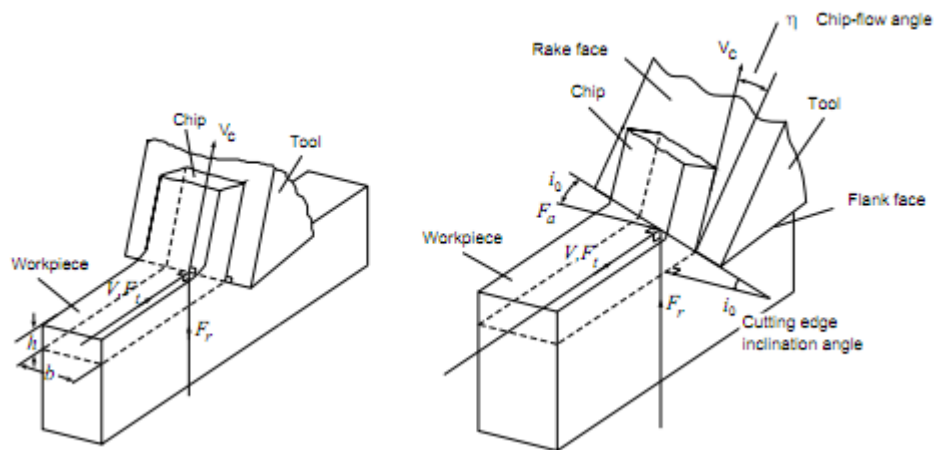


Figure 4.6: Orthogonal and oblique cutting geometries [11]

Using measured orthogonal cutting forces, i.e. feed (F_{rc}) and tangential (F_{tc}) forces, cutting parameters which are shear stress, shear angle and friction angle can be obtained [3];

$$\tau_s = \frac{(F_{tc} \cos \phi_c - F_{rc} \sin \phi_c) \sin \phi_c}{b.h} \quad (4.22)$$

$$\phi_c = \tan^{-1} \left(\frac{r_c \cos \alpha_r}{1 - r_c \sin \alpha_r} \right) \quad (4.23)$$

$$\beta_f = \alpha_r + \tan^{-1} \left(\frac{F_{rc}}{F_{tc}} \right) \quad (4.24)$$

where b is the width of cut, h is the instantaneous uncut chip thickness, r_c is the chip ratio defined as the ratio uncut chip thickness h to the cut chip thickness h_c .

In milling, force coefficients identified from orthogonal database may not be sufficiently accurate due to the obliquity introduced by the helical cutting edges. For this reason, coefficients are transformed into oblique cutting conditions using an approach proposed by Armarego [11].

$$\begin{aligned} K_{tc} &= \frac{\tau_s}{\sin \phi_n} \frac{\cos(\beta_n - \alpha_n) + \tan i_0 \tan \eta \sin \beta_n}{\sqrt{\cos(\phi_n + \beta_n - \alpha_n)^2 + \tan \eta^2 \sin \beta_n^2}} \\ K_{rc} &= \frac{\tau_s}{\sin \phi_n \cos i_0} \frac{\sin(\beta_n - \alpha_n)}{\sqrt{\cos(\phi_n + \beta_n - \alpha_n)^2 + \tan \eta^2 \sin \beta_n^2}} \\ K_{ac} &= \frac{\tau_s}{\sin \phi_n} \frac{\cos(\beta_n - \alpha_n) \tan i_0 - \tan \eta \sin \beta_n}{\sqrt{\cos(\phi_n + \beta_n - \alpha_n)^2 + \tan \eta^2 \sin \beta_n^2}} \end{aligned} \quad (4.25)$$

where α_n , β_n and ϕ_n are the normal cutting parameters defined on the oblique shear plane;

$$\alpha_n = \tan^{-1}(\tan \alpha_r \cos i_0) \quad (4.26)$$

$$\phi_n = \tan^{-1} \left(\frac{r_c \cos \alpha_n}{1 - r_c \sin \alpha_n} \right) \quad (4.27)$$

$$\beta_n = \tan^{-1}(\tan \beta \cos \eta) \quad (4.28)$$

where η is defined as the chip flow angle. Due to the obliquity in milling, the chip flow direction is not parallel to the cutting velocity direction as is the case of orthogonal cutting. Stabler [49] proposed that the chip flow direction can be assumed to be orthogonal to the cutting edge, resulting in the equality of the chip flow angle and helix angle, ie. $\eta = i_0$. Edge force coefficients on the other hand are assumed to be insensitive to the changes in oblique/helix angle [11]. Furthermore, it is shown that K_{ae} being the edge force coefficient in axial direction along the cutting edge can be taken as 0.

4.4 Model verification and experimental results

The presented general force model for general milling cutters is verified with several available and custom milling tools. For the verification tests utilized equipment are as follows;

- Deckel Maho DMU 50evo 5 axis milling center
- Kistler table type dynamometer (Type 9275BA)
- Kistler signal conditioner (Type 5233A1) with 200Hz integrated low pass filter

4.4.1 Multi-axis cutting force verification for a ball end mill tool

First 5-axis milling test case involves cutting Ti₆Al₄V workpiece with a standard ball end mill tool. The tool and process properties are given in Table 4.1.

Table 4.1: Tool and process properties for 1st force model verification test case

Tool (Ball end mill)					
<i>Radius</i>	<i>Edge #</i>	<i>Helix angle</i>			
<i>R</i>	<i>N_t</i>	<i>i₀</i>			
6mm	2	30°			

Process					
<i>Axial DoC</i>	<i>Radial DoC</i>	<i>Lead angle</i>	<i>Tilt angle</i>	<i>Feed</i>	<i>Spindle speed</i>
1.5mm	slotting	+10°	-15°	600mm/min	3000rpm

The material database for Ti₆Al₄V is formulated by Budak et al. [11] and corresponding database parameters are given below for cutting speed range of 3-47 m/min with varying rake angles from 0° to 15°.

Table 4.2: Material database parameters for Ti₆Al₄V

$\tau_s = 613 \text{ MPa}$ $\beta_f = 19.1 + 0.29\alpha_r$ $r_c = r_o \cdot t^a$ $r_o = 1.755 - 0.028\alpha_r$ $a = 0.331 - 0.0082\alpha_r$
$K_{te} = 24 \text{ N/mm}$ $K_{re} = 43 \text{ N/mm}$ $K_{ae} = 0 \text{ N/mm}$

In Figure 4.7, the comparison of measured forces and simulated forces are plotted with the addition of corresponding cutter engagement boundaries.

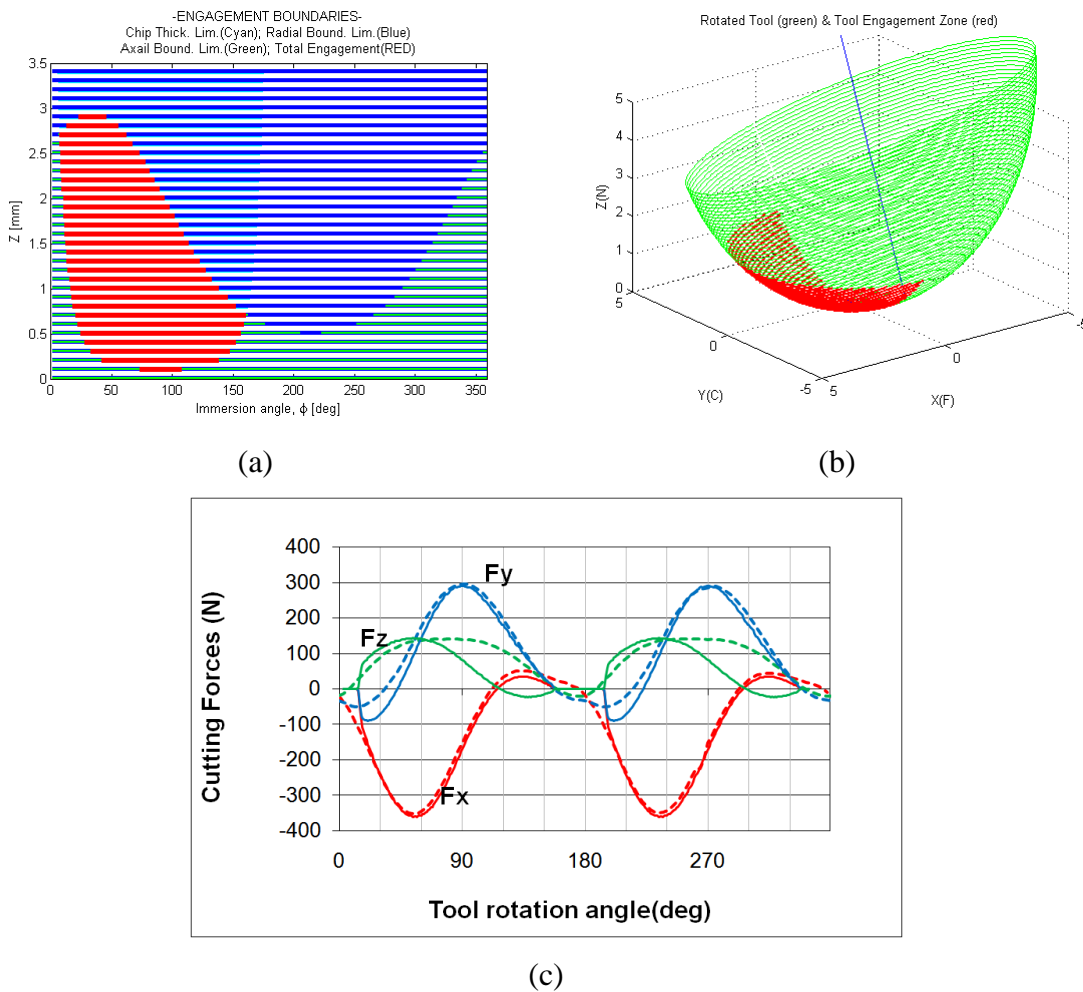


Figure 4.7: Results of the 1st force verification test (a) cutter engagement boundary, (b) cutter engagement zone on tool, (c) simulated versus measured forces (simulated in thin line, measured in dashed)

For the presented test case, 0.25mm of axial elevation step size (dz) and 3° of rotation angle step size is utilized. The cutting force results for the 5-axis ball end milling case are in good agreement with the simulation results.

4.4.2 Multi-axis cutting force verification for a standard milling tool

For the second verification test, a standard inverted cone bull end mill tool (ISCAR MMHT) (tool is shown in Figure 4.8) is utilized in a 5-axis operation where an Al7075-T6 material is machined. The tool and process properties are given in Table 4.1.

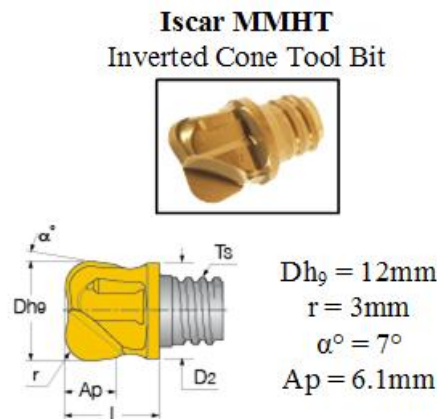


Figure 4.8: Inverted cone bull end mill tool (ISCAR MMHT) geometrical parameters

Table 4.3: Tool and process properties for 2nd force model verification test case

Tool (Inverted cone bull end mill)

<i>Geometrical properties</i>	<i>Edge #</i> N_t	<i>Helix angle</i> i_0
Figure 4.8	2	0°

Process

<i>Axial DoC</i>	<i>Type</i>	<i>Lead angle</i>	<i>Tilt angle</i>	<i>Feed</i>	<i>Spindle speed</i>
3mm	following up milling $s = 7\text{mm}$	$+30^\circ$	-15°	2000mm/min	4000rpm

The identified orthogonal database parameters for Al7075-T6 is given in the below table [16].

Table 4.4: Material database parameters for Al7075-T6

$\tau_s = 297.05 + 1.05\alpha_r$ MPa $\beta_f = 18.79 + 6.7h + 0.0076V_c + 0.256\alpha_r$ $\phi_c = 24.2 + 36.67h + 0.0049V_c + 0.3\alpha_r$
$K_{te} = 23.41$ N/mm $K_{re} = 35.16$ N/mm $K_{ae} = 0$ N/mm

In Figure 4.9, the comparison of measured forces and simulated forces are plotted together with the corresponding cutter engagement boundaries.

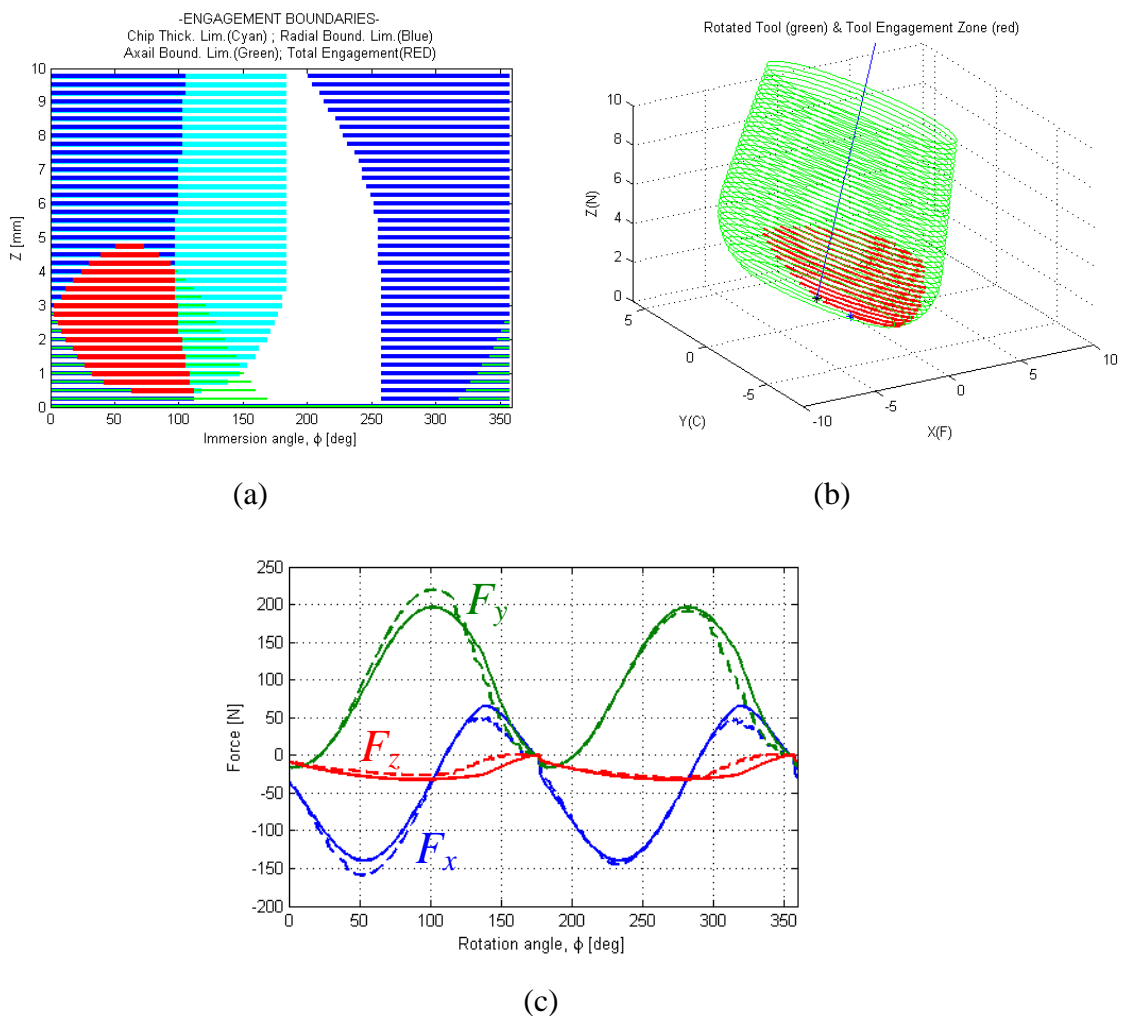


Figure 4.9: Results of the 2nd force verification test (a) cutter engagement boundary, (b) cutter engagement zone on tool, (c) simulated versus measured forces (simulated in thin line, measured in dashed)

For the presented test case, 0.25mm of axial elevation step size (dz) and 1° of rotation angle step size is utilized for precision. The test results and the simulation results are in very good agreement for this test case. The deviation of the peak force amplitudes of the measurements can be attributed to the run-out errors of deflection during cutting operation.

4.4.3 Cutting force verification for a custom profiling tool with multiple profile segments

In order to verify the presented multi segmented tool definition, a custom profiling tool provided by Makina Takım Endüstrisi (MTE) is utilized. The tool profile geometry is extracted using an optic CMM machine (Dr. Schneider WM1 400) and the representative profile directly taken from the software of the CMM is given in Figure 4.10a.

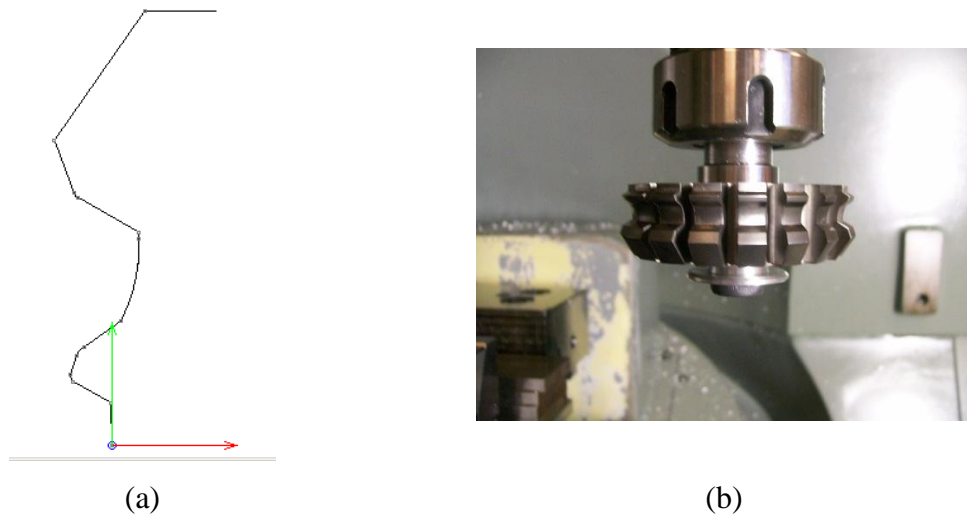


Figure 4.10: Custom profiling tool (a) CMM output of the profile for the custom multi-segmented tool, (b) actual tool photograph

The tool has straight 18 cutting edges to ensure better surface finish and the tool profile is composed of 8 linear and 4 circular segments. Tool diameter and height are measured as 68.3mm and 20.2mm respectively.

These types of custom profiling tools are often utilized for slotting in order to engrave the edge profile directly to the material. For this reason, the verification test should be a $2\frac{1}{2}$ axis operation where the axial depth of cut is chosen greater or equal to the tool

length. In the test case, an Al7075-T6 (material database presented in Table 4.4) workpiece is cut and tool and process properties are given in the below table.

Table 4.5: Tool and process properties for 2nd force model verification test case

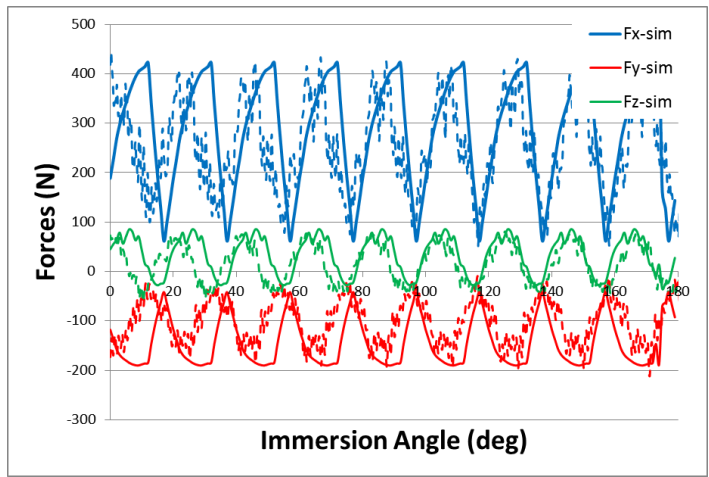
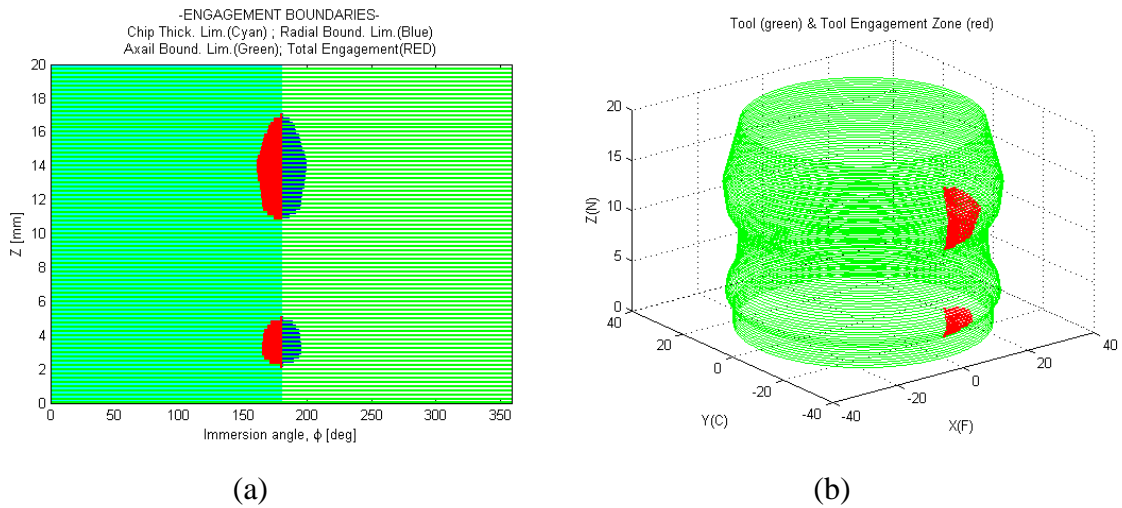
Tool (Custom profiling tool)

<i>Profile geometry</i>	<i>Tool diameter</i>	<i>Tool height</i>	<i>Edge # N_t</i>	<i>Helix angle i_0</i>
Figure 4.10	68.3mm	20.2mm	18	0°

Process

<i>Axial DoC</i>	<i>Type</i>	<i>Radial DoC</i>	<i>Feed</i>	<i>Spindle speed</i>
20.2mm	down milling	2mm	1260mm/min	1400rpm

In Figure 4.7, the comparison of measured forces and simulated forces are plotted with the addition of corresponding cutter engagement boundaries.



(c)

Figure 4.11: Results of the 3rd force verification test (a) cutter engagement boundary, (b) cutter engagement zone on tool, (c) simulated versus measured forces (simulated in thin line, measured in dashed)

For the presented test case, 0.2mm of axial elevation step size (dz) and 1° of rotation angle step size is utilized to capture the geometric variation of the cutting tool segments. Both simulation and experimental results are in good agreement where the basic trend and peak force amplitudes are satisfied. On the other hand, the measurement is noisy however no chatter vibration is detected during cutting. There exists a small delay in the tooth periods considering the simulation and measurement results which can be due to the deviation in the spindle speed during cutting.

4.4.4 Cutting force verification for inserted face milling tool

The proposed model is also verified for inserted face milling tools. GH210 steel is cut with Fette FCT 11355 (Figure 4.12) tool having 5 circular uncoated carbide inserts.

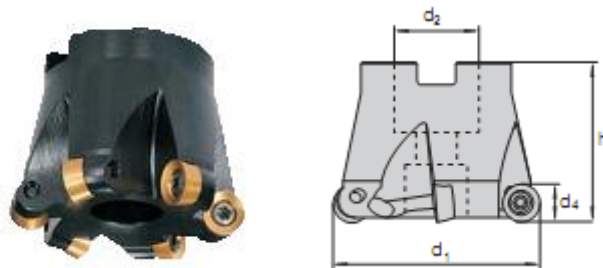


Figure 4.12: Inserted face milling tool (Fette FCT 11355) and respective geometry

The cutting coefficients are acquired again through conversion of the orthogonal cutting calibration with the specified material and tool couple. For orthogonal database generation, calibration tests were performed in the range of 30-200 m/min for cutting speed and in the range of 0.1-0.3 mm/tooth for feed per tooth. It was observed that effect of the feed per tooth on the orthogonal database is negligible. Oblique angle is negative of the axial rake angle, α and rake angle on the cutting edge α_r depends on index angle β and rake angle of the insert (Figure 2.16), α_{ins} , as follows:

Table 4.6: Orthogonal database for GH210 steel

$\tau_s = 348.78 - 0.0289V_c$ (MPa) $\beta_f = 29.937 - 0.0805V_c$ (°) $\phi_c = 32.351 + 0.0403V_c$ (°)
$K_{te} = 42.539 + 0.2465V_c$ (N/mm) $K_{re} = 35.16 + 0.1348V_c$ (N/mm) $K_{ae} = 0$ (N/mm)

The tool geometry is given in Table 2.2 under the properties of Tool 2. Roughly, the tool can be described as; 66mm tool diameter, 16mm insert diameter with 7° of axial rake angle α and 18° of index angle β . The process parameters chosen for the verification test are presented in Table 4.7.

Table 4.7: Process parameters for inserted face milling tool force verification test

<i>Axial DoC</i>	<i>Type</i>	<i>Radial DoC</i>	<i>Feed</i>	<i>Spindle speed</i>
0.5mm	down milling	33mm	4000mm/min	1200rpm

The obtained comparison plots including simulation and experiment data for each direction are as follows;

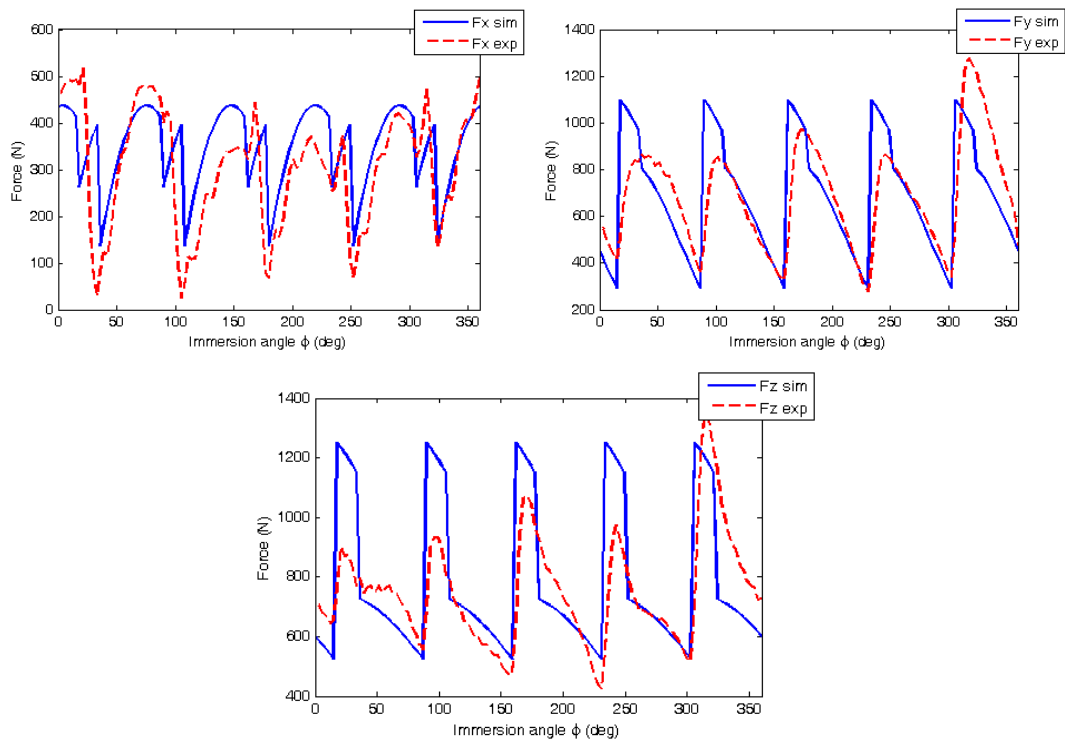


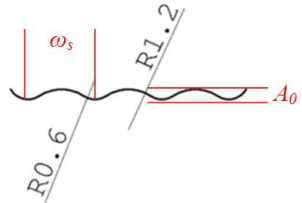
Figure 4.13: Force verification results of the inserted face milling tool

The cutting force comparison shows an acceptable correlation between simulated and calculated forces. The trend of the force variation is predicted however the changes in the peaks of the measured forces indicates a run-out error during cutting which is often the case in face milling operations.

4.4.5 Cutting force verification tests for a serrated end mill

In the following verification test, the cutting forces measured during cutting AL7075 – T6 with a serrated end mill with circular serration profile is compared to the simulation results. The cutting tool has a standard circular serration profile dictated by the DIN 844 NF standard. The geometrical tool parameters with the addition of serration profile definition are given in Table 4.8.

Table 4.8: Tool properties for serrated flat end mill verification tests

<i>Tool diameter</i>	<i>Edge #</i> N_t	<i>Helix angle</i> i_0	<i>Serration profile type</i>	<i>Serration geometry</i>
12mm	3	30°	Circular $A_0 = 0.3\text{mm}$ $\omega_s = 2\text{mm}$	

In order to demonstrate the effect of chip thickness several tests cases are presented with varying feed rate values. The test conditions for two representative experiment are given in Table 4.9.

Table 4.9: Process conditions for serrated end mill force verification tests

	<i>Axial DoC</i>	<i>Type</i>	<i>Radial DoC</i>	<i>Spindle speed</i>	<i>Feed rate</i>
<i>1st Test</i>	4mm	down milling	9mm	1200rpm	0.015mm/tooth
<i>2nd Test</i>					0.075mm/tooth

In Figure 4.14, the simulated and measured forces are compared for the 1st test condition (4mm axial depth, 9mm radial immersion with 1500rpm spindle speed and 0.015mm/tooth feed rate)

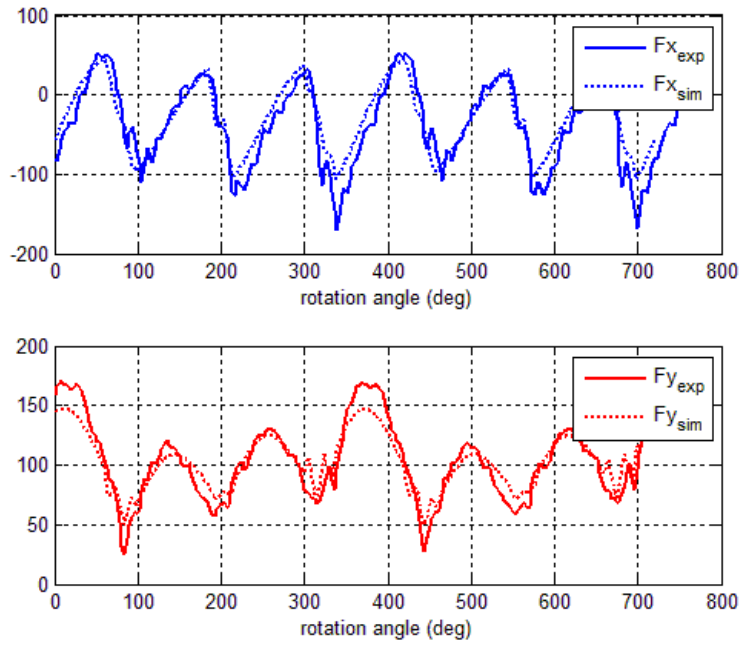


Figure 4.14: Force verification results for serrated end mills the 1st test condition

In Figure 4.15, the simulated and measured forces are compared for the 1st test condition (4mm axial depth, 9mm radial immersion with 1500rpm spindle speed and 0.015mm/tooth feed rate)

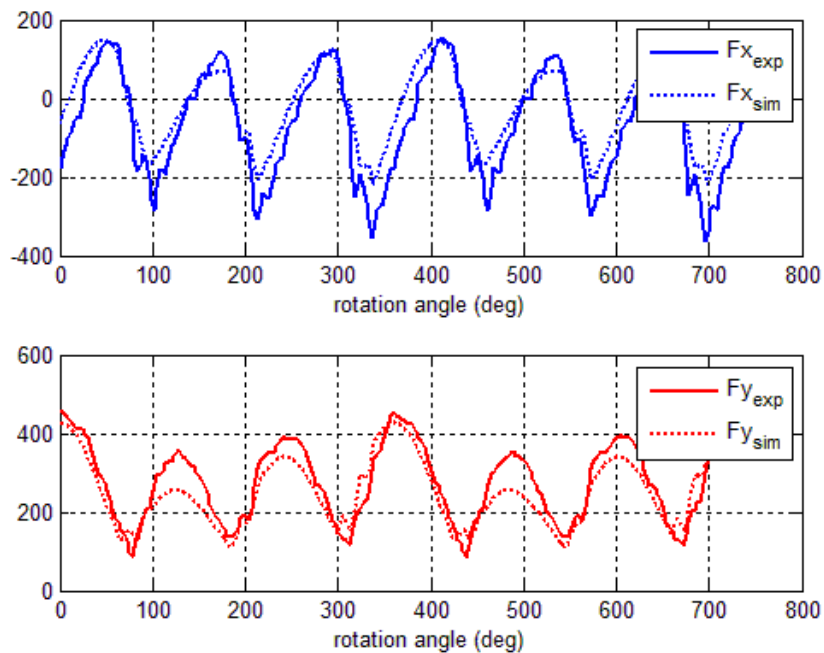


Figure 4.15: Force verification results for serrated end mills the 2nd for test condition

4.4.6 Cutting force verification for variable helix/pitch cutters

Flat end custom tools with variable cutting edge geometries presented in Table 2.4 are utilized for the force verification tests. For AOT.318.002 and AOT.318.003, the cutting force results are shown in this section. For clarity the geometrical parameters of these tools are restated in Table 4.10;

Table 4.10: Cutting edge geometric parameters for variable helix/pitch tools used for force verification tests

Tool code	Helix angle (deg), $i_{0,1...4}$	Pitch distribution type	Pitch angles (deg) $\phi_{p,1...4}(\theta)$
AOT.318.002	30 – 32 – 34 – 36	-	90 – 90 – 90 – 90
AOT.318.003	30 – 33 – 30 – 33	Alternating	87 – 93 – 87 – 93

For the verification case, an Al707 – T6 block is machined with process parameters shown on Table 4.11.

Table 4.11: Process parameters for milling tools with variable cutting edge geometry

<i>Axial DoC</i>	<i>Type</i>	<i>Radial DoC</i>	<i>Feed</i>	<i>Spindle speed</i>
7.5mm	down milling	5mm	530mm/min	2650rpm

In order to capture the differentiation of the separation angle along tool body, a rather deep cutting condition is chosen. The measured cutting forces are compared with the simulation results in Figure 4.16 and Figure 4.17.

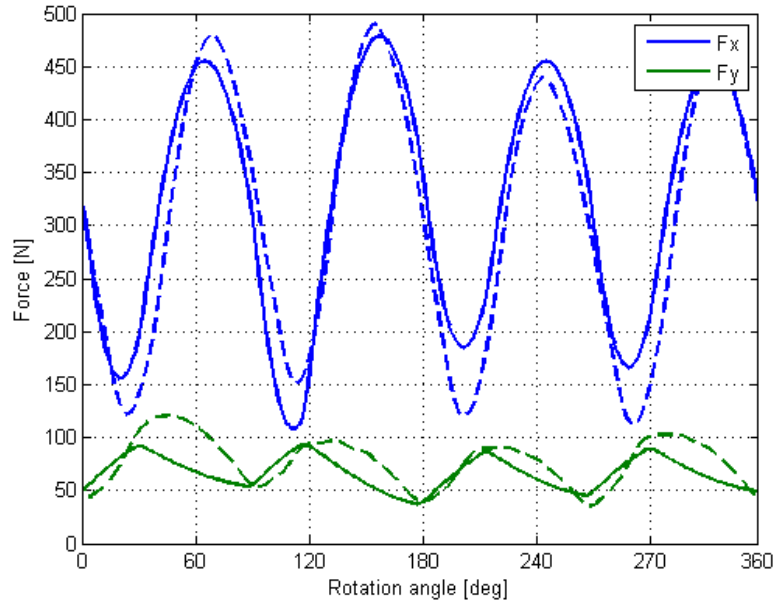


Figure 4.16: Force verification results for AOT.318.002 variable helix tool

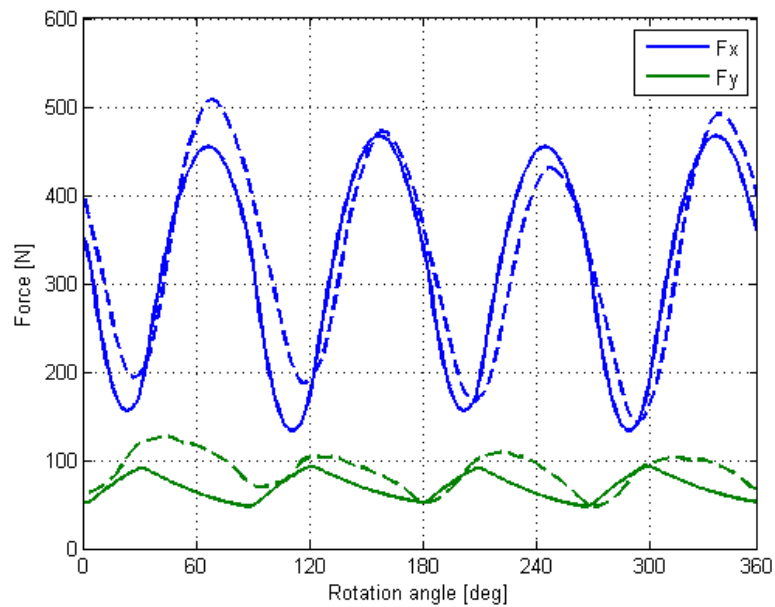


Figure 4.17: Force verification results for AOT.318.003 variable helix/pitch tool

The results indicate that the simulation output forces are comparable to the measured forces even though there are mismatches. However, in general the model is able to predict the force variation trend. Regarding the force in X direction, the effect of the edge geometry variation can be observed. For the first case (Figure 4.16), it was expected and seen from the measured forces that due to linearly increasing helix angle values from tooth to tooth, the forces starting from the 1st teeth increases and fluctuate accordingly. The difference between measured and simulation results can be attributed

to run-out errors, nevertheless for the forces in Y direction, the model should be reconsidered; the error might be originating from the employed cutting force coefficients.

4.4.7 Cutting force verification for a process simulation case employing Z-mapping

In this section, the proposed force model is integrated into a Z-map process modeler developed by Tunc [52]. The proposed model decodes the rough surface information stored in the STL file format. The workpiece is divided into grids on XY plane and a vector cluster is formed for each grid point for which the height denotes the rough surface of the position in machine +Z direction. The CL file containing the tool path information of the cutting process including the tool tip position, tool axis unit vector direction and corresponding feed value is parsed to model the cutting tool motion. The cutter position is updated for each CL point and a Boolean operation is conducted to find the polygon intersections between the mapped surface and previously modeled tool body using the model proposed in CHAPTER 2 in order to update the Z-map vector heights and find the cutter engagement boundaries. The schematic of the Z-map process model is depicted in Figure 4.18.

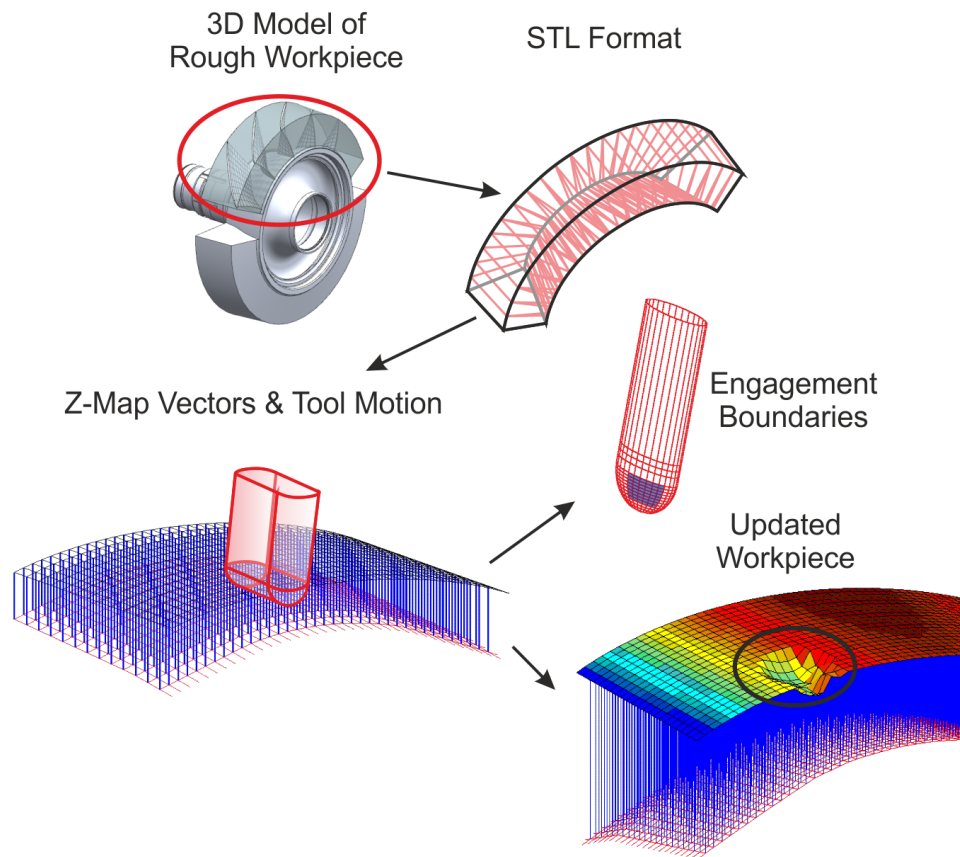


Figure 4.18: Application of the Z-map method [52]

To verify the process simulation module, four different test cases are compared with experimental results. During the experiment a Ti6Al4V (see Table 4.2 for orthogonal database) block is machined with a carbide ball end mill tool having a diameter of 12mm, 2 cutting flutes with 30° helix angle. The stock is cut following linear tool paths to achieve a sinusoidal face profile. For each test case cutting parameters are shown in Table 4.12

Table 4.12: Cutting conditions for process simulation verification tests

	<i>Step no</i>	<i>Cutting type</i>	<i>Lead</i>	<i>Tilt</i>
I	1	Slotting	0	0
	2	%50 radial	0	0
	3	%50 radial	0	0
II	4	Slotting	15	25
	5	%50 radial	15	25
	6	%50 radial	15	25
III	7	Slotting	15	25
	8	%50 radial	15	25
IV	9	Slotting	20	30
	10	%50 radial	20	30

In the below figure, virtual CAM operation and resulting machined surfaces using NX7.5 is shown. First three operations (I, II, III) involve cutting an intact surface however in the IVth operation previously machined surface is cut diagonally.

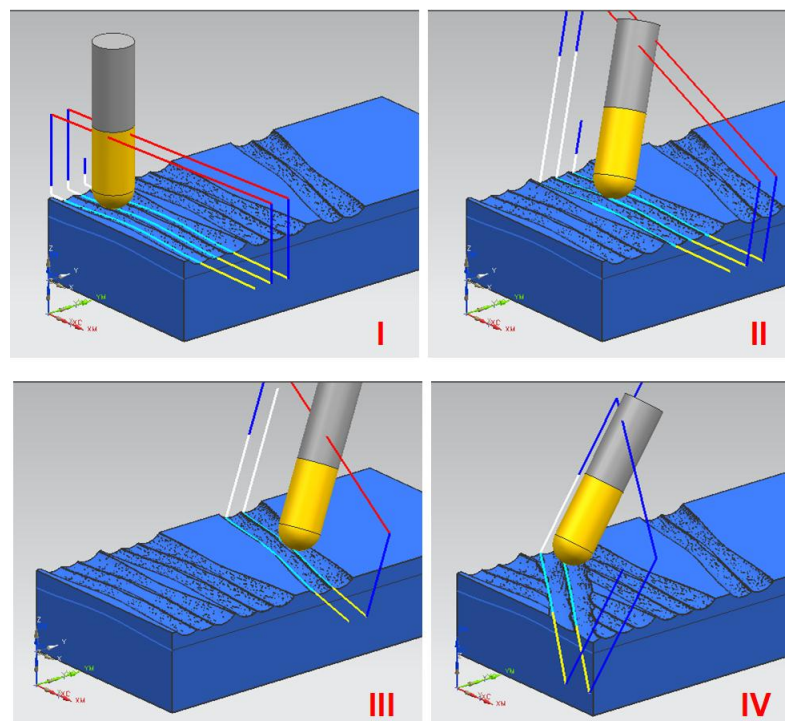


Figure 4.19: Virtual CAM operation and resulting surfaces

In order to both capture details of the process and to be able to find accurate engagement boundaries the STL solid body is mapped using 0.25mm meshes in X and Y directions. The tool is divided into axial elements with a separation height of 0.1mm

and cutter envelope points are calculated and generated for each 3° increment around the tool axis for each level.

Simulations are carried out in MATLAB 2010a using a PC having Intel i5-450M processor (2.40GHz – DualCore) and 4Gb of RAM. Simulation times are as follows;

Table 4.13: Simulation times for the process model

<i>Operation</i>	<i>Total step number</i>	<i>Sim. time</i>
I	617 steps	172.32s
II	614 steps	230.095s
III	232 steps	84.26s
IV	449 steps	252.616s

In Figure 4.20, the obtained machined surfaces are shown;

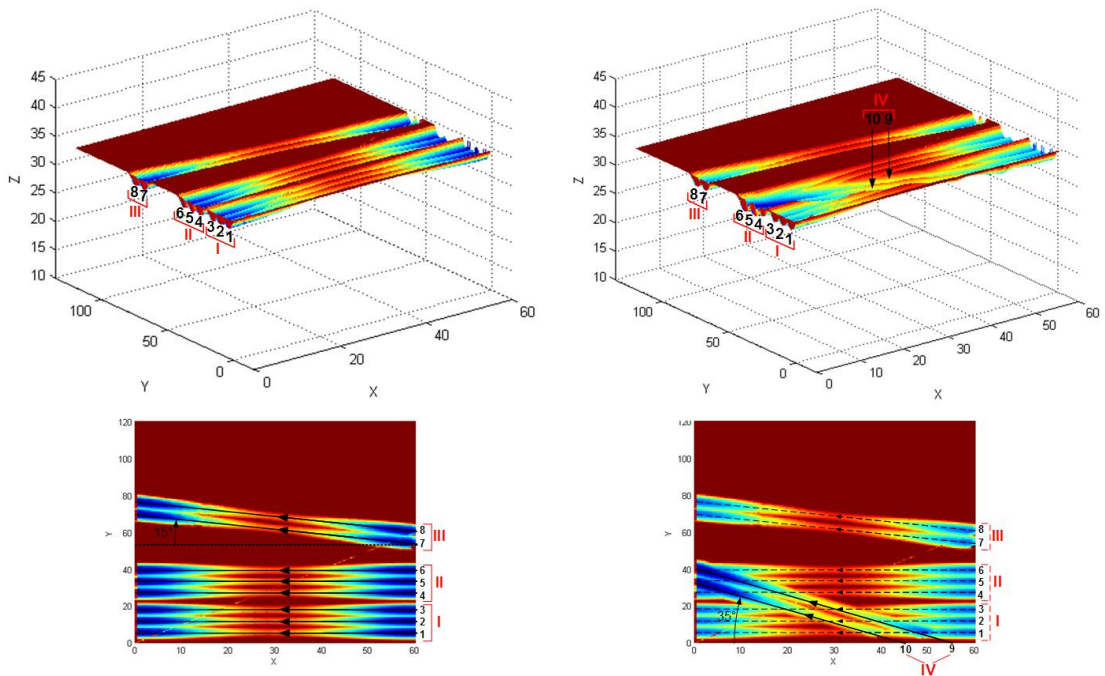


Figure 4.20: Simulated machined surface profiles from Z-mapping algorithm

Cutting forces are measured during the experiment using the rotary dynamometer (Kistler 9123). The results are not filtered. During the test no sign of chatter vibration is observed.

The process model utilizes the mechanistic force modeling approach represented in CHAPTER 2 and it is directly used in the process model as an auxiliary function. In the below figures, the calculated and measured force values in XY workpiece coordinates

are shown for each operation at every step. The simulated forces corresponds to F_{xy} forces which is the resultant force of F_x and F_y . Only the maximum force values are compared for simulation and measurement results

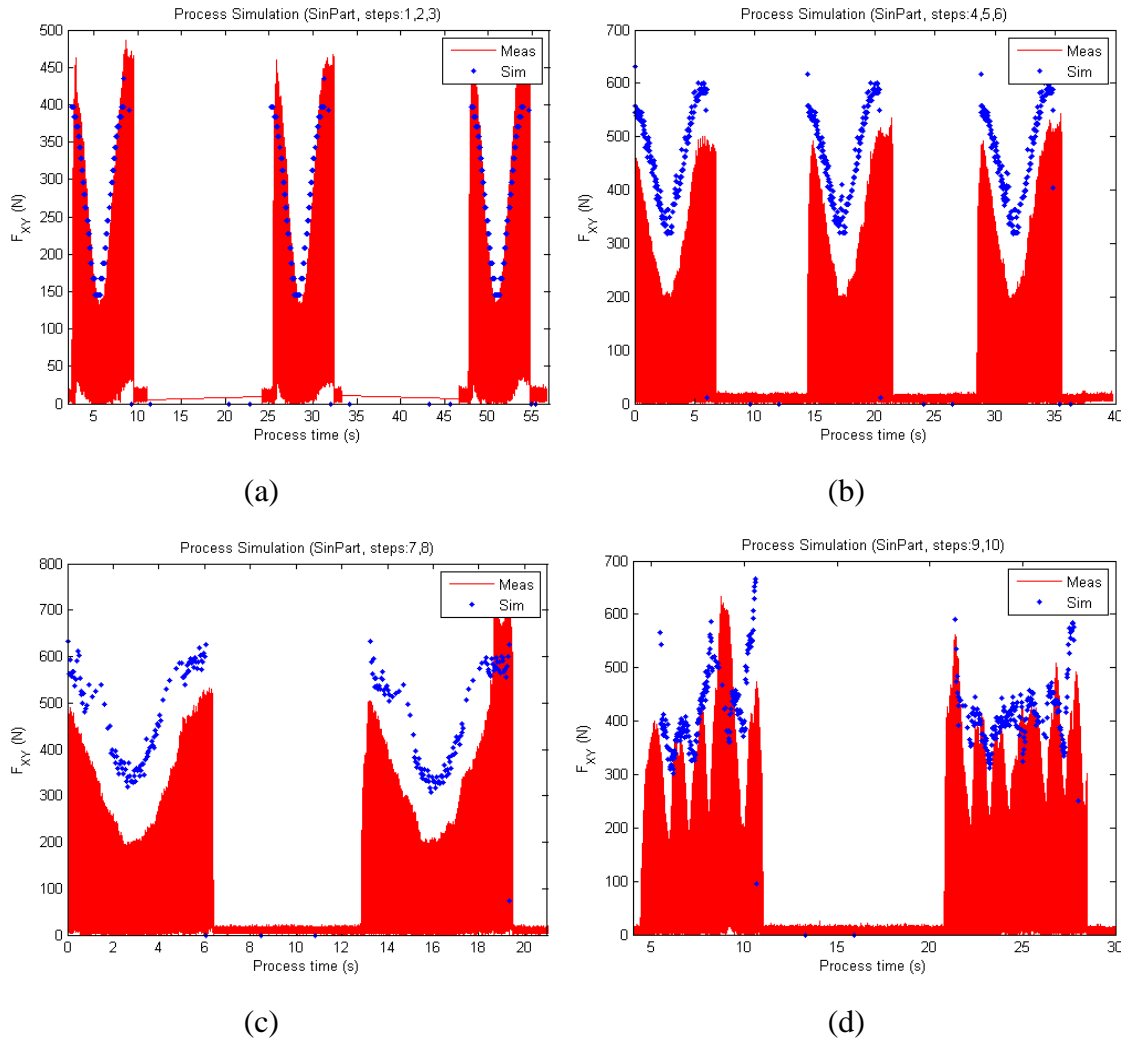


Figure 4.21: Simulated and measured process forces

The results show that for 3axis operations the process model can very closely predict the realistic measured forces (Figure 4.21a). However in 5-axis machining cases, even though the varying cutting force trends are satisfied with the simulation results, there is an offset between maximum force values (Figure 4.21b). For the final case where a previously machined surface is cut, the even though the overall trend is captured, the simulation variation of the cutting forces is not very satisfactory (Figure 4.21c). This difference can be attributed to the chosen simulation step numbers and the mesh size; increasing these values may yield better results. Moreover for the last case, the utilized Z-mapping algorithm was unable to capture the variation of the previously cut surface.

The mapping and intersection method can be reconsidered and further improved, however this is not in the scope of this study.

4.5 Summary

In this chapter, the force model for generalized milling tools with multiple profile segments and irregular cutting edge geometries is presented. Mechanistic approach is utilized where chip area and engaged cutting edge length is related to cutting forces using force coefficients. The formulation for uncut chip thickness calculation at a given tool elevation level and immersion angle is also given. Initially, differential elemental cutting forces acting on the cutting edges are determined and then transformed to machine coordinates. To accurately adjust force coefficients orthogonal to oblique transformation methodology is followed.

CHAPTER 5

DYNAMIC STABILITY MODEL

Chatter being a self-excited closed loop regenerative vibration is directly related with the dynamic chip thickness and corresponding dynamic cutting forces. In the closed loop system dynamic cutting forces causes oscillatory displacements affecting the chip thickness and then as a result the chip thickness alter the dynamic cutting forces for the next tooth periods. The closed loop block diagram where the milling dynamic is represented in Laplace domain which will be referred throughout the chapter is represented in figure 5.1.

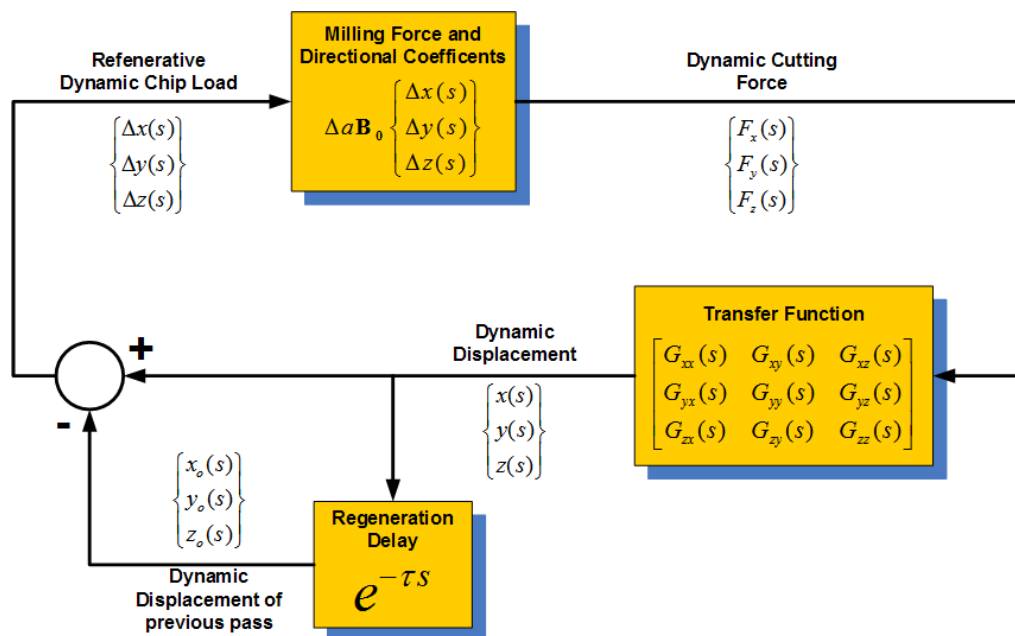


figure 5.1: Block diagram for the closed loop chatter generation system

In Section 5.1, single frequency solution method represented by Ozturk and Budak [43] is extended for generalized milling tools with uniformly distributed straight helical flutes. For these types of tools the regeneration delay between consecutive tooth periods are constant. For serrated and variable helix cutters the regeneration delay term due to

nonuniform distribution of consecutive edges which are cutting, the solution differs. In order to tackle this problem, an averaging technique to determine effective regeneration terms is incorporated into Ozturk and Budak's [43] model. For each section, first the dynamic chip thickness model is presented, secondly the formulation of the stability problem is given and finally an iterative method to generate stability lobes is explained.

5.1 Chatter stability model for constant time delayed systems

The chatter stability model is formed as an eigenvalue problem where the closed loop system is described in terms of dynamic chip thickness variation and corresponding dynamic forces. Similar to force model approach the tool is divided into axial cross-sectional elements with height dz and the differential dynamic forces are represented for each level.

The dynamic chip thickness is described as the scalar product of dynamic displacement vector d and cutting edge point unit outward vector \hat{n} [43];

$$h_d = \hat{n} \cdot d \quad (5.1)$$

where \hat{n} is presented in equation (4.11) and the displacement vector d is defined as the difference between current displacement and the displacement one tooth period before (Figure 5.2);

$$d = \begin{bmatrix} \Delta x \\ \Delta y \\ \Delta z \end{bmatrix} = \begin{bmatrix} x_d(t) - x_d(t - \tau) \\ y_d(t) - y_d(t - \tau) \\ z_d(t) - z_d(t - \tau) \end{bmatrix} \quad (5.2)$$

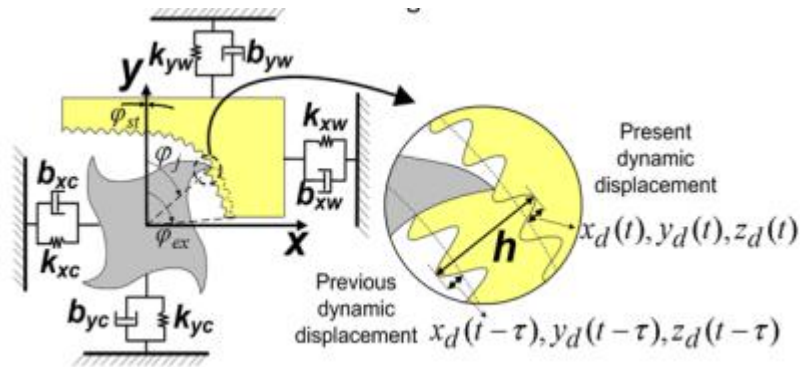


Figure 5.2: The chatter vibration on the tool and corresponding dynamic chip thickness definition

The dynamic part of cutting forces affecting the oscillatory displacement of the system is expressed as follows;

$$\begin{bmatrix} F_x(\phi_j, z) \\ F_y(\phi_j, z) \\ F_z(\phi_j, z) \end{bmatrix} = T \begin{bmatrix} K_{rc} \\ K_{tc} \\ K_{ac} \end{bmatrix} h_d db \cdot \delta(z) \quad (5.3)$$

where T is the transformation matrix relating radial, tangential and axial direction to tool coordinate system xyz (eq. (4.5)); K_{rc} , K_{tc} and K_{ac} are the local cutting force coefficients obtained from orthogonal to oblique transformation; db is the chip width formulated in eq. (4.3); and $\delta(z)$ is the cutter engagement criteria defined in eq. (4.2) (Figure 5.3).

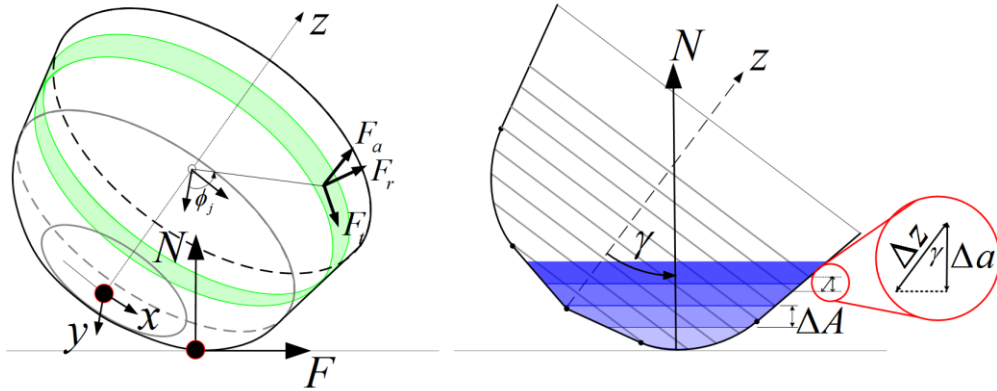


Figure 5.3: Dynamic cutting forces and discrete height definitions

For simplifying the above equation by defining the directional coefficient matrix $B_j(\phi_j, z)$ is defined as follows;

$$B_j(\phi_j, z) = \frac{1}{\cos \gamma \sin \kappa} T \begin{bmatrix} K_{rc} \\ K_{tc} \\ K_{ac} \end{bmatrix} \hat{n} \quad (5.4)$$

where the inclination angle between tool axis z and surface normal N on the FN plane;

$$\gamma = \cos^{-1} \left(\frac{\Delta a}{\Delta z} \right) \quad (5.5)$$

Thus eq. (5.3) can be rewritten as follows;

$$\begin{bmatrix} F_x(\phi_j, z) \\ F_y(\phi_j, z) \\ F_z(\phi_j, z) \end{bmatrix} = \Delta a \mathbf{B}_j(\phi_j, z) \begin{bmatrix} \Delta x \\ \Delta y \\ \Delta z \end{bmatrix} \quad (5.6)$$

Summing up the contribution of each cutting edge, dynamic cutting forces at immersion angle ϕ on axial level z is expressed as;

$$\begin{bmatrix} F_x(\phi_j, z) \\ F_y(\phi_j, z) \\ F_z(\phi_j, z) \end{bmatrix} = \Delta a \mathbf{B}(\phi_j, z) \begin{bmatrix} \Delta x \\ \Delta y \\ \Delta z \end{bmatrix} \quad (5.7)$$

Since the immersion angle changes in time domain during the rotation at each period of the tool, eq. (5.7) can be expressed in terms of time as;

$$\begin{bmatrix} F_x(t, z) \\ F_y(t, z) \\ F_z(t, z) \end{bmatrix} = \Delta a \mathbf{B}(t, z) \begin{bmatrix} \Delta x \\ \Delta y \\ \Delta z \end{bmatrix} \quad (5.8)$$

$\mathbf{B}(t, z)$ is a periodic function with tooth passing period τ and can be represented by Fourier series expansion. Altintas and Budak [1] showed that using only the first term of the Fourier series expansion, stability diagrams can be predicted accurately unless radial immersion is very low. This method is called single frequency or zero order solution method. Hence, $\mathbf{B}(t, z)$ matrix is replaced by the first term of the Fourier series expansion which is \mathbf{B}_o . It can be represented in time and angular domain as follows;

$$\mathbf{B}_o(z) = \frac{1}{\tau} \int_0^{\tau} \mathbf{B}(t, z) dt = \frac{1}{\phi_p} \int_0^{\phi_p} \mathbf{B}(\phi, z) dt \quad (5.9)$$

where ϕ_p is the tooth separation angle between equally spaced cutting edges which in this case is equal to $2\pi/N_t$. The dynamic displacement vector at the limit stability in terms of the transfer function matrix of the system and cutting forces can be written as follows;

$$d = \begin{bmatrix} \Delta x \\ \Delta y \\ \Delta z \end{bmatrix} = (1 - e^{-i\omega_c \tau}) \mathbf{G}(i\omega_c) \begin{bmatrix} F_x(t) \\ F_y(t) \\ F_z(t) \end{bmatrix} \quad (5.10)$$

Therefore, substituting \mathbf{B}_o into eq. (5.10), cutting forces corresponding to the tool cross-section at level z at the limit of stability takes the following form;

$$\begin{bmatrix} F_x(t, z) \\ F_y(t, z) \\ F_z(t, z) \end{bmatrix} e^{i\omega_c \tau} = \Delta a \mathbf{B}_o(z) (1 - e^{-i\omega_c \tau}) \mathbf{G}(i\omega_c) \begin{bmatrix} F_x(t) \\ F_y(t) \\ F_z(t) \end{bmatrix} e^{i\omega_c \tau} \quad (5.11)$$

where ω_c is the chatter frequency and $(1 - e^{-i\omega_c \tau})$ is defined as the regeneration coefficient denoted as \mathbf{b} . For cutting tools with non-serrated equally spaced cutting edges, this term is always constant for each axial level and cutting edge. However, in the following section it will be shown that due to the variation of the time delay τ between each tooth period for every axial level, this term should be updated.

In eq. (5.10), the transfer function matrix $\mathbf{G}(i\omega_c)$ is expressed in the machine coordinate system as;

$$\mathbf{G}(i\omega_c) = \begin{bmatrix} G_{xx} & G_{xy} & G_{xz} \\ G_{yy} & G_{yx} & G_{yz} \\ G_{zx} & G_{zy} & G_{zz} \end{bmatrix} \quad (5.12)$$

The terms of the transfer function matrix corresponds to the measured transfer function in the denoted directions whereas G_{yx} is the transfer function denoting the Y direction output of the input in X direction.

Up to this point, the cutting forces for the tool cross-section at level z have been written in terms of total forces. However, in order to solve for the stability limits, all of the axial elements should be solved simultaneously. For that reason eq. (5.11) is written for all tool cross-section elements in the analysis and these equations are summed side by side. Then the following expression is obtained where the left hand side of the equation represents the total dynamic cutting forces;

$$\begin{bmatrix} F_x(t, z) \\ F_y(t, z) \\ F_z(t, z) \end{bmatrix} e^{i\omega_c \tau} = \Delta a (1 - e^{-i\omega_c \tau}) \left(\sum_{z=1}^m \mathbf{B}_o(z) \right) \mathbf{G}(i\omega_c) \begin{bmatrix} F_x(t) \\ F_y(t) \\ F_z(t) \end{bmatrix} e^{i\omega_c \tau} \quad (5.13)$$

where m is the number of cross-sectional disc elements in the analysis at the current iteration which is equal to $a/\Delta a$. After the terms are collected at the left hand side, the equation turns into an eigenvalue problem;

$$\left[\mathbf{I} - \Delta a (1 - e^{-i\omega_c \tau}) \left(\sum_{z=1}^m \mathbf{B}_o(z) \right) \mathbf{G}(i\omega_c) \right] \begin{bmatrix} F_x(t) \\ F_y(t) \\ F_z(t) \end{bmatrix} = 0 \quad (5.14)$$

where \mathbf{I} defines the identity matrix. Equation (5.14) has nontrivial solution only if the following determinant is equal to 0;

$$\det \{ \mathbf{I} - \lambda \Phi \} = 0 \quad (5.15)$$

where Φ and the complex eigenvalue λ are defined as follows;

$$\Phi = \left(\sum_{z=1}^m \mathbf{B}_o(z) \right) \mathbf{G}(i\omega_c) \quad (5.16)$$

$$\lambda = -\Delta a (1 - e^{-i\omega_c \tau}) = \lambda_R + i\lambda_I \quad (5.17)$$

The solution of eq. (5.15) produces three different eigenvalues and for each of them the elemental critical limiting cutting depth is calculated;

$$\Delta a_{\text{lim}} = -\frac{1}{2} \lambda_R (1 + \kappa_\lambda^2) \quad \text{where } \kappa_\lambda = \lambda_I / \lambda_R \quad (5.18)$$

The minimum positive limiting depth is search among three possible solutions and used as the limiting depth in the stability diagram. Since at each iteration an increasing m number of discs are taken into account, the cumulative limiting cutting depth for a given chatter frequency ω_c is found as;

$$a_{\text{lim}} = m \Delta a_{\text{lim}} \quad (5.19)$$

Finally, after the all of the limiting depth of cut for a possible frequency range around the dominant system modes are found by sweeping the frequency domain iteratively, the corresponding spindle speeds starting from 1st lobe (k=1) should be calculated. The procedure is proposed and explained in detail by Altintas and Budak [1]. First, the relation between the chatter frequency ω_c and tooth passing period τ is established;

$$\omega_c \tau = \varepsilon + k2\pi \quad (5.20)$$

which yields the tooth passing frequency as follows;

$$\tau = \frac{\varepsilon + k2\pi}{\omega_c} \quad (5.21)$$

where ε is the phase shift between inner and outer modulation waves corresponding to present and previous surface waves imprinted by the consecutive cutting edges and k is the number of full waves marked during the cut denoting the lobe numbers in the stability lobe diagram. The phase shift is a function of the phase angle ϕ_{ph} ;

$$\varepsilon = \pi - 2\phi_{ph} = \pi - 2(\tan^{-1} \kappa_\lambda) \quad (5.22)$$

As the final step, corresponding spindle speed on lobe k is calculated;

$$n = \frac{60}{N_t \tau} \quad (5.23)$$

The procedure to form stability lobe diagrams for non-time varying systems is summarized as a pseudocode in Figure 5.4.

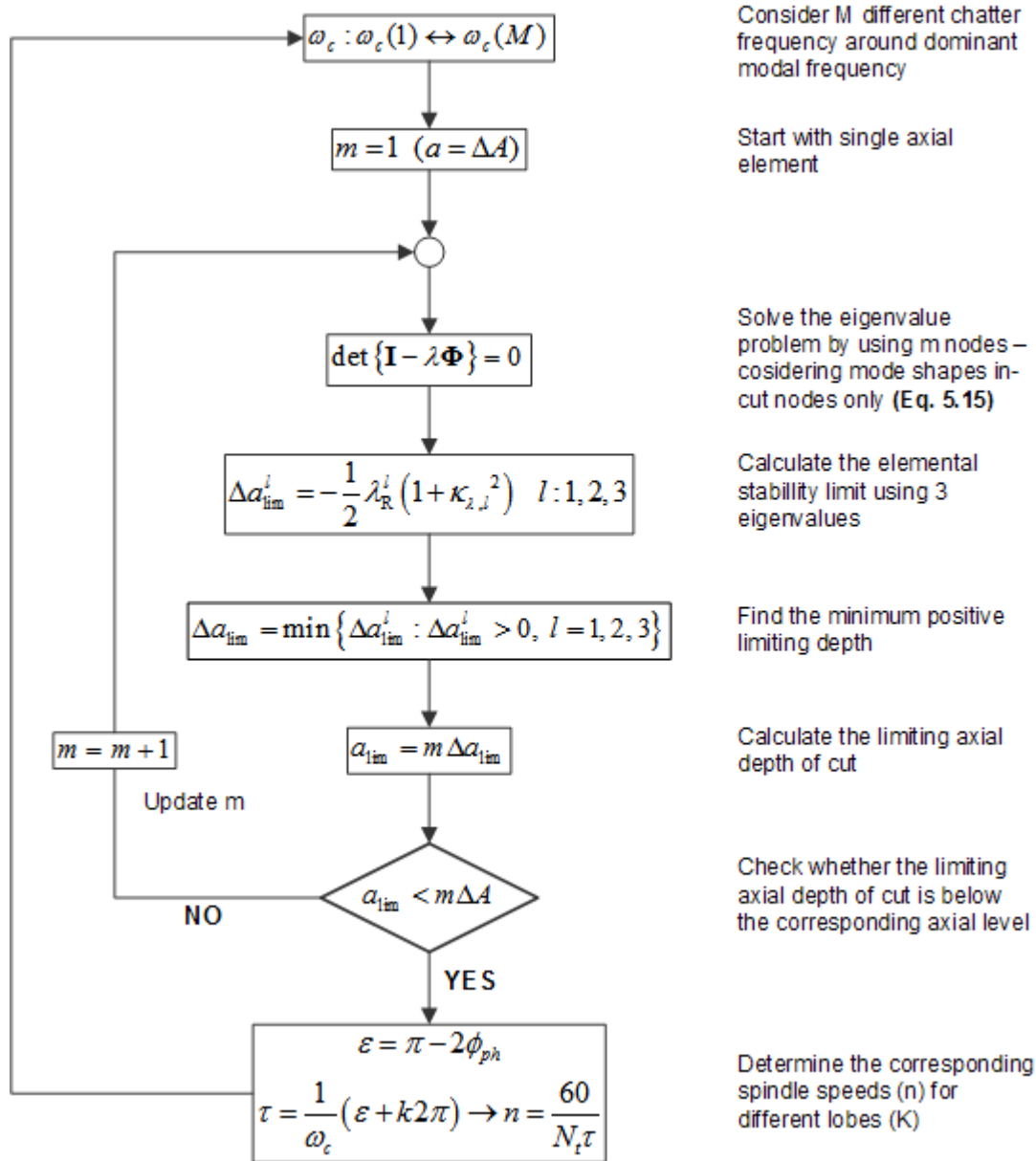


Figure 5.4: Pseudocode for generating stability diagrams for non-time varying machine tool systems

5.2 Chatter stability model for varying time delayed systems

The stability of a milling system depends mainly on the phase difference and between outer and inner modulation waves imprinted on the cutting surface by present and previous cutting edges. Depending on the frequency of chatter and on the time delay τ , the phase shift can cause system to become stable or unstable. For regular milling tools where the straight cutting edges are identical and equally separated the time delay is always constant for a specified rotational speed and is equal to;

$$\tau = \frac{2\pi}{N_t \Omega} \quad (5.24)$$

where N_t is the teeth number and Ω is the spindle speed in terms of rps. As the time delay does not vary along the cutting edge, the regeneration term, $\mathbf{b}=(1-e^{-i\omega_c \tau})$, is independent of the axial elevation and the stability limit for a single chatter frequency is always constant. The regeneration term For milling cutter with variable flute separation changing along the tool axis, the time delay term can simply be written considering the separation angle $\delta\phi_j(z)$ (see eq. (2.33) for formulation) between consecutive cutting edges for each axial level as;

$$\tau_j(z, \phi) = \frac{\delta\phi_j(z)}{\Omega} \quad (5.25)$$

On the other hand for serrated and variable helix/pitch milling tools for which the separation between consecutive cutting teeth at elevation z differ from each other the variation of the time delay must be considered. For serrated cutters the time delay for an angular position ϕ of tooth j for the axial elevation level z is calculated numerically by finding the number of preceding flutes which formed the currently cutting surface in the previous passes;

$$k \rightarrow \max_{m=1 \dots N_t} \left[\Delta r_{eff} - \left(\sum_{p=1}^m f_{t,j}(z) \right) \hat{f}_x \sin \phi_j \right] \quad (5.26)$$

the number k giving the largest value for the above equation gives the number of cutting edges skipped during the cut for that specific location. This expression is derived from the chip thickness formulation given in eq. (4.17) as an improvement to the Campomanes' [14] formulation in order to handle the multi-axis machining cases. Finally the time delay term can be written as;

$$\tau_j(z, \phi) = \sum_{i=1}^k \frac{\delta\phi_j(z)}{\Omega} \quad (5.27)$$

Thus, the regeneration coefficient for the j^{th} cutting edge at elevation level z is updated as follows;

$$\mathbf{b}_j(\phi, z) = 1 - e^{-i\omega_c \tau_j(z, \phi)} \quad (5.28)$$

Finally, the dynamic closed loop equation presented in eq. (5.13) is updated and the characteristic equation of the milling system is obtained as;

$$\begin{bmatrix} F_x(t, z) \\ F_y(t, z) \\ F_z(t, z) \end{bmatrix} = \Delta a b_j(\phi, i\omega_c) \left(\sum_{z=1}^m \mathbf{B}_o(z) \right) \mathbf{G}(i\omega_c) \begin{bmatrix} F_x(t) \\ F_y(t) \\ F_z(t) \end{bmatrix} \quad (5.29)$$

By following the formulation and methodology in the previous section the stability limit values can be calculated by finding the eigenvalues of presented the characteristic equation.

However the presented stability lobe formation formulation is invalid for varying time delayed system because of the varying regeneration coefficient introducing multiple chatter frequencies. It is therefore necessary to establish a new iterative loop formulation where for every spindle speed to be inspected, the possible chatter frequency values are swept in order to find corresponding time delays for every position. The new iterative cycle is presented in Figure 5.5.

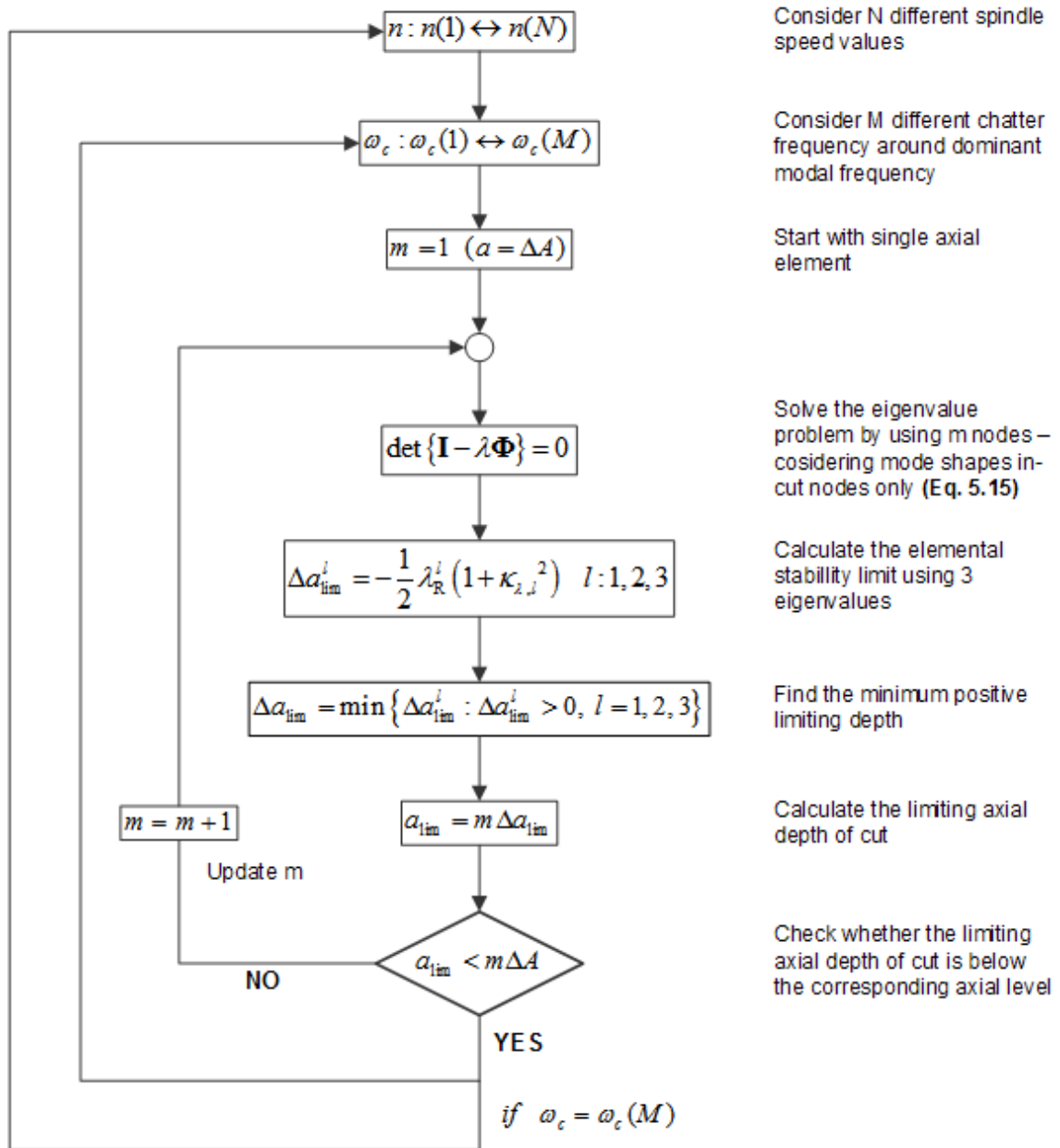


Figure 5.5: Pseudocode for generating stability diagrams for varying time delay machine tool systems

5.3 Model verification and simulation results

The proposed chatter stability models are validated with several cases involving different types of cutting geometries and some simulation results are shown in this section.

In order to construct the stability lobe diagrams, first the dynamic of the machine tool system should be known. The dynamic response information referred as the transfer function of the system is obtained through FRF (Frequency Response Function) measurements. To obtain the transfer function of the system the displacement output in terms of mm and the force input in terms of N must be measured. Even though many methods can be utilized to acquire FRF information, impact test setup is one the most inexpensive and easy to use setup. An impact hammer, which has a piezoelectric load cell on it, is used to excite the cutting tool at the tool tip and the response at the tool tip is acquired using an accelerometer (Figure 5.6a) or a vibrometer (Figure 5.6b). The output signal of the accelerometer in mm/s^2 or the vibrometer in mm/s is integrated to obtain a displacement output data in terms of m/s. Using the force and the displacement data, frequency response functions of the cutting tools in X and Y directions are obtained. Since the cutting tools are much more rigid in Z direction compared to X and Y directions, the flexibility in Z direction is neglected.

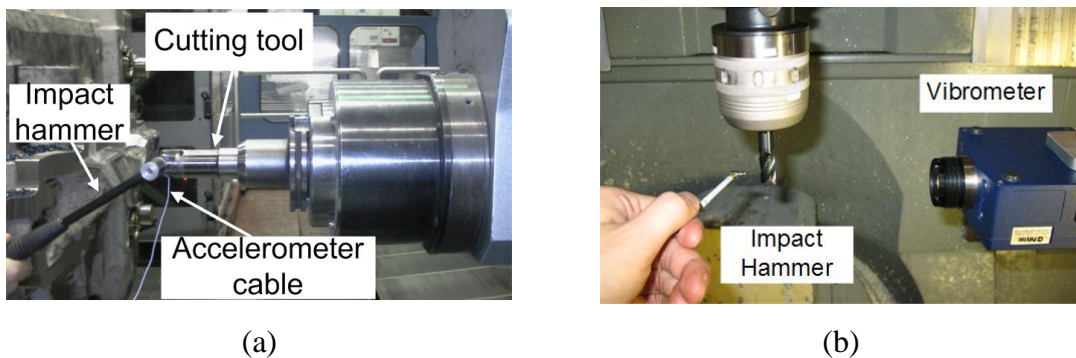


Figure 5.6: Frequency response function (FRF) measurement setups (a) impact hammer with accelerometer, (b) impact hammer with vibrometer

The raw data of the FRF can be directly used in the simulation by taking the real and the imaginary parts of the corresponding frequency through the iteration loops or the dynamic parameters can be extracted from the FRF for analysis where noise and non-dominant vibration modes can be neglected. The dynamic parameters for each different vibration mode constitute of the natural frequency ω_n in terms of Hz , the damping ratio ξ in terms of % and the modal stiffness K . Utilizing these parameters, the transfer function in a single direction is obtained as the sum for all the corresponding vibration modes as follow;

$$G(i\omega_c) = \sum_{i=1}^m \frac{\omega_n / K}{\omega_n^2 - \omega_c^2 + 2\zeta\omega_n\omega_c i} \quad (5.30)$$

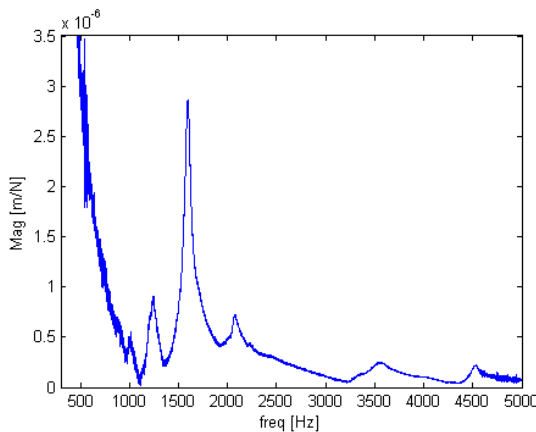
where m is the total number of vibration modes.

5.3.1 Stability analysis of an inverted cone bull end mill during 5-axis operation

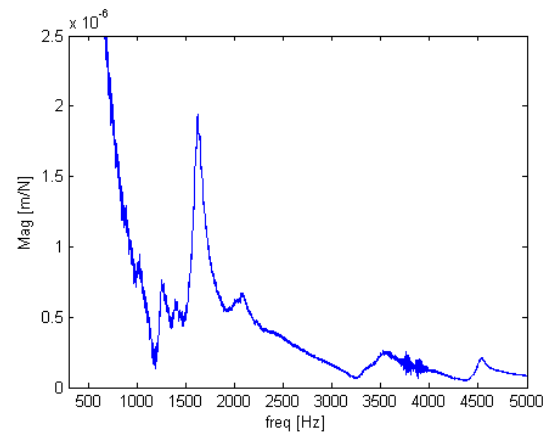
For the first test case the inverted cone bull end mill tool represented in Figure 4.8 is investigated for stable cutting conditions. Al7075 – T6 workpiece is through a multi-axis operation where the $+15^\circ$ lead angle and -10° tilt angle tool orientation values are chosen. A slotting case is simulated and the feed rate is kept constant at 0.05mm/tooth. The test is conducted with tool overhang length equal to 94mm. In Table 5.1, the modal parameters of the most dominant modes for X and Y directions are presented in addition to the FRF plots Figure 5.7. The workpiece is assumed to be rigid with respect to the milling tool.

Table 5.1: Modal parameters for the inverted cone bull end mill cutter with 94mm overhang length

	<i>mode</i>	ω_n (Hz)	ξ (%)	K (N/m)
X	1	1237.01	3.972	1.5e7
	2	1590.69	1.784	9.65e6
	3	2071.28	1.61	6.15e7
Y	1	1619.47	2.966	9.431e6
	2	2088	2.817	5.51e7



(a)



(b)

Figure 5.7: Frequency response function plots for inverted cone bull end cutter in X (a) and Y (b) directions

For the stability analysis, the system is considered unstable if there exist chatter marks on the machined surface, chatter noise is heard and a dominant chatter frequency suppressing the tooth pass and other process noises. For the test case, the simulated stability lobe diagram is presented in Figure 5.8 with corresponding verification points. For seven different spindle speeds, the stability of the system is analyzed using sound and vibration data by seeking dominant chatter frequencies. The axial depth for each spindle speed is increased as far as chatter is detected and stable and unstable point are marked with green and red points respectively.

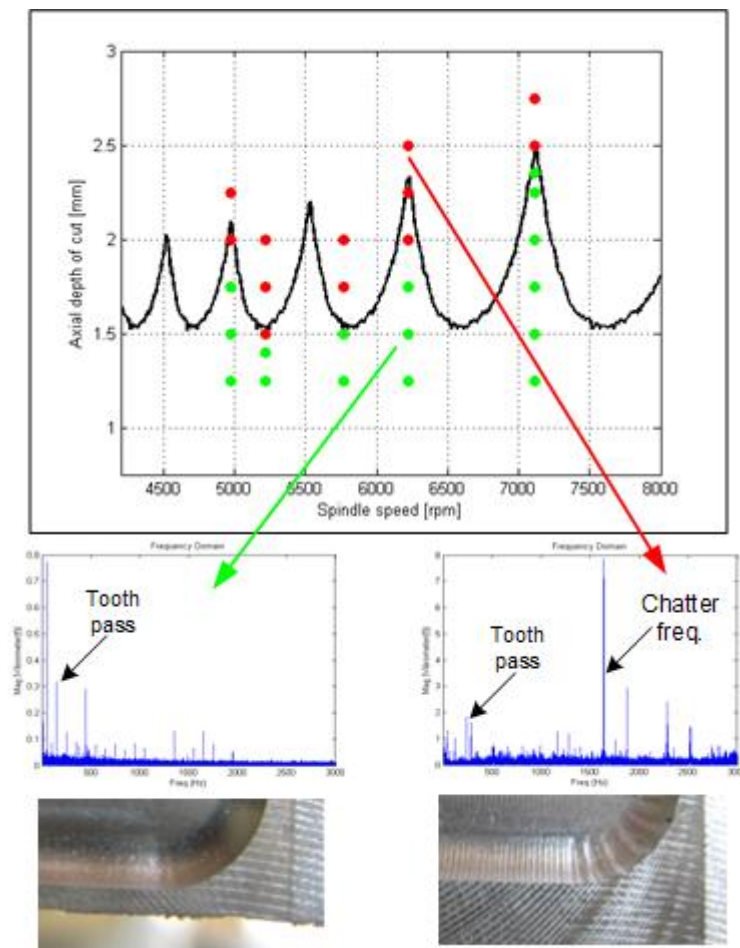


Figure 5.8: Stability lobe diagram for inverted bull end mil with corresponding stability test points (green dot representing stable operations, red dot representing chatter vibrations)

5.3.2 Radial stability analysis of multi-segmented profiling tool

For most of the profiling tools, in order to generate the desired surface, the entire tool profile envelope must engage with the workpiece. Hence, as axially the entire tool length is utilized, for stability the radial limits must be sought. The final surface geometry can be generated in many radial passes and in this example the radial stability limit for the first cutting pass is examined. The aim is to choose the highest possible radial depth of cut value for a productive operation.

Predicting the radial stability limits is rather easy for simple operations such as $2\frac{1}{2}$ flat end where the start and exit immersion angles can be expressed as a function of radial depth of cut. However, in multi-axis operations and especially for intricate milling tools, the cutter engagement boundary cannot be expressed as function and varies along the cutter axis both due to the differentiating tool local radii and tool axis orientations. For the stated reason, the radial stability boundaries are found iteratively by identifying the stability lobes for several cases where the radial depth of cut is altered. Finally, for each generated axial stability lobe diagram, the axial limit points equal to the tool height are extracted with the corresponding spindle speed values and plotted with respect to the radial depth of cut values.

For the test case, the custom profiling tool provided by MTE which is described in section 4.4.3 is investigated. Radial cutting of AL7075 – T6 workpiece simulation is conducted. The measured FRF of the cutting tool is shown in Figure 5.9 where only a single dominant mode is found and the modal parameters are listed in Table 5.2. The FRF measured in X and Y directions are compatible.

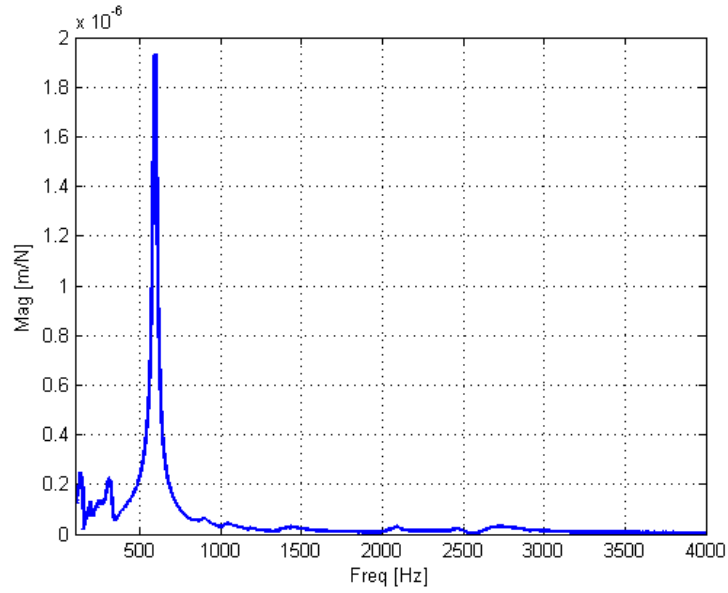


Figure 5.9: Magnitude of FRF for custom profiling tool with tool overhang length 190mm

Table 5.2: Modal parameters for custom profiling tool with tool overhang length 190mm

<i>mode</i>	ω_n (Hz)	ξ (%)	K (N/m)
1	594.9	1.371	6.44e7

The axial stability lobe diagrams are generated for every 0.2mm radial depth of cut increment starting from 0.2mm up to 2mm. All of the obtained graphs are plotted with respect to their corresponding radial depth of cuts in Figure 5.10. In the figure, the yellow surface designates the total tool cutting profile height. To decide on radial stability limits and construct the radial stability lobe diagram, the intersection points of the obtained axial stability lobe diagrams are extracted. These points with their corresponding radial depth of cuts are plotted in Figure 5.11.

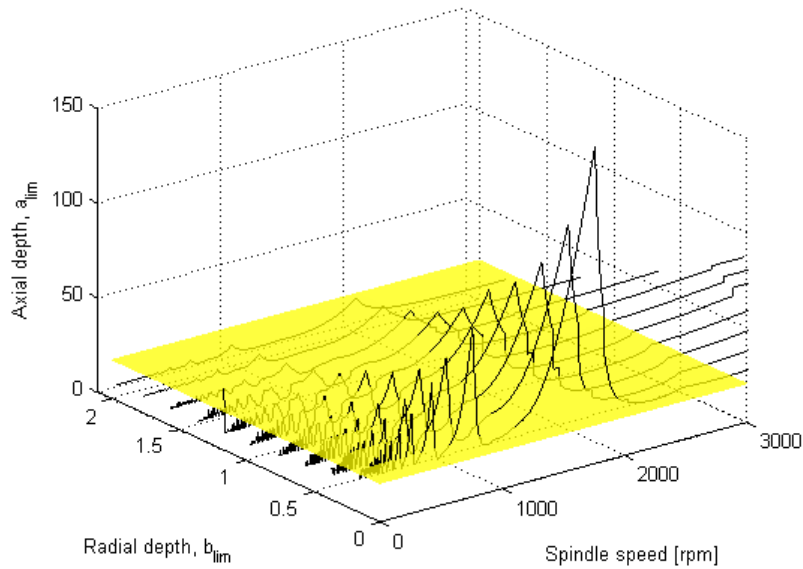


Figure 5.10: 3D plot of axial stability lobe diagrams with corresponding radial depth of cuts for custom profiling tool

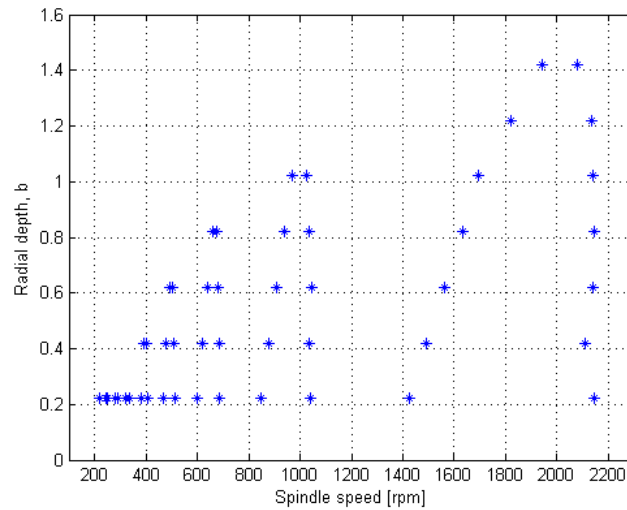


Figure 5.11: Radial stability limit diagram for custom profiling tool

The radial stability limit diagram plotted in Figure 5.11 can be evaluated as a normal stability diagram where the region below the plotted points designates the stable cutting region. For this simulation case, for example, when spindle speed is chosen as 2000rpm, it is possible to choose a radial depth of cut of 1.4mm which for a stable operation.

This example shows that the proposed model can be flexibly utilized to predict radial stability limits. The accuracy depends on the chosen radial immersion interval and step size.

5.3.3 Stability limit verification of inserted milling tool

In this section, the stability limit prediction and verification for an inserted cutting tool is presented. In the test case, a GH210 steel workpiece is cut with 6 circular inserted face milling tool presented in Table 2.2 under the properties of Tool 2. The overhang length of the tool is 170 mm. A half immersion case ($b=33\text{mm}$) is presented where the feed rate is chosen as 0.3mm/tooth . The frequency response function of the tool in X and Y direction is measured. Due to the symmetry of the structure, they are quite similar to each other. Hence, the measured frequency response function in X direction, which is plotted in Figure 5.12, is used in the simulation for both X and Y directions. Predicted stability diagram and results of chatter tests are given in Figure 5.13.

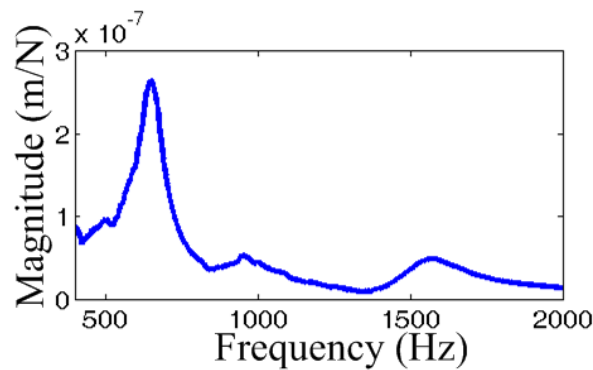


Figure 5.12: Magnitude of FRF for inserted tool (Table 2.2 - Tool 2) with overhang length 170mm

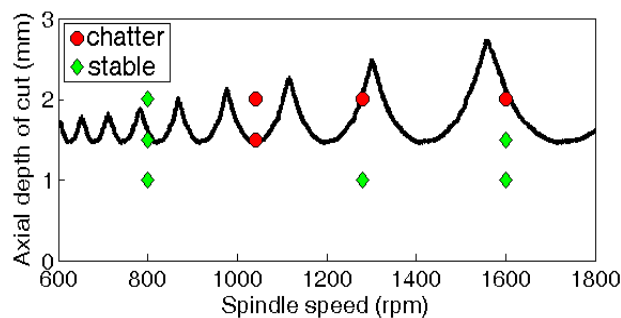


Figure 5.13: Stability lobe diagram for inserted tool (Table 2.2 - Tool 2)

Although, there is some discrepancy between experiments and simulations, the difference is reasonable and can be attributed to the measurement errors in FRFs and errors in predictions of cutting force coefficients.

5.3.4 Stability limit of serrated milling tool

In this simulation example, the effect of feed rate on the stability of serrated milling tools is shown. As previously mentioned, the serration profile due to varying time delay along the cutting edge, increases the stability of the cutting operation dramatically.

The serrated milling tool introduced in Table 4.8 is utilized for the stability simulation. The modal parameters from the measured FRF data are stated in Table 5.3.

Table 5.3: Modal parameters for serrated milling tool (see Table 4.8)

	<i>mode</i>	ω_n (Hz)	ξ (%)	K (N/m)
X	1	1569.441	3.206	1.619e7
	2	1960.55	1.46	5.931e6
Y	1	1577.23	2.89	2.061e7
	2	1966.9	1.247	6.473e6

Stability lobe diagrams for varying feed per tooth values are plotted in Figure 5.14. The radial depth is chosen to be 6mm and force coefficients for Al7075- T6 workpiece are utilized.

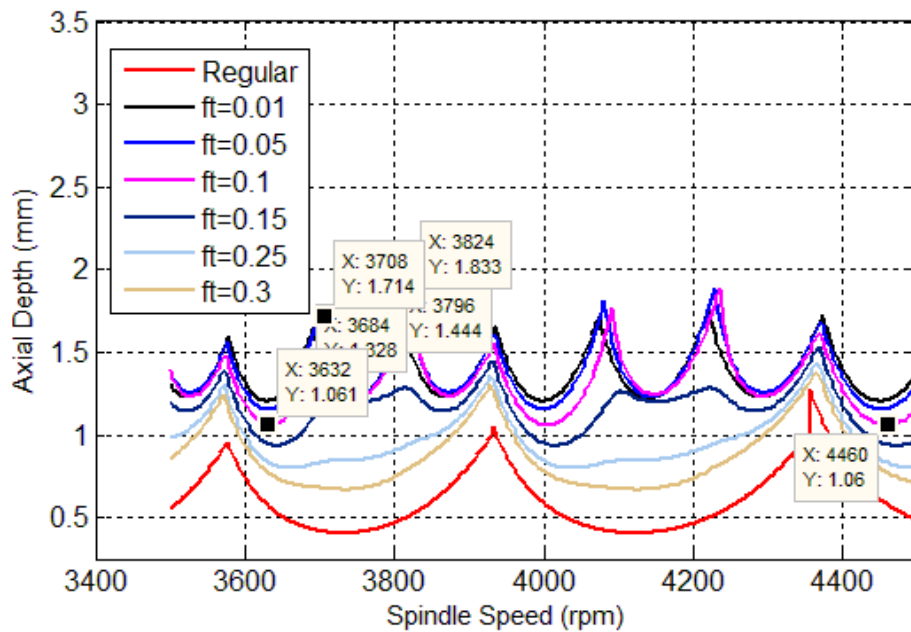


Figure 5.14: Stability lobe diagram serrated milling tool (see Table 4.8)

The resulting stability diagrams verify the previously stated hypothesis. The time delay during cutting depends on the selected feed rate in serrated cutter as it dictates how many teeth will be skipped during cutting for a given axial level. This mechanism introduces multiple chatter frequencies to the system and new lobes are formed as seen for example comparing the stability lobe diagram for a regular end mill and the lobe diagram for a serrated mill cutting with low feed rate (ie. $f_t = 0.05\text{mm/tooth}$). Moreover, the stability limits are increasing dramatically under this effect.

CHAPTER 6

CONCLUSION

Among many different manufacturing processes, multi-axis milling is one of the most flexible and reliable operations and it is widely used in industries requiring high precision. For all manufacturing process, the key to productivity is to choose operation parameters properly. In machining operations, poor choices can lead to dimensional inaccuracies, machine tool malfunctions and tool breakages, etc. due to unpredicted high cutting forces or chatter vibrations. Process models are utilized to predict feasible process parameters through geometrical and mathematical modeling without relying on empirical methods. In the literature, there are vast amount of proposed process models for machining operations, however most of them are either cutting tool or operation specific.

6.1 Summary and contributions

In this study, a general numerical model is proposed for multi-axis milling operations using any type of tool considering the tool profile geometry and cutting edge variation. The tool body and cutting edges are represented as a point cloud where the tool is divided into radial cross-sections cutting edge points corresponding to a cross-section are represented in cylindrical coordinates. Thus, a multi-segmented tool composed of linear and circular profile elements could be represented no matter how intricate the tool is in terms of profile geometry. The methodology is adapted to both solid milling tools and inserted cutters. Moreover, using the proposed method any geometrical variation of the cutting edge can be considered and in this study the effect of serrated and variably distributed edge geometries are investigated.

Both the mechanics and the dynamics of the multi-axis milling process are investigated. Linear edge force model is adapted to the multi-segmented, variably distributed, serrated edges milling tools. For each tool cross-section the differential orthogonal

cutting forces are calculated and for each immersion angle value, considering the contribution of each cutting edge at different axial levels, the total cutting forces are found using transformations. Uncut chip thickness definition is given for the most general case in multi-axis milling where the tool has both serration profile and variable edge distribution. Using orthogonal to oblique transformation method, the associated force coefficients are calibrated for each cutting point making use of the orthogonal databases obtained for different workpiece materials. For the dynamics of the milling process, the force model is utilized as the basis and the characteristic function of the multi-axis milling system is identified considering the regenerative closed-loop dynamic system. The limiting axial depths of cuts are identified corresponding to a range of chatter frequencies and spindle speeds and stability lobe diagrams are generated. For regular milling tools where the straight cutting edges are identical and equally separated, the model proposed by [43] is adapted and improved. For milling tools with variably distributed serrated edges, a new stability model is developed and introduced where the time variation between consecutive cutting edges is considered. The proposed mechanical and dynamic models are verified for different milling tool geometries. In general, especially for the force model, the simulation results are in good agreement with the measured data. Moreover, the proposed force model is integrated into the Z-mapping algorithm developed by Tunc [52] and the forces are simulated for continuous multi-axis milling processes and simulated results are compared with measured ones.

Finally, the models proposed in this study fill the gap of the mechanical and dynamical analysis of multi-axis milling and introduces a complete model where multi-segmented milling tools with variably distributed serrated cutting edges are investigated for the first time in the literature. The proposed models can be further adapted to any new tool geometries due to the robustness of the numerical point-wise approach. Nevertheless, because the models are numerical, the accuracy mainly depends on the chosen step sizes which directly effects the computation time. In this respect, analytical models are more advantageous in terms of computation time and accuracy. However due to their narrow perspective considering the tool geometry and operation type, analytical models are not considered as robust as the proposed one in this thesis. Moreover, the proposed model can be easily adapted into CAM systems and the mechanic and the dynamic of the process can be simulated in the real time during a continuous cycle. An exemplary case is presented by integrating the model into a Z-mapping algorithm.

6.2 Future works

In this section possible future works topics are listed. First, issues requiring further investigation which are not included in this study are mentioned;

1. The force coefficient identification for serrated milling tools technique can be further improved because the orthogonal to oblique transformation methodology is first proposed for regular milling tools. For serrated cutters the variation is not limited with the deviation of the helix angle; the deviation of the rake and clearance angles must be also considered in the first glance.
2. Different serration geometries such as circular, triangular, trapezoid, blended, etc. can be modeled for the completeness of the model.
3. Milling tool designers and manufactures introduces new tooling options where each cutting edge geometry varies dramatically from each other (ie. one serrated one straight edges milling tools, krest cut tools with sinusoidal helix angle variation, etc.). The proposed model can be adapted to these types of cutters for completeness.
4. The surface generation errors and in extreme cases tool breakages are the outcome of the tool deflections. In this study, the investigation of the tool deflection is not included, however as the total cutting forces acting on the cutting tool is known for each tool cross-section, the tool deflection can be easily calculated using Timoshenko beam equations.

A brief list of future works which can be based on the proposed models in this study are listed;

1. Due to the numerical approach, the proposed models can be directly integrated into CAM systems to monitor continuous process cycles. Thus, this academical study can be utilized in the industrial applications to obtain high productivity.
2. To adjust the time delay introduced by variable or serrated cutting edges is a possible way to suppress chatter vibrations which can be utilized in milling operations where process parameters are not allowed to be changed are the

variation range is not sufficient to avoid chatter. Using the proposed dynamical model, the cutting edge geometry can be optimized using heuristic methods.

3. Process optimization techniques are often utilized for continuous cycle simulations to increase productivity without violating the limits of the operation in terms of stability and mechanics of the system. Feed rate scheduling is one of the most common technique where for each step of the tool path the feed rate are adjusted such that resulting maximum cutting forces are constant throughout the process. The proposed Z-map integrated mechanical model can be utilized for feed rate scheduling.

Bibliography

- [1] Altintas, Y., Budak, E., “Analytical prediction of stability lobes in milling”, *Annals of the CIRP*, Vol.44/1, pp.357-362, 1995.
- [2] Altintas, Y., Engin, S., Budak, E., “Analytical stability prediction and design of variable pitch cutters”, *Journal of Manufacturing Science and Engineering*, Vol.121, pp.173-178, 1999.
- [3] Altintas, Y., *Manufacturing Automation*, Cambridge University Press, 2000.
- [4] Altintas, Y., Spence, A., “End milling force algorithms for CAD systems”, *CIRP Annals*, Vol. 40, pp.7-22, 1991.
- [5] Altintas, Y.; Shanoto, E.; Lee, P.; Budak, E.; “Analytical Prediction of Stability Lobes in Ball End Milling”; *ASME Jour. of Manufacturing Science and Engineering*, Vol.121, pp596-592; 1999.
- [6] Armarego, E.J.A, Epp, C.J., “An Investigation of Zero Helix Peripheral Up-Milling”, *International Journal of Machine Tool Design and Research*, Vol.10, pp. 273-291, 1970.
- [7] Barber, A., *Handbook of Noise and Vibration Control*, 6th edition, Elsevier Science Publishers, Oxford, UK, 1992.
- [8] Bayly, P.V.; Halley, J.E., Mann, B.P.; Davies, M.A.; “Stability of Interrupted Cutting by Temporal Finite Element Analysis”, *ASME Journal of Manufacturing Science and Engineering*, Vol.125, pp.220-225, 2003.
- [9] Budak, E., “An analytical design method for milling cutter with nonconstant pitch to increase stability”, *Journal of Manufacturing Science and Engineering*, Vol.125, pp.35-38, 2003

- [10] Budak, E., “Analytical models for high performance milling. Part I: Cutting forces, structural deformations and tolerance integrity”, *International Journal of machine Tools & Manufacture*, Vol. 46, pp. 1478-1488, 2006.
- [11] Budak, E., Altintas, Y., Armarego, E.J.A., “Prediction of Milling Force Coefficients from Orthogonal Cutting Data”, *Transactions of ASME*, Vol. 118, pp. 216-224, 1996.
- [12] Budak, E.; Altintas, Y.; “Analytical Prediction of Chatter Stability in Milling. Part I-II”; *ASME Journal of Dynamic System Measurement and Control*; Vol.120; pp.22-36, 1998.
- [13] Campa, F.J., Lopez de Lacalle, L.N., Lamikiz, A., Sanchez, J.A., 2007, Selection of Cutting Conditions for a Stable Milling of Flexible Parts with Bull-Nose End Mills, *Journal of Materials Processing Technology*, 191: 279-282.
- [14] Campomanes, M. L., “Kinematics and dynamics of milling with roughing endmills”, *Metal Cutting and High Speed Machining*, Kluwer Academic/Plenum Publishers, 2002.
- [15] Choi, B.K., Jerard, R.B., *Sculptured Surface Machining: Theory and Applications*, Kluwer Academic Publishers, The Netherlands, 1998.
- [16] Dombovari, Z. , Altintas, Y., Stephan G., “The effect of serration on mechanics and stability of milling cutters”, *International Journal of Machine Tools & Manufacture*, Vol.50, pp.511-520, 2010.
- [17] Engin, S. and Altıntaş, Y.,“Mechanics and dynamics of general milling cutters. part I: helical end mills”, *Int. Journal of Machine Tools & Manufacture*. Vol.41, pp. 2213-2231, 2001.
- [18] Engin, S. and Altıntaş, Y.,“Mechanics and dynamics of general milling cutters. part II: inserted cutters”, *Int. Journal of Machine Tools & Manufacture*. Vol.41, pp. 2195-2212, 2001.

- [19] Ferry, W. B., Altintas, Y., “Virtual five-axis flank milling of jet engine impellers – part I-II”, *Journal of Manufacturing Science and Engineering*, Vol.130, pp.011005, 2008.
- [20] Ferry, W. B.S.; “Virtual 5axis flank milling of jet engine impellers”, Ph.D. Thesis; University of British Columbia Mechanical Engineering Program; Vancouver, Canada; 2008.
- [21] Gradisek, J., kalveram, M., Weinert, K., “Mechanic identification of specific force coefficients for a general end mill”, *International Journal of Machine Tools and Manufacture*, Vol.44, pp.401-404, 2004.
- [22] *High Performance Solid Carbide End Mills*, Product catalog, Guhring INC., 2010
- [23] Insperger, T., Stephan, G., “Semi-discretization method for delayed systems”, *International Journal for Numerical Methods in Engineering*, Vol.55, pp.503-518, 2002
- [24] Insperger, T., Stephan, G., “Updated semi-discretization method for periodic delay-differential equations with discrete delay”, *International Journal for Numerical Methods in Engineering*, Vol.67, pp.117-141, 2004.
- [25] Kapoor, S. G., DeVor, R. E., Zhu, R., Gajjela, R., Parakkal, G. and Smithey, D. “Development of Mechanistic Models for the Prediction of Machining Performance: Model Building Methodology”, *Machining Science and Technology*, Vol.2:2, pp.213, 1998.
- [26] Kim, G. M., Cho, P. J., Chu, C. N., “Cutting force prediction of sculptured surface ball-end milling using Z-map”, *International Journal of machine Tools and Manufacture*, Vol.40, pp.277-291, 2000.
- [27] Kim, G. M., Ko, S. L., “Improvement of cutting simulation using Octree method”, *International Journal of Advance Manufacturing Technology*, Vol.28, pp.1152-1160.

- [28] Kim, S.-J., Lee, H.-U., Cho, D.,W., “Feedrate Scheduling for Indexable End Milling Process Based on an Improved Cutting Force Model”, *International Journal of Machine Tools and Manufacture*, Vol. 46, pp.1589-1597, 2006.
- [29] Kline W.A., DeVor R. E., “The Effect of Runout on Cutting Geometry and Forces in End Milling”, *International Journal of Machine Tool Design & Research*, Vol. 23, No. 2-3, pp. 123-140, 1983.
- [30] Kline, W. A., DeVor, R. E., Lindberg, J. R., “The prediction of cutting forces in the end milling with application to cornering cuts.”, *International Journal of Machine Tool Design and Research*, Vol. 22, pp.7-22, 1982.
- [31] Lazoglu I., Liang, S. Y., “Modelling of ball-end milling forces with cutter inclination” *Journal of Manufacturing Science and Engineering*, Vol.122., pp.3-11, 1996.
- [32] Lee, P. and Altintas, Y., “A General Mechanics and Dynamics Model for Helical End Mills”, *Annals of the CIRP*, Vol.45, pp. 59-64, 1996.
- [33] Lee, P., Altintas, Y., “Prediction of ball end milling forces from orthogonal cutting data”, *International Journal of machine Tools and Manufacture*, Vol.36, pp.1059-1072, 1996.
- [34] Lia, X.P., Zhenga, H.Q., Wonga, Y.S., Neea, A.Y.C., 2000, An Approach to Theoretical Modeling and Simulation of Face Milling Forces , *Journal of Manufacturing Processes*, Vol. 2, Issue 4: 225-240
- [35] Lopez de Lacalle , L.N., Lamikiz, A. , Munoa, J., Salgado, M.A., Sanchez, J.A., 2006, Improving the High-Speed Finishing of Forming Tools for Advanced High-Strength Steels (AHSS), *International Journal of Advanced Manufacturing Technology*, 29: 49-63.
- [36] Maeng, S. R., Baek, N., Shin, S.Y., Choi, B. K., “A Z-map update method for linear moving tools”, *Computer-Aided Design*, Vol. 35, pp.995-1009, 2003.
- [37] Martelotti, M. E., “An analysis of milling process”, *Transactions of ASME*, Vol. 122, pp.3-11, 1941.

- [38] Merchant, M.E., "Basic Mechanics of the Metal Cutting Process", Transactions of ASME Journal of Applied Mechanics, pp. 168-175, 1994.
- [39] Merdol, S.D., Altintas, Y., "Mechanics and dynamics of serrated cylindrical and tapered end mills", Journal of Manufacturing Science and Engineering, Vol.126, pp.217-236, 2004.
- [40] Minis, I., Yanushevsky, T., Tembo, R., Hocken, R., "Analysis of linear and nonlinear chatter in milling", Annals of CIRP, Vol.39, pp.459-462, 1990.
- [41] National Bureau of Standards, "Digital representation for communication of product definition data", NBSIR 80-1978, 1980.
- [42] Olgac, N., Sipahi, R., "Dynamics and stability of variable-pitch milling" Journal of Vibration and Control, Vol.13, pp.1031-1043, 2007.
- [43] Ozturk, E., Budak E., "Dynamics and stability of five-axis ball-end milling", Journal of Manufacturing Science and Engineering, Vol.132, pp. 021003-1-13, 2010.
- [44] Ozturk, E., Budak E., "Modeling of 5-axis milling processes", Machine Science and Technology, Vol. 11/3, pp. 287-311, 2007.
- [45] Patel, B. R., Mann, B. P., Young, K. A., "Uncharted islands of chatter instability in milling", International Journal of Machine Tools and Manufacture, Vol.48, pp.124-134, 2008
- [46] Ramaraj, T.C., Eleftheriou, E., "Analysis of mechanics of machining with tapered end milling cutters", Transactions of the ASME, Vol.116, pp. 398-404, 1994.
- [47] Siller, H. R., Vila, C., Rodriguez, C. A., Abellan, J. V., "Study of face milling of hardened AISI D3 steel with a special design of carbide tools", International Journal of Advanced Manufacturing Technologies, Vol. 40, pp. 12-25, 2008.
- [48] Sims, N. D., Mann, B., Huyanan, S., "Analytical prediction of chatter stability for variable pitch and variable helix milling tools", Journal of Sound and Vibration, Vol.137, pp.664-686, 2008

- [49] Stabler, G.V., "The Chip Flow Law and Its Consequences", *Advances in Machine Tool Design and Research*, pp. 243-251, 1964.
- [50] Tlustý, J., Ismail, F., Zaton, W., "Milling cutters with irregular pitch", Technical report, McMaster Engineering Society, Canada
- [51] Toolex Inc., "Machine tool catalog", 2010.
- [52] Tunc, L. T., "Selection of cutting strategy and parameters in multi-axis machining operations for improved productivity" PhD Thesis, Sabanci University, Turkey, 2010.
- [53] Turner, S., Merdol D., Altintas. Y., Ridgway, K., "Modelling of stability of variable helix end mills", *International Journal of Machine Tools and Manufacture*, Vol.47, pp.1410, 2010
- [54] Wang J.-J. Junz, Liang S. Y., "Chip Load Kinematics in Milling with Radial Cutter Runout", *Transactions of the ASME*, Vol. 118, pp. 111-118, 1996.
- [55] Yusoff A.R., Sims, N. D., "Optimization of variable helix end milling tools by minimizing self-excited vibration", 7th International Congerence on Modern Practice in Stress and Vibration Analysis, 2009.
- [56] Zatarain, M., Munoa, G., Peigne, T., Insperger, T., "Anaylsis of the influence of mill helix angle on chatter stability", *Annals of CIRP*, Vol.55, 2006.
- [57] Zhang, Z., Zheng, L. "A cutting force model for waved-edged end milling cutters", *International Journal of Advance Manufacturing Technology*, Vol.21, pp.403-410, 2003.